

Experimental and Theoretical Modelling of CO₂ Injectivity

Effect of Fines Migration and Salt Precipitation

by

Yen Adams Sokama-Neuyam

Thesis submitted in fulfilment of
the requirements for the degree of
PHILOSOPHIAE DOCTOR
(PhD)



Faculty of Science and Technology
Department of Petroleum Engineering
2017

University of Stavanger
NO-4036 Stavanger
NORWAY
www.uis.no

©2017 Yen Adams Sokama-Neuyam

ISBN: [Click to enter ISBN.](#)

ISSN: [Click to enter ISSN.](#)

PhD: Thesis UiS No. [Click to enter PhD No.](#)

To Susan, with love...

Acknowledgements

All glory and honour to the LORD for His grace, encouragement and guidance.

I would like to express my deepest appreciation to my supervisor, Professor Jann Rune Ursin, for his special mentorship, support and trust. I truly appreciate the rare trust and opportunities he gave me to acquire vital research and teaching skills. I am also grateful to Professor Aly Anis Hamouda as my co-supervisor.

Special gratitude is extended to Professor Zhixin Yu for providing space in the laboratory for my experimental apparatus. I thank Dr. Ingebret Fjelde and Dr. Aruoture Voke Omekeh for their encouragement during my work.

Kim Andre N. Vorland is kindly acknowledged for his pivotal role in setting up the CO₂ core-flood laboratory. Great thanks are extended to Ola Ketil Siqveland, Per Eirik Krossgått Widvey and Svein Myhren for all their help in the laboratory instrumentation work. My sincere gratitude to Inger Johanne M. Olsen for her support to purchase various laboratory apparatus and materials. I am also thankful to Reidar Inge Korsnes for his help in SEM analysis.

I would also like to acknowledge the help and support of my colleagues, Dori Yosef Kalai, Kun Guo and Kristian Stangeland for their collegiality in the laboratory. I am thankful to all the bachelor and master students who worked with me in the laboratory, especially Pahmi U. R. Ginting and Bikram Timilsina.

PGNiG Upstream International AS and the Department of Petroleum Engineering, Faculty of Science and Technology, University of Stavanger are acknowledged for their financial support.

The LORD bless you.

Abstract

Adequate well injectivity is required to inject large volumes of CO₂ at acceptable rates through a minimum number of wells. Mineral dissolution and salt precipitation could impair CO₂ injectivity and reduce the quality and capacity of deep saline reservoirs for carbon storage. Convincing evidence of CO₂ injectivity impairment induced by salt precipitation has encouraged the need to investigate other potential injectivity impairment mechanisms.

Under typical storage conditions, CO₂-brine-rock reactions could generate secondary minerals in the form of fine particles into the pore fluid. Drilling fluids and cement particles may also contaminate the wellbore region. If these particles are mobilized during CO₂ injection, injectivity could be severely impaired through fines entrapment. The special properties of supercritical CO₂ and the high injection rates required to meet emission reduction targets, demand extension of conventional findings to understand the mechanisms of fines mobilization in relation to CO₂ injection. In addition, the drying effect of supercritical CO₂ makes fines mobilization and salt precipitation effects inseparable.

We investigated the impact of fines mobilization on CO₂ injectivity through sandstone core-flood experiments and theoretical modelling. The impact of fines mobilization was then compared to the effects of salt precipitation. Attempt was made to investigate the coupled effect of fines mobilization and salt precipitation as the two mechanisms are inseparable under typical storage conditions. Important parameters such as CO₂ injection flow rate, initial rock permeability, concentration and size of particles and saturating brine salinity were identified and studied.

We found that, mineral dissolution and fines mobilization could impose severe injectivity impairment. Up to 26 % injectivity impairment was recorded during carbonated water flooding into Berea sandstone rocks. Injectivity impairment decreased when carbonated water injection rate was increased. This implies that, under storage conditions, injectivity impairment induced by mineral dissolution and fines mobilization increases with storage time as the number of particles generated increases with CO₂-brine-rock reaction rate.

Fines mobilization was also found to induce injectivity impairment comparable to salt precipitation effects. About 0.3 wt.% of particles in the pore fluid induced over two-fold injectivity impairment compared to about 10 wt.% of total dissolved solid in the formation water. About 1.0 wt.% of particles in the pore fluid almost plugged the rock. Under storage conditions, mineralization may be more pronounced away from the wellbore. However, the present findings suggest that even small amount of fine particles in the pore fluid around the immediate injection area could induce severe CO₂ injectivity impairment. Although salt precipitation is expected to be the dominant injectivity impairment mechanism under radial flow conditions, the current finding shows that fines mobilization could further impair injectivity.

We also found that salt precipitation could aggravate injectivity impairment induced by fines mobilization. The precipitated salts reduce the CO₂ flow area and render the pores more susceptible to fines entrapment. However, while salt precipitation within the plugged pores could be limited by flow restrictions, the injected CO₂ could also dislodge pore-bridging particles. The net impact of these competing mechanisms on injectivity is not fully understood.

Although the findings are largely based on linear core-flood studies, insights gained, adequately describe the mechanisms and impact of fines mobilization in the immediate injection area of the wellbore. The findings further underpins the need to reconsider the impact of fines mobilization on CO₂ injectivity. We have also shown that previous findings cannot sufficiently describe the mechanisms of fines mobilization in the context of CO₂ injection under storage conditions.

List of Papers

- I. **Sokama-Neuyam Y. A.**, Ursin, J. R., 2017. Experimental Investigation of the Impact of Salt Precipitation on CO₂ Injectivity. Published in proceedings of *International Symposium of the Society of Core Analysts*, August 28 – 31, Vienna, Austria.
- II. **Sokama-Neuyam Y. A.**, Ursin, J. R., 2015. The Effect of Mineral Deposition on CO₂ Well Injectivity. Published in proceedings of *SPE EUROPEC Conference*, June 1 – 4, Madrid, Spain.
- III. **Sokama-Neuyam Y. A.**, Ursin, J. R., 2017. Experimental and Theoretical Study of Salt Precipitation, Development of the Dry-out zone and CO₂ injectivity. To be submitted for Publication.
- IV. **Sokama-Neuyam Y. A.**, Ursin, J. R., 2015. CO₂ Well Injectivity: Effect of Viscous Forces on Precipitated Minerals. Published in proceedings of *International Petroleum Technology Conference*, December 6 – 9, Doha, Qatar.
- V. **Sokama-Neuyam Y. A.**, Ursin, J. R., 2016. Experimental and Theoretical Investigations of CO₂ Injectivity. *AGH Drilling, Oil, Gas* **33**, 245 – 258.
- VI. **Sokama-Neuyam Y. A.**, Ginting, P. U. R., Timilsina, B., Ursin, J. R., 2017. The Impact of Fines Mobilization on CO₂ Injectivity: An Experimental Study. *International Journal of Greenhouse Gas Control* **65**, 195 – 202.
- VII. **Sokama-Neuyam Y. A.**, Forsetløyken, S. L., Lien, J., Ursin J. R., 2017. The Coupled Effect of Fines Mobilization and Salt Precipitation on CO₂ Injectivity. *Energies*, **10**(8), 1125.

Contents

Acknowledgements.....	iii
Abstract.....	v
List of Papers.....	vii
List of Figures.....	xi
List of Tables.....	xiii
Abbreviations and Symbols.....	xv
1 Introduction.....	1
1.1 Geological Storage of CO ₂	1
1.1.1 Storage in saline aquifers.....	1
1.1.2 CO ₂ Enhanced Oil Recovery.....	2
1.1.3 CO ₂ Enhanced Coal Bed Methane Production.....	3
1.2 Prerequisites for CCUS.....	4
1.2.1 Storage Potential.....	4
1.2.2 Well Injectivity.....	6
1.2.3 Containment Efficiency.....	6
1.3 CO ₂ Well Injectivity Impairment Mechanisms.....	7
1.3.1 Geochemical Effects.....	8
1.3.2 Transport Effects.....	10
2 Objectives.....	13
3 Materials and Methods.....	15
3.1 Materials.....	15
3.1.1 Core Samples.....	15
3.1.2 Brine.....	16
3.1.3 Gas.....	16
3.1.4 Carbonated Water.....	16

3.1.5	Colloids.....	17
3.2	Experimental Setup.....	18
3.3	Methods	19
3.3.1	Procedure	19
3.3.2	Calibrations.....	20
3.3.3	Uncertainty in Experimental Data.....	21
4	Results.....	23
4.1	Salt precipitation	23
4.1.1	Salt cake development	23
4.1.2	Drying effects	25
4.1.3	CO ₂ alternating LSW flooding.....	35
4.2	Mineral dissolution and fines mobilization.....	36
4.2.1	Evidence of dissolution and fines entrapment	37
4.2.2	Effect of dissolution and fines entrapment	38
4.3	Salt precipitation and fines mobilization	40
4.3.1	Comparing fines and salt effects.....	40
4.3.2	Coupling fines and salt effects.....	43
5	Discussion.....	47
5.1	Results compared to literature	47
5.2	Limitations of the work.....	49
5.3	Field relevance	49
5.4	Proposed further work	51
6	Conclusion	53
7	Bibliography	55
	Papers.....	65

List of Figures

Figure 1.1. Factors affecting CO ₂ injectivity (after Lombard et al., 2010).....	8
Figure 3.1 Schematics of the experimental setup used to prepare carbonated water.	17
Figure 3.2 Schematics of the core-flooding apparatus used in the tests – the CO ₂ flow rig.....	19
Figure 4.1 Photographs of Bentheimer core after CO ₂ was injected at 1 mL/min into the core initially saturated with 120 g/L NaCl brine.	24
Figure 4.2 Photographs showing salt cake development at the core inlet when supercritical CO ₂ injection rate was increased from (A) 1 mL/min to (B) 5 mL/min.	25
Figure 4.3 Photographs showing salt cake development at the core inlet when brine salinity was decreased from (A) 120 g/L to (B) 75 g/L.....	25
Figure 4.4 Effect of drying and salt precipitation on CO ₂ injectivity..	26
Figure 4.5 Schematics of the bundle-of-tubes model.	28
Figure 4.6 The impact of the dry-out length (L_d) on CO ₂ injectivity impairment (β) induced by salt precipitation..	31
Figure 4.7 The impact of CO ₂ injection flow rate on the effect of drag on permeability after salt precipitation.	33
Figure 4.8 Effect of initial core permeability on permeability change induced by the effect of drag forces on precipitated salts. Berea core (1484 mD) and Kirby core (372 mD) were tested.....	34
Figure 4.9 Effect of diluent brine Salinity on CO ₂ injectivity change induced by alternate injection of supercritical CO ₂ and LSW.....	36
Figure 4.10 Pressure drop profile recorded during injection of carbonated water into a Bentheimer core at flow rate of 0.25 mL/min at 80 bar and 60 °C.....	37
Figure 4.11 Effect of injection flow rate on injectivity impairment induced by fines plugging..	39
Figure 4.12 Pressure drop profiles recorded during supercritical CO ₂ injection into Berea Sandstone cores initially saturated with FW, 0.3 wt.% and 0.5 wt.% colloid solutions with average particle size of 0.08 μm	41
Figure 4.13 The relative impact of fines mobilization and salt precipitation on CO ₂ injectivity..	42

Figure 4.14 The coupled effect of fines mobilization and salt precipitation on
CO₂ injectivity..45

List of Tables

Table 3.1 Characteristics and petrophysical properties of outcrop sandstone cores used in the experiments.	15
Table 3.2 Properties of fumed alumina stock solution used to prepare colloid solutions.	18
Table 4.1 EDS elemental analysis of effluent samples collected during carbonated water flooding into Bentheimer core.	38

Abbreviations and Symbols

Abbreviations

CCS	CO ₂ Capture and Storage
CCUS	CO ₂ Capture, Utilization and Storage
CSC	Critical Salt Concentration
CO ₂ – ECBM	CO ₂ Enhanced Coalbed Methane Recovery
CO ₂ – EOR	CO ₂ Enhanced Oil Recovery
CO ₂ – LSWAG	CO ₂ Low Salinity Water Alternating Gas flooding
EOR	Enhanced Oil Recovery
FW	Formation Water
H – P	Hagen – Poiseuille
HS	High Salinity NaCl Brine
I	Injectivity
LS	Low Salinity NaCl Brine
LSW	Low Salinity Water prepared from FW
MMP	Minimum Miscibility Pressure
PV	Pore Volumes
RF	Recovery Factor
RIC	Relative Injectivity Change
WAG	Water Alternating Gas Injection

Symbols

β	Relative injectivity change index
μ	Fluid viscosity, (Pa.s)
μ_{CO_2}	Viscosity of CO ₂ under reservoir conditions, (Pa.s)
ρ	Mass density of the fluid, (Kg/m ³)
ρ_{aq}	Density of the aqueous phase, (Kg/m ³)
ρ_{CO_2}	Density of CO ₂ at reservoir conditions, (Kg/m ³)
$\rho_{CO_2,res}$	Density of CO ₂ under reservoir conditions, (Kg/m ³)
$\rho_{CO_2,sc}$	Density of CO ₂ under standard conditions, (Kg/m ³)
ρ_s	Density of precipitated salt, (Kg/m ³)
ϕ	Porosity after impairment
ϕ_o	Porosity of the clean porous medium
ϕ_T	Total porosity of the aquifer
ΔI_{avg}	Estimated uncertainty in injectivity
Δp	Pressure drop, (bar)

ΔP_f	Final pressure drop, (bar)
ΔP_i	Initial pressure drop, (bar)
Δr_i	Precipitated salt thickness in capillary tube i , (m)
A	Reference area, (m ²)
C_D	Drag coefficient
C_i	Molar concentration of ion i , (mol/L)
E_s	Storage efficiency
I_{avg}	Mean value of injectivity (m ³ /Pa.s)
I_f	Final injectivity, (m ³ /Pa.s)
I_i	Initial injectivity, (m ³ /Pa.s)
I_{max}	Maximum measured injectivity, (m ³ /Pa.s)
$I_{measured}$	Measured injectivity, (m ³ /Pa.s)
I_{min}	Minimum measured injectivity, (m ³ /Pa.s)
k	Permeability of the impaired porous medium, (mD)
K_f	Final measured permeability, (mD)
kh	Permeability-thickness product, (m ³)
K_i	Initial measured permeability, (mD)
k_o	Original permeability of the porous medium, (mD)
L	Total length of core, (m)
L_1	Length of the dry-out zone, (m)
l_d	Dimensionless dry-out length
M_{CO_2}	Mass of CO ₂ that can be stored, (Kg)
N	Total number of capillary tubes
Q	Total fluid flow rate, (m ³ /s)
q	Volumetric injection flow rate, (m ³ /s)
q_f	Final injection flow rate, (m ³ /s)
q_i	Initial injection flow rate, (m ³ /s)
R	Core radius, (m)
R_i	Initial spherical radius in a close packed structure, (m)
r_i	Radius of tube i , (m)
r_e	Radius of the reservoir boundary, (m)
\bar{r}_i	Average tube/pore radius, (m)
\bar{r}_i^2	Average of the square of the tube radii, (m ²)
r_w	Well radius, (m)
s	Skin factor
$\bar{S}_{CO_2,d}$	Average CO ₂ saturation behind the dry-out front
S_s	Solid salt saturation
v	Flow velocity relative to the object
V_A	Bulk volume of the aquifer, (m ³)

V_{CO_2}	Volume of injected CO ₂ , (m ³)
V_{HC}	Hydrocarbon pore volume, (m ³)
V_{iw}	Volume of the reservoir invaded by water, (m ³)
V_p	Pore volume of the core, (m ³)
V_{pore}	Accessible reservoir pore volume for CO ₂ storage, (m ³)
V_{pw}	Reservoir volume of produced water, (m ³)
X_s	Mass fraction of salt dissolved in the aqueous phase
Z_i	Charge number of the ion i

1 Introduction

A concise background of CO₂ Capture, Utilization and Storage (CCUS) is presented in this chapter. The main focus is on CO₂ injectivity impairment mechanisms.

1.1 Geological Storage of CO₂

CO₂ capture and storage (CCS) is a promising approach to mitigate global climate change. The technique involves large scale capture of CO₂ from anthropogenic and industrial sources, safe transportation usually through pipelines and eventual storage of the gas in subsurface geological traps (Ha-Duong and Keith, 2003). The oceans and deep subsurface geological structures are the two main locations proposed for CO₂ storage (Michael Sheppard, 2017). However, because of political and technical challenges associated with CO₂ sequestration in the oceans, geological storage is more plausible.

CO₂ is commonly stored in three different geological formations: deep saline aquifers, depleted oil and gas reservoirs and unmineable coal beds (Leung et al., 2014a). Storage in deep saline reservoirs is less attractive as the CO₂ is injected without any positive economic benefit other than to the environment. However, CO₂ could be injected to recover residual oil through various Enhanced Oil Recovery (EOR) techniques. The recovered hydrocarbons is then used to improve the economics of the capture and transportation processes (Baines et al., 2009; Li et al., 2013). CO₂ injection has also shown enormous promise in coal-bed methane production.

1.1.1 Storage in saline aquifers

In terms of accessibility and volumetric capacity, deep saline formations have the highest potential for CO₂ storage (Baines et al., 2009; Gunter et al., 1998; Holloway, 2001; Li et al., 2013). Davison et al., (2001) claimed that on a global scale, deep saline reservoirs could account for between 20% and 500% of the projected CO₂ emissions by 2050. Thus, worldwide CO₂ storage potential of deep saline reservoirs ranges from 400 – 10,000 Gt CO₂.

Deep saline aquifers, usually at depths between 700 – 1000m, hold large volumes of high salinity formation brines (Singh, 2008). The natural contents of these reservoirs have no direct commercial value. However, the chemical composition of the formation fluids makes them suitable for CO₂ mineralization. In deep saline aquifers, CO₂ could be sequestered through hydrodynamic trapping where the gas is trapped beneath a caprock, residual trapping where the rock contains residual saturation of CO₂, solubility trapping where the gas dissolves in the formation brine and mineral trapping where CO₂ reacts with Ca, Fe or Mg to form stable carbonate precipitates (Reichle et al., 1999).

A practical example of CO₂ storage in deep saline formation is the Sleipner field on the Norwegian continental shelf, where CO₂ is injected into saline aquifer, about 800m below the sea bed (Baines et al., 2009). Lack of additional economic benefits except carbon tax incentives, makes CO₂ storage in saline aquifers less attractive to the oil and gas industry, where large quantities of CO₂ are still produced from fossil fuel.

1.1.2 CO₂ Enhanced Oil Recovery

CO₂-EOR is a tertiary oil recovery technique where CO₂ and usually water or brine is injected into the reservoir (IEA, 2015). In addition to extraction of residual oil, the injected gas provides pressure support and could remain stored permanently after the recovery process. Under subsurface conditions, CO₂ mixes with oil above a certain minimum miscibility pressure (MMP), reducing the capillary effect that retain the oil in place (Gozalpour et al., 2005). There are four underlying mechanisms of CO₂-EOR presented by Rojas and Ali, (1986) and Tunio et al., (2011) as: (1) oil swelling; (2) reduction of oil viscosity; (3) reduction of oil and water density; and (4) extraction of oil components.

Different forms of CO₂-EOR have been developed over the past years, including continuous CO₂ injection, continuous CO₂ injection followed by water, water-alternating gas (WAG) and WAG followed by gas or water (Jarrell, 2002). To improve sweep efficiency of CO₂ flooding, carbonated water injection could be a viable alternative (Christensen, 1961; Dong et al., 2011; Hickok et al., 2013; Riazi et al., 2009). Recently, Wilson, (2015) proposed CO₂ low salinity water alternating gas (CO₂-LSWAG) injection under miscible CO₂

displacement conditions which they claim could improve both the microscopic displacement and sweep efficiency.

The largest CO₂-EOR project is the Weyburn field in Canada which started in 2000 (Moberg, 2001). This project is expected to produce 130 million barrels of incremental oil and extend field life by about 25 years. Although the project was not intended for CO₂ storage, over 30 million tonnes of CO₂ is expected to be stored in the reservoir at the end of the project (Leung et al., 2014b).

IEA, (2015) suggested a modification of the conventional CO₂-EOR techniques to increase capacity for long term CO₂ storage. They proposed three models: “Conventional EOR+”, “Advanced EOR+” and “Maximum Storage EOR+”. They believe these models could exploit possibilities to profit from both improved oil recovery and maximum CO₂ storage. The cost of implementing these proposed CO₂-EOR models could be extremely high as they require additional reservoir characterization and risk assessment to evaluate storage capacity, improvement in reservoir monitoring and changes in plug and abandonment practices. However, to make CO₂ storage a business objective of EOR practices, the E&P industry will need a suitable carbon price or other regulatory benefits to offset the additional cost to conventional CO₂-EOR.

Depleted oil and gas reservoirs are also attractive candidates for CO₂ storages. In addition to the potential to reuse some of the production equipment, geological data collected over the production life of the reservoirs could lower exploration cost and reduce risk associated with CO₂ storage. Davison et al., (2001) asserted that depleted oil and gas reservoirs could hold about 45% of the projected CO₂ emissions by 2050.

1.1.3 CO₂ Enhanced Coal Bed Methane Production

CO₂ enhanced coalbed methane recovery (CO₂-ECBM) has the potential to store large volumes of CO₂ in deep unmineable coal seams while improving the efficiency of coal bed methane recovery (Shi and Durucan, 2005). The injected CO₂ displaces methane and remain sequestered in the coal seams as CO₂ is preferentially adsorbed onto coal seams, thus releasing the coal bed methane which can then be produced as free gas (Reeves, 2003). The sale of produced methane could help to offset the cost of the recovery process.

Reeves, (2001) reported about 75% increase in methane production from coal beds through CO₂ injection in a pilot project in San Juan, New Mexico. Based on the simple assumption that, for every CH₄ molecule, two molecules of CO₂ can be stored, IEA-GHG, (1998) estimated that about 220 GT of CO₂ could be stored in deep unminable coal formations worldwide.

1.2 Prerequisites for CCUS

A viable candidate for CCUS must have a threshold well injectivity to inject the desired quantity of CO₂ at acceptable rates through a minimum number of wells, adequate storage capacity to hold large volumes of CO₂ and robust containment to permanently isolate the sequestered gas from the environment (IEA, 2013). Storage capacity and well injectivity are the main factors required to define the storage potential of a geological CCUS candidate (Cinar et al., 2007; Yang et al., 2010).

1.2.1 Storage Potential

To store large volumes of CO₂, implementation of CCUS technology require accurate estimation of available CO₂ storage capacity (Bachu et al., 2007; Bradshaw et al., 2007). Bachu, (2015) and Miri, (2015) have used the term “CO₂ storage reserve” to express the amount of CO₂ that can be commercially sequestered in a reservoir within a specific period, using available technology, under current economic conditions, operating methods and governmental regulations. The USDOE, (2007) developed a simple expression to quantify the storage capacity of deep saline formations:

$$M_{CO_2} = V_A \phi_T \rho_{CO_2} E_s \quad (1.1)$$

In Eq. (1.1), M_{CO_2} is the mass of CO₂ that can be stored, V_A is the bulk volume of the aquifer, ϕ_T is the effective porosity of the aquifer, ρ_{CO_2} is the density of CO₂ at reservoir conditions and E_s is the storage efficiency.

The storage efficiency expresses the degree of filling the reservoir (Miri, 2015), also defined as the ratio of the volume occupied by CO₂ to the total accessible pore volume of the reservoir (Bachu, 2015b):

$$E_s = \frac{V_{CO_2}}{V_{pore}} \quad (1.2)$$

In Eq. (1.2), V_{CO_2} is the volume of injected CO₂ and V_{pore} is the accessible reservoir pore volume available for CO₂ storage. Eq. (1.1) and (1.2) can be combined to estimate the volumetric CO₂ storage capacity of a given deep saline reservoir.

CO₂ storage efficiency in deep saline formations depends on the reservoir rock properties (porosity, permeability, net to gross, thickness and area), the efficiency of water displacement by injected CO₂ and the degree of conformance of the aquifer (Miri, 2015).

Bachu et al., (2004) proposed a model to estimate the theoretical CO₂ storage capacity of depleted oil and gas reservoirs, based on the assumption that the entire pore space originally occupied by hydrocarbons can be filled by CO₂ and that CO₂ can be injected until the reservoir pressure reaches the original pressure of the virgin reservoir. These assumptions can be valid if the reservoir is not in contact with an aquifer or already flooded during secondary and tertiary recovery. Under such ideal conditions, CO₂ storage capacity can be estimated from:

$$M_{CO_2} = \rho_{CO_2} [RF \cdot V_{HC} - V_{iw} + V_{pw}] \quad (1.3)$$

In Eq. (1.3), ρ_{CO_2} is density of CO₂ under reservoir conditions, RF is the recovery factor, V_{HC} is the hydrocarbon pore volume, V_{iw} is the volume of the reservoir invaded by water and V_{pw} is the reservoir volume of produced water.

For practical purposes, an effective storage capacity could be defined to incorporate other important parameters such as displacement efficiency, gravity effects, residual oil and water saturation, reservoir heterogeneity, rock-fluid interactions and formation damage.

1.2.2 Well Injectivity

The injectivity of a reservoir measures the amount of CO₂ an injection well can receive without fracturing the formation (Miri, 2015). Well injectivity can be expressed with an injectivity index, I , often defined as the ratio of volumetric injection flow rate to the pressure drop (Dake, 1983; Schembre-McCabe et al., 2007). For a homogeneous and isotropic reservoir, the steady-state CO₂ well injectivity index can be expressed as:

$$I = \frac{q}{\Delta p} = \frac{\rho_{CO_2, res}}{\rho_{CO_2, sc}} \frac{2\pi kh}{\left[\ln \left(\frac{r_e}{r_w} \right) + s \right] \mu_{CO_2}} \quad (1.4)$$

In Eq. (1.4), q is the volumetric injection flow rate, Δp is the pressure drop, $\rho_{CO_2, res}$ is the density of CO₂ under reservoir conditions, $\rho_{CO_2, sc}$ is the density of CO₂ under standard conditions, kh is the permeability-thickness product, r_e is the radius of the reservoir boundary, r_w is the well radius, s is the skin factor and μ_{CO_2} is the viscosity of CO₂ under reservoir conditions.

Well injectivity determines the number of wells required to inject a specific quantity of CO₂ into the reservoir. This makes injectivity an important factor for both technical and economic evaluation of CO₂ storage projects (Birkholzer et al., 2015; Schembre-McCabe et al., 2007).

1.2.3 Containment Efficiency

The ultimate objective of CCUS project is to permanently isolate the sequestered CO₂ from the environment. The injected CO₂ may be trapped in the subsurface in folded or fractured rocks which are often sealed by an impermeable caprock (structural trapping), immobilized by capillary forces (residual trapping), dissolved in the resident formation brine through physical and chemical interactions (solubility trapping) or react with rock and fluid minerals to form more stable secondary components (mineral trapping)(Miri, 2015). Containment efficiency characterizes the assurance of containment of the injected CO₂.

Since formation water is denser than supercritical CO₂, the CO₂ plume tends to rise to the top of the reservoir, where it accumulates beneath the caprock. The containment efficiency of a geological trap is therefore strongly dependent on the seal potential or the ability of the caprock to confine the injected gas and prevent leakage into overlying formations and eventually back into the atmosphere (Kaldi et al., 2013). The caprock must have the lateral extent and geomechanical strength to retain the full CO₂ column height.

The integrity of the caprock could be compromised by mechanical deformation induced by pressure from CO₂ injection or through geochemical CO₂-rock-brine interactions which may dissolve or precipitate minerals to increase the permeability of the caprock (Daniel and Kaldi, 2009). Wells have also been identified as probable leakage pathways. Therefore, robust wellbore integrity is important to prevent leakage through wells.

1.3 CO₂ Well Injectivity Impairment Mechanisms

CO₂ injectivity impairment is a major constraint on the storage capacity of reservoirs (Miri and Hellevang, 2016; Peysson et al., 2014; Pruess, 2009). Under typical storage conditions, several factors could influence CO₂ injectivity because of the complex interplay of chemical and physical phenomena in the reservoir (Cinar et al., 2009, 2007; Sundal et al., 2013). Lombard et al., (2010) identified three groups of parameters responsible for CO₂ injectivity impairment (Figure 1.1). We discuss these parameters in the rest of the section.

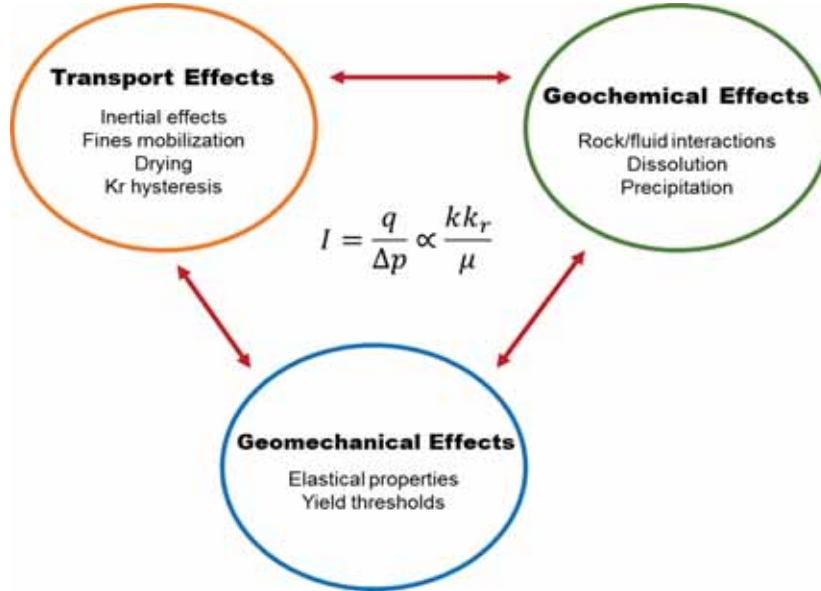
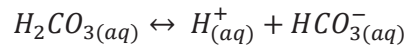
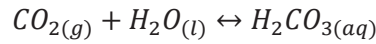


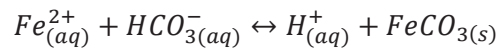
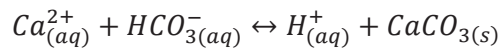
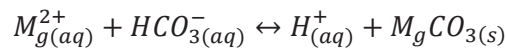
Figure 1.1. Factors affecting CO₂ injectivity (after Lombard et al., 2010)

1.3.1 Geochemical Effects

Mineral dissolution and salt precipitation are the two main geochemical CO₂ injectivity impairment mechanisms (Lombard et al., 2010). Under storage conditions, CO₂ could dissolve in the pore fluid to form carbonic acid and then bicarbonates according to the following equations:



The bicarbonates could react with cations in the rock and formation water to form stable carbonates:



These carbonates in solution ($MgCO_{3(s)}$, $CaCO_{3(s)}$, $FeCO_{3(s)}$, etc.) could form other secondary minerals, aggregate into tiny particles in the bulk liquid or form a scale on the pore walls (Patton et al., 1981; Sayegh et al., 1990; Tobergte and Curtis, 2013). CO₂-brine-rock batch reaction under typical storage conditions have shown various amounts of dissolved minerals in solution (Dawson et al., 2015; Ilgen and Cygan, 2016; Kaszuba et al., 2005; Tobergte and Curtis, 2013). Under static conditions, mineral dissolution could increase rock permeability temporally as new pore spaces are etched and old pore channels could widen (Lombard et al., 2010). However, mineral precipitates could aggregate into fine particles in the pore fluid which could form a scale on the pore walls and reduce the flow area.

Salt precipitation is an existing injectivity challenge in natural gas production. Kleinitz et al., (2003) reported field experience of severe halite-scaling in the injection region during natural gas production. The wells were shut down as complete plugging of the flow path by precipitated salts reduced the production rate to the barest minimum. Similar field experiences have been reported during injection, storage and production of gas (Golghanddashti et al., 2013; Jasinski et al., 1997; M.C. Place Jr., 1984). In the context of field CO₂ injection, Baumann et al., (2014) and Grude et al., (2014) reported evidence of salt precipitation effects in the Ketzin pilot reservoir and the Snøhvit field, respectively.

Permeability impairment between 13 % and 83% and porosity reduction between 2 % and 15% have been reported from laboratory core-flood experiments (André et al., 2014; Bacci et al., 2011; Kim et al., 2013; Muller et al., 2009; Sokama-Neuyam and Ursin, 2016; Tang et al., 2015). These experimental findings have been found to be consistent with theoretical and numerical simulations (Giorgis et al., 2007; Hurter et al., 2007; Pruess, 2009; Zeidouni et al., 2009). While numerical experiments by Roels et al., (2016) suggested that local salt accumulates far from the wellbore, several research works (Bacci et al., 2011; Kleinitz et al., 2001; Peysson et al., 2014; Pruess and Muller, 2009) shows that precipitated salt accumulates near the wellbore, where brine vaporization rates are the highest.

Pruess and Muller, (2009) suggested that pre-flush of the injection region with freshwater could reduce salt precipitation. However, Kleinitz et al., (2003) have

shown that freshwater injection could not mitigate salt precipitation if the flow area is completely plugged by solid salt. Fresh water also has a high tendency to react with rock minerals, leading to other injectivity impairment challenges such as clay swelling.

1.3.2 Transport Effects

The mechanisms of fines migration and the impact of particle transport on the petrophysical properties of reservoir rocks have been previously researched. Khilar and Fogler, (1998) presented the mechanisms of colloidal and hydrodynamic induced release of fine particles in porous media. Muecke, (1979) investigated parameters controlling the movement of fines particles within the pore spaces. They identified the pH and salinity of formation brine, flow rate and temperature as some of the underlying parameters. Khilar and Fogler, (1983) asserted the existence of a critical salt concentration below which the pore fluid could weaken the Van der Waal's forces holding fine particles to the pore wall. Gruesbeck and Collins, (1982) investigated the effect of hydrodynamic forces on the release and transport of fines. They identified a minimum interstitial velocity for fines entrainment. The effect of two-phase flow and rock wettability on fines entrainment has been experimentally investigated by Sarkar and Sharma, (1990). They found that, the wettability of the core could affect the extent and rate of permeability impairment induced by migratory fines. Analytical models have been developed by Sharma and Yortsos, (1987) to investigate the mechanisms of size exclusion and quantify the effect of particle entrapment on rock permeability. A thorough analysis of formation damage induced by migratory fines can be found in Civan, (2007).

Geochemical CO₂-brine-rock reactions could generate secondary minerals into the pore fluid (Hangx, 2005; Ilgen and Cygan, 2016; Wilkinson et al., 2009). In addition, CO₂-brine interactions could alter the pH of formation fluid which could induce the release of formation fines from the pore walls (Gruesbeck and Collins, 1982; Khilar and Fogler, 2010). While flowing with the injected fluid, the mineral particles could clog pore channels and impair injectivity. Whether entrapment or piping of fines will dominate the flow depends on characteristics of the generated fine particles, the porous medium and the permeating fluid in which the particles are suspended (Aji, 2014; Sen and Khilar, 2006; Vaidya and

Fogler, 1990). Pore structure, the size and concentration of the minerals and the hydrodynamic and colloidal conditions of the suspending medium could also affect their impact on CO₂ injectivity. Under radial flow conditions, plugging effects could be limited to the near well region where fluxes are highest.

The general mechanisms of fines mobilization are well understood and documented. However, supercritical CO₂ has unique combination of gas-like viscosity and liquid-like density (Nalawade et al., 2006). In addition, very high CO₂ injection rates are required to meet global emission reduction targets. For example, CO₂ injection rate in the Weyburn project is between 74 – 588 tonnes per day per well (Verdon, 2012). The drying effect of supercritical CO₂ also makes salt precipitation and fines mobilization inseparable under typical storage conditions. These special properties of supercritical CO₂, coupled with the high injection rates required to meet global reduction targets need adaptation and extension of previous findings to understand the mechanisms and impact of fines migration within the context of CO₂ injection.

Introduction

2 Objectives

The present work is part of a grand project, born out of a collaborative effort between three institutions (IPT/UiS, AGH University of Science and Technology, Krakow and PGNiG Upstream International AS, Norway) to investigate challenges related to CO₂ injection and storage. The research team at IPT/UiS was tasked to develop a suitable laboratory model to investigate CO₂ injectivity impairment mechanisms applicable to a vertical well centered in a cylindrical reservoir. The initial idea was to develop a “pancake” reservoir framework, where gas could be injected into the narrow end of the model and allowed to expand in a parabolic flow into the reservoir. However, this idea was found to be mechanically unstable. A cylindrical cone model was then to be designed to retain the parabolic flow behavior in the “pancake” model. It was later found that the cylindrical cone model was not technically and financially feasible at the target operating conditions. Therefore, linear laboratory core-flood experiments and theoretical modelling were used to investigate the governing physical parameters of CO₂ injectivity impairment.

Two main CO₂ injectivity impairment mechanisms were investigated: geochemical effects (salt precipitation and mineral dissolution) and transport effects (fines mobilization). The objective of the study can be split into the following themes:

1. To investigate the mechanisms and impact of mineral dissolution and fines mobilization on CO₂ injectivity.
2. To investigate the relative contribution of fines mobilization and salt precipitation to CO₂ injectivity impairment.
3. To investigate the coupled effect of fines mobilization and salt precipitation on CO₂ injectivity.

The studies were based mostly on laboratory sandstone core-flood experiments and theoretical modelling. We discuss the above themes based on both published and unpublished data.

Objectives

3 Materials and Methods

3.1 Materials

3.1.1 Core Samples

Cylindrical outcrop sandstone core plugs were used in the experiments. General characteristics of the rock samples are shown in Table 3.1. Outcrop sandstone rocks were used because they are clean and some of their properties are predictable. Each type of core was drilled from the same block in the same direction. With exception of Bandera core plugs, the core samples can be considered homogenous in the linear direction with respect to permeability. Each core was 20 cm long with diameter of 3.81 cm.

Table 3.1 Characteristics and petrophysical properties of outcrop sandstone cores used in the experiments.

Rock Sample	Permeability (mD)	Porosity (%)
Berea	90 – 105	17 – 19
Bentheimer	1600 – 2400	22 – 24
Bandera	30 – 40	19 – 21
Kirby	15 – 20	16 – 18

The Bentheimer rock is composed mainly of quartz (91.70 wt.%), feldspars (4.86 wt.%), clay minerals (2.68 wt.%), pyrite and iron oxides (0.17 wt.%) (Peksa et al., 2015a). According to measurements conducted by Peksa et al., (2015), the Bentheimer rock has average pore body diameter of 0.014mm and pore throat diameter of 0.012 mm.

Berea sandstone core samples were used as the main reservoir rock in most of the experiments, partly because of their suitable range of porosity and permeability and because their properties are well known. The Kipton Berea sandstone rock used in this study is composed mainly of Silica (86.47 wt.%), Alumina (7.31 wt.%) and Oxides (Iron Oxide, Titanium Oxide, Calcium Oxide and Magnesium oxide)(Mohammed et al., 2014). Dullien and Dhawan, (1974)

reported pore throat sizes between 0.5 and 5.0 μm and pore body sizes ranging from 5.0 to 50 μm for Berea sandstone.

3.1.2 Brine

Synthetic formation water (FW), representative of North Sea reservoir pore fluid, with brine salinity of about 105.5 g/L (NaCl, 77.4 g/L; $\text{CaCl}_2 \cdot 2\text{H}_2\text{O}$, 21.75 g/L; $\text{MgCl}_2 \cdot 6\text{H}_2\text{O}$, 3.56g/L; $\text{SrCl}_2 \cdot 6\text{H}_2\text{O}$, 2.25 g/L; Na_2SO_4 , 0.13 g/L; KCl 0.42 g/L) (Fjelde et al., 2014) was used as the main saturating wetting fluid. Dilute solutions of FW were also used to investigate the effect of reduced brine salinity.

NaCl brine was also used in some of the experimental work. Jeddizahed and Rostami, (2016) asserted that injectivity impairment induced by salt precipitation is mainly dependent on the total dissolved solid in the brine. Since FW is predominantly composed of NaCl, the NaCl brine with same ionic strength as FW would induce almost the same salt precipitation effect as FW. On the other hand, the use of NaCl brine reduces challenges associated with modelling the effect of several ionic components and chemical interactions in FW. NaCl brine with salinity of about 150 g/L and 75 g/L were used to investigate the effect of high brine salinity and low salinity respectively.

3.1.3 Gas

Liquid CO_2 was used to measure injectivity impairments induced by salt precipitates and entrapped fines because these pore-plugging materials are insoluble in CO_2 . Liquid CO_2 was obtained by injecting the gas at 80 bar and 26 °C. Supercritical CO_2 – the main displacement and drying fluid, was injected at 80 bar and 50 °C.

3.1.4 Carbonated Water

Carbonated water was used to generate fine particles in the rock. Figure 3.1 shows schematics of the setup used to prepare carbonated water. CO_2 is soluble in brine, with solubility strongly dependent on temperature, pressure and brine salinity. A tight piston cell was filled with about 1000 mL of FW. Liquid CO_2 was then injected into the brine at a constant pressure of 80 bar and 20 °C for

about 48 hours. The injection pressure was kept at 80 bar until the pump delivered insignificant volume of CO₂ (<0.001 mL/min) into the brine, signifying complete saturation. Experimental data reported by Portier and Rochelle, (2005) suggests CO₂ solubility in Utsira formation pore water which has similar composition to the FW used in this experiment, under the current working conditions is in the range of 1.26 – 1.36 mol Kg⁻¹ H₂O. The connected pressure gauge was used to monitor the fluid pressure in the piston cell.

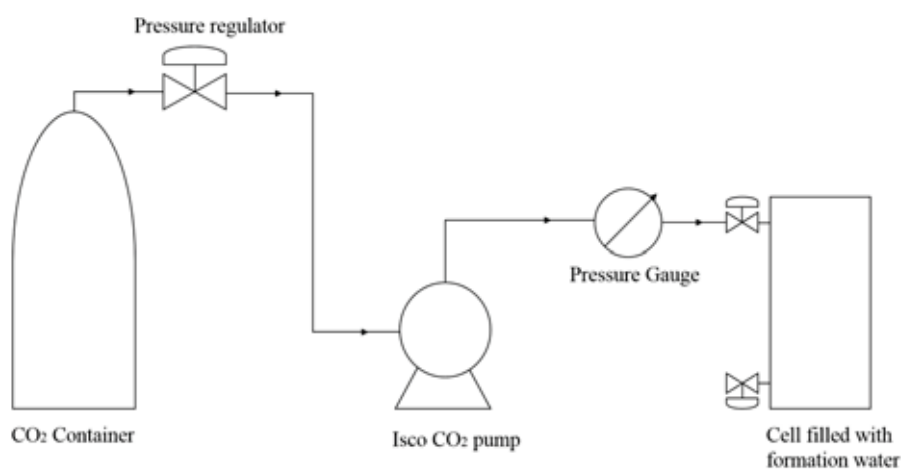


Figure 3.1 Schematics of the experimental setup used to prepare carbonated water.

3.1.5 Colloids

Mono-disperse colloid solutions were used to investigate the effect of fines migration on CO₂ injectivity. The mono-disperse colloids were prepared from concentrated fumed alumina latex particles. Alumina was selected for this study because of its high resistance to wear and its stability in CO₂. The particles are oil wet and this also minimizes attachment to the pore walls.

The alumina particles were stabilized in low salinity brine at near-neutral pH conditions to prevent particle aggregation. A 5 g/L (0.086 mol/L) NaCl brine was used to dilute the concentrated colloid stock solution into mono-disperse colloidal solutions at specific particle concentrations. It has been found that below a critical salt concentration (CSC) of about 0.071 mol/L, NaCl brine could detach formation fine particles from the pore walls into the flowing

stream (Fogler, 1984). Brine concentration of 0.086 mol/L was selected to minimize this effect. Brine salinity in this region is also low enough to prevent salt precipitation which could introduce uncertainty into estimation of fines migration effects. Typical formation fines have average particle diameter between 0.01 μm and 1 μm (Khilar and Fogler, 2010). Two particle sizes were selected for the experiments: I and II with average particle diameter of 0.08 μm and 0.14 μm respectively. Characteristics of the stock solution used to prepare the mono-disperse colloid solutions are presented in Table 3.2.

Table 3.2 Properties of fumed alumina stock solution used to prepare colloid solutions.

Properties	I	II
Particle size (μm)	0.08	0.14
Al ₂ O ₃ content (%)	39 – 41	29 – 31
Viscosity (mPa/s)	< 90	<2000
pH	6.0 – 9.0	3.0 – 5.0
Density (g/cc)	1.39	1.26

3.2 Experimental Setup

The schematics of core flooding apparatus used in the tests are shown in Figure 3.2. Prior to the test, the core was mounted in the horizontal hassler core-holder. To measure the effect of mineral impairment at different sections of the core, the hassler core-holder was replaced with a pressure-tapped core-holder. The Quizix pump delivers fluid through the connected piston cell into the core inlet. Either brine, colloid suspension or carbonated water was injected depending on the nature of the tests. The ISCO CO₂ pump receives liquid CO₂ from the gas container through a pressure regulator. Depending on the injection conditions, either liquid or supercritical CO₂ are injected. The injected fluid passes a piston cell, positioned in the oven to hold the fluid and secure a preset temperature in the oven. A differential pressure gauge and a pressure transducer are used to monitor the pressure drop across the core and record the absolute pore pressure respectively. A backpressure of 80 bar was set at the outlet during CO₂ injection and the effluent fluid was safely collected in a piston cell for analysis and safe disposal.

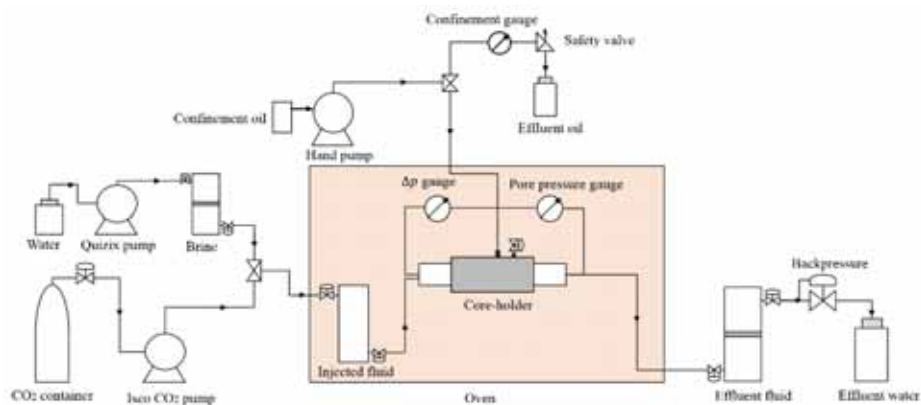


Figure 3.2 Schematics of the core-flooding apparatus used in the tests – the CO₂ flow rig.

3.3 Methods

3.3.1 Procedure

The clean core sample was first dried at 65 °C for about 24 hours. The core was then wrapped in shrinking Teflon sleeve to prevent leakage before it was inserted into a rubber sleeve and horizontally mounted in the core holder. A confining pressure of about 150 bar was applied in the annular space between the core and the core holder during supercritical CO₂ injection. The confining pressure was reduced to 20 bar during injection of FW. The experimental procedure consists of the following general steps:

1. Initial injectivity of the clean dry core sample is measured.
2. The core is saturated with the aqueous solution.
3. The saturated core sample is flooded with supercritical CO₂ to displace and vaporize the aqueous phase to dryness.
4. The core is inspected for filter cake at the injection inlet and the extent of dryness is estimated.
5. Final injectivity of the impaired core is measured.

In Step 2, the core was first vacuum-saturated with either FW, NaCl brine or colloid solution and mounted into the core-holder followed by injection of the saturating fluid at 1 mL/min until a stable pressure drop is obtained to ensure complete saturation. In Step 3, about 100 - 300 pore volumes (PV) of

supercritical CO₂ was injected into the saturated core at constant injection rate to displace and vaporize the aqueous phase and possibly precipitate minerals into the pores. Pressure drop profiles were monitored during supercritical CO₂ injection. In Step 1 and Step 5, liquid CO₂ or FW was injected at constant rate to measure permeability before and after vaporization and mineral impairment. Each test either followed all or some of the steps in slightly modified form.

3.3.2 Calibrations

Fluid injectivity, I is defined as the ratio of volumetric injection flow rate, q to the pressure drop, Δp . Assuming the core has constant absolute permeability k_i and k_f before and after it is exposed to mineral impairment respectively and that the viscosity of the fluid used in the measurement (liquid CO₂) is constant, the injectivity before and after salt deposition can be expressed with Darcy's law as:

$$I_i = \frac{q_i}{\Delta p_i} = k_i \cdot C \quad (3.1)$$

$$I_f = \frac{q_f}{\Delta p_f} = k_f \cdot C \quad (3.2)$$

In Eq. (3.1) and (3.2), C is a constant defined as $C = \frac{A}{\mu L}$, for constant cross-sectional area A and length L . If liquid CO₂ is injected at a constant rate during injectivity measurements ($q_i = q_f$), we define a Relative Injectivity Change (RIC) index β as:

$$\beta = \left(\frac{I_i - I_f}{I_i} \right) = 1 - \left(\frac{I_f}{I_i} \right) \quad (3.3)$$

Substituting Eq. (3.1) and (3.2) into (3.3) yields:

$$\beta = 1 - \left(\frac{\Delta p_i}{\Delta p_f} \right) = 1 - \left(\frac{k_f}{k_i} \right) \quad (3.4)$$

Plugging of the core by precipitated minerals may reduce the flow area and increase pressure drop across the core, Δp . Thus, in Eq.(3.4), $\Delta p_f > \Delta p_i$ and $k_i > k_f$ after injectivity impairment. Consequently, a positive β indicates injectivity impairment. In most cases, β was expressed as a percentage. Although, β is rather linear injectivity measurement technique, it provides an indirect method for estimating injectivity impairment independent of the chemical properties of the pore-plugging material

3.3.3 Uncertainty in Experimental Data

Particle transport in natural porous media is a highly uncertain process. The particles are displaced in random flow path into highly tortuous pore network distribution. Therefore, the repeatability of particle flow experiments in even homogeneous natural rocks is expected to be low. However, attempt was made to quantify and minimize the uncertainty in the measurements.

The measured injectivity data I , was reported as:

$$I_{measured} = I_{avg} \pm \Delta I_{avg} \quad (3.5)$$

In Eq. (3.5), I_{avg} is calculated from the mean value of the stabilized liquid CO₂ or brine Δp across the core before and after supercritical CO₂ injection, mineral precipitation and particle entrapment and ΔI_{avg} is the estimated uncertainty in I_{avg} . Initial and final pressure drop measurements are recorded when the liquid CO₂ or brine pressure drop across the core stabilizes. I_{avg} and ΔI_{avg} are calculated from:

$$I_{avg} = \frac{\sum I}{N} \quad (3.6)$$

$$\Delta I_{avg} = \frac{I_{max} - I_{min}}{\sqrt{N}} \quad (3.7)$$

In Eq. (3.6) and (3.7), N is the total number of recorded data points, I_{max} and I_{min} are the maximum and minimum recorded injectivity values respectively.

Materials and Methods

It was found that, the uncertainty in injectivity was dependent upon the differential gauge pressure, injection flow rate and the type of mineral plugging. A very sensitive differential pressure gauge which measures to an accuracy of about 0.009% was used. We found that, low injection flow rate minimized the uncertainty. Similarly, colloidal entrapment induced higher uncertainty compared to salt precipitation. Injection flow rate of about 5 mL/min was found to be the optimal liquid CO₂ injection rate that minimized the uncertainty in the fines migration experiments. The maximum calculated uncertainty was then applied to the data.

4 Results

4.1 Salt precipitation

We present results from core-flood experiments and theoretical studies conducted to investigate physical mechanisms of salt precipitation and the impact of deposited salts on CO₂ injectivity. The mechanisms of salt precipitation are grouped into two successive processes: salt cake development at the injection inlet and drying effects. Salt cake forms on the surface of the core inlet during early stages of brine vaporization prior to drying. As drying commences, salt precipitates into pore spaces in the dry-out zone. Each stage is investigated and important parameters are identified and studied. We then propose a mitigation technique which involve alternate injection of CO₂ and diluent low salinity brine.

4.1.1 Salt cake development

To investigate the development of salt cake on the surface of the injection inlet, a clean Bentheimer core was vacuum-saturated with 120 g/L NaCl brine and flooded with about 100 PV of dry supercritical CO₂ at a rate of 1 mL/min. Pressure drop profiles were monitored during the CO₂ flooding. The core was inspected when abnormality in pressure drop was detected. Figure 4.1 shows photographs of the core taken during inspection.

In Figure 4.1 (A), we observe that no salt was formed at the core outlet. Figure 4.1 (B) shows massive salt cake deposition at the core inlet. Figure 4.1 (C) shows that the entire length of the core was still wet. At the onset of injection, when the core is fully saturated with brine, the injected supercritical CO₂ leaves brine behind the inlet due to poor sweep. Salinity of the brine increases as water is removed through vaporization. If the initial brine salinity is high enough, the brine left behind could reach supersaturation and precipitate salt onto the inlet before it is swept into the core. The precipitated salt creates a saturation gradient that draws more brine into the inlet region through capillary backflow to precipitate more salts at the inlet. Thus, salt cake formation will thrive on: (1) High brine salinity and (2) Poor brine displacement at the injection inlet.

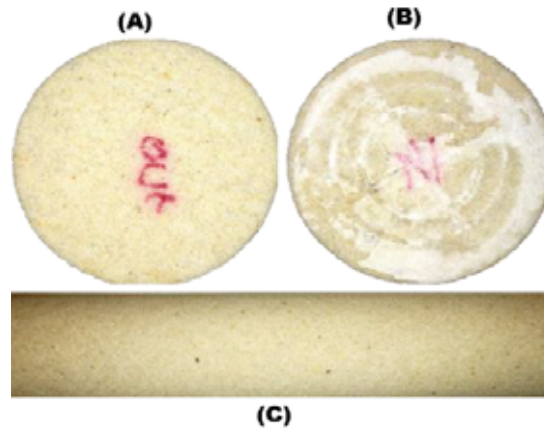


Figure 4.1 Photographs of Bentheimer core after CO₂ was injected at 1 mL/min into the core initially saturated with 120 g/L NaCl brine. (A) No salt cake observed at the core outlet. (B) Massive salt cake found at the injection inlet. (C) The entire core remains wet.

To investigate the impact of sweep on salt cake development, supercritical CO₂ injection flow rate was increased from 1 mL/min to 5 mL/min. The amount of deposited salts at the injection inlet decreased when the displacing flow rate was increased from 1 mL/min to 5 mL/min (Figure 4.2). Under linear flow conditions, the CO₂ – brine sweep improves with increasing injection flow rate. As sweep is improved, less brine is left behind the injection inlet for salt precipitation.

The initial brine salinity was then reduced from 120 g/L to 75 g/L, keeping the CO₂ injection flow rate constant at 5 mL/min. The amount of salt cake precipitated at the injection inlet further decreased significantly when brine salinity was decreased (Figure 4.3). At constant vaporization rate, lowering the saturating brine salinity delays supersaturation, allowing a significant portion of the brine left behind at the injection inlet to be swept into the core. This probably reduced the amount of salt cake formed.

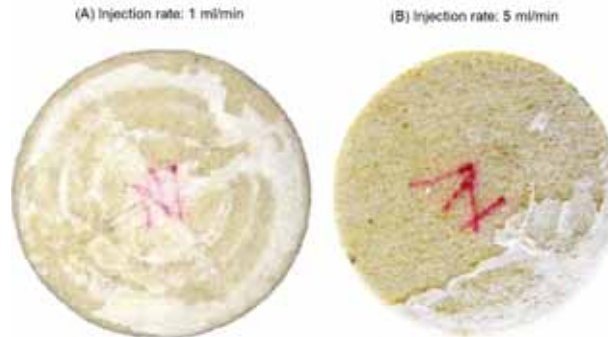


Figure 4.2 Photographs showing salt cake development at the core inlet when supercritical CO₂ injection rate was increased from (A) 1 mL/min to (B) 5 mL/min. Increase in CO₂ injection rate decreased the amount of deposited salt.

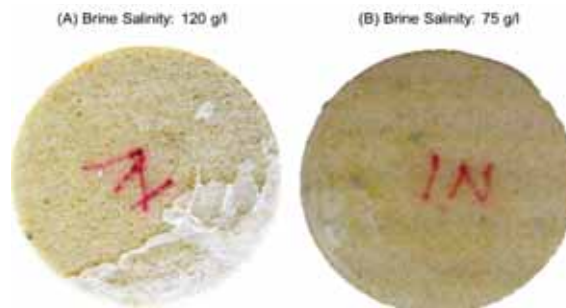


Figure 4.3 Photographs showing salt cake development at the core inlet when brine salinity was decreased from (A) 120 g/L to (B) 75 g/L. Decrease in brine salinity further decreased the amount of deposited salts.

Therefore, salt cake could develop at the injection inlet during CO₂ injection into saline porous media if the saturating brine salinity is above a certain threshold and the sweep efficiency is low. Under these conditions, brine left behind the inlet could reach supersaturation before it is swept into the core. Details of the experimental work have been published in Paper I.

4.1.2 Drying effects

Mechanisms of brine vaporization and salt precipitation at dry-out are presented. The effect of salt precipitation on CO₂ injectivity are quantified and effect of some important parameters are investigated. Underlying mechanisms

of the development and extension of the dry-out zone and other post-precipitation effects are also investigated.

4.1.2.1 The impact of salt precipitation on CO₂ injectivity

A clean Berea core with known permeability was initially saturated with FW and flooded with about 300 PV of supercritical CO₂ at a rate of 1 mL/min until the core was completely dried. The permeability of the core after drying was measured and β was calculated. The experiment was then repeated for CO₂ injection flow rate of 5 mL/min and 10 mL/min, keeping all other parameters constant, to study the effect of injection flow rate. Details of the experimental work can be found in Paper II. Figure 4.4 shows results of injectivity impairment induced by drying and salt precipitation at varying CO₂ injection flow rates.

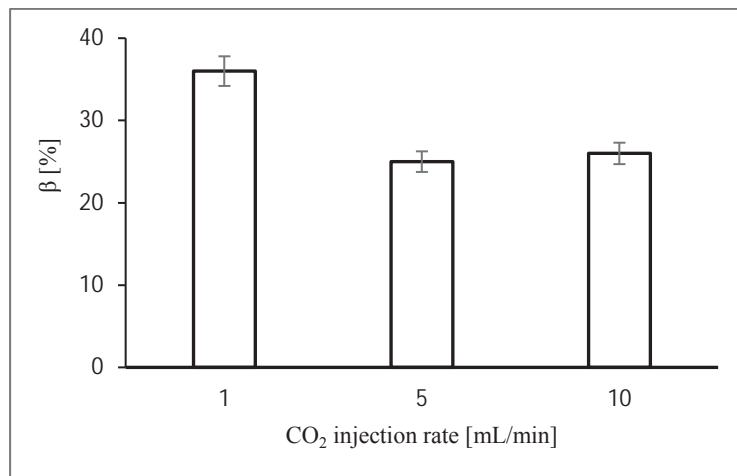


Figure 4.4 Effect of drying and salt precipitation on CO₂ injectivity. Injectivity impairment, β increased with decreasing CO₂ injection rate.

CO₂ injectivity was impaired by about 36 % for drying rate of 1 mL/min (Figure 4.4). Injectivity impairment decreased from 36% to about 25% when drying rate was increased to 5 mL/min and remained practically unchanged when the drying rate was further increased to 10 mL/min. Several researchers (Bacci et al., 2013; Muller et al., 2009; Peysson, 2012; Tang et al., 2015) have earlier reported CO₂ injectivity impairment within a range (13% - 83%) that agree

favorably with the current figures. During drying and brine vaporization, when the concentration of brine exceed supersaturation, salt precipitates into the pores in the dry-out region as observed by Zuluaga et al., (2001). The deposited salts reduce the CO₂ flow area, impairing permeability and injectivity.

As drying progresses, a saturation gradient is established which draws more brine into the dry-out region through capillary backflow. Capillary backflow of brine leads to more salt deposition in the dry-out region. The capillary backflow of brine increases with decreasing drying rate because at high CO₂ injection flow rates, viscous forces overcome capillary forces. Therefore, less amount of salts are precipitated in the dry-out region at high injection flow rates, inducing low injectivity impairment as observed in Figure 4.4.

Injectivity impairment remained practically unchanged when drying rate was further increased from 5 mL/min to 10 mL/min because at these injection flow rates, the resident brine is quickly swept out of the core, leaving out only immobile brine for salt precipitation. Thus, for core flow, at high injection rates, salt precipitation depends mostly on the immobile brine saturation rather than the drying rate.

4.1.2.2 Development of the dry-out zone

During injection of dry supercritical CO₂ into brine-saturated sandstone cores, the dry-out region close to the injection inlet, extends into the core as more CO₂ is injected. The effect of extension of the dry-out zone on CO₂ injectivity could be very vital for understanding the underlying mechanisms of brine vaporization and salt precipitation. A tractable bundle-of-tubes model was developed to track the development of the dry-out zone and estimate the impact of extension of the dry-out region on CO₂ injectivity. Core-flood experiments were conducted to validate the model. Details of the experimental and modelling work can be found in Paper III.

4.1.2.2.1 The bundle-of-tubes model

The cylindrical core, radius R and length L was reconstructed into a bundle of parallel, non-interacting cylindrical capillary tubes with varying radii ($r_1, r_2, r_3, \dots, r_N$) (Figure 4.5). The model is sectioned into a dry-out zone (L_1)

where salt has been precipitated into the core and the uncontaminated region (L_2), representing the part of the core yet to be dried by supercritical CO_2 . In the dry-out zone, we assume the precipitated salt accumulates on the walls of the pores (dark shades). We further assume the accumulated salt in the dry-out region would reduce the cross-flow area by say Δr_1 for r_1 ; Δr_2 for r_2 ... for total of N capillary tubes in the core.

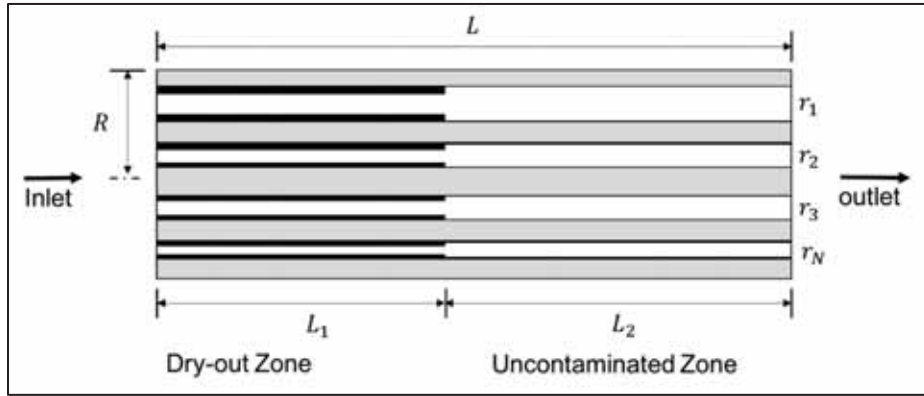


Figure 4.5 Schematics of the bundle-of-tubes model. The core of length L and radius R was reconstructed into a bundle of parallel cylindrical capillary tubes with varying radii.

A dimensionless dry-out length, l_d , is defined as the ratio of the length of the dry-out zone to the total length of the core.

$$l_d = \frac{L_1}{L}, l_d \in [0,1] \quad (4.1)$$

The dry-out length, l_d , tracks the development of the dry-out zone during brine vaporization and salt precipitation.

From the Hagen–Poiseuille (H–P) equation, it can be shown that the injectivity impairment induced by precipitated salts, β for any dry-out length l_d is given by:

$$\beta = 1 - \frac{\sum_{i=1}^N \left[\frac{(r_i - \Delta r_i)^4}{l_d + (1 - l_d) \left(1 - \frac{\Delta r_i}{r_i}\right)^4} \right]}{\sum_{i=1}^N r_i^4} \quad (4.2)$$

Eq. (4.2) can be used to quantify injectivity impairment, β as a function of the dry-out length, l_d if the total number of tubes, N is known and the thickness of precipitated salt Δr_i in each tube, r_i is known.

The total number of capillary tubes depends on the porosity of the core, ϕ , average tube radius, \bar{r}_i , and the radius of the core, R given by:

$$N \approx \frac{3}{4} \phi \left(\frac{R}{\bar{r}_i} \right)^2 \quad (4.3)$$

The average pore size of the porous medium is used as \bar{r}_i . We calibrated our model to an average pore size of $6\mu\text{m}$ using lognormal distribution of tube radii. Radii greater than $20\mu\text{m}$ make up less than 5% of the total number of tubes. The minimum tube radius was set to $0.38\mu\text{m}$.

The average coordination number in sandstones is between 4 and 8 (Lin and Slattery, 1982; Yanuka et al., 1984). The pore size distribution used in the present study compares favorably with this range of coordination number. Under linear flow, the amount and distribution of precipitated salt depend on the linear interconnection of pores which controls capillary backflow of brine towards the injection inlet during brine vaporization. Thus, the bundle-of-tubes model can be used to adequately characterize the principal mechanisms of salt deposition and distribution, where the horizontal interconnection of pores are represented as capillary tubes.

By fitting experimental data, we derived a correlation for solid salt saturation as:

$$S_s = (0.85 + 0.1l_d) \frac{\rho_{aq} X_s}{\rho_s} \quad (4.4)$$

From mass balance, it can be shown that the thickness of solid salt in each capillary tube is given by:

$$\Delta r_i \approx \frac{2 S_s r_i}{3 l_d} \quad (4.5)$$

Eq. (4.5) shows that, the thickness of solid salt, Δr_i in each capillary tube, r_i depends on the total precipitated solid salt saturation, S_s and the distribution of salt which is determined by the dry-out length l_d .

4.1.2.2.2 *The model validated with experimental data*

A Berea sandstone core with known initial permeability was saturated with 75 g/L NaCl brine prior to the drying experiment. The core was then flooded with supercritical CO₂ at 5mL/min. After every 100 PV of CO₂ injection, the core was inspected and the advancing dry-out zone was measured to estimate l_d . CO₂ injectivity change as a function of the dry-out length l_d was measured and β computed. To investigate the effect of brine salinity, the experiment was repeated by doubling the brine salinity from 75 g/L (LS) to 150 g/L (HS). Figure 4.6 shows impact of the advancing dry-out zone, l_d on CO₂ injectivity impairment β .

Figure 4.6 also shows a favorable agreement between the simulation and the experimental data. CO₂ injectivity impairment peaked at the onset of drying. Injectivity impairment decreased to a minimum at l_d of about 0.45 and then rose slightly as the dry-out zone approached the core effluent end.

At the start-up of drying, two mechanisms could impair CO₂ injectivity; salt precipitation and relative permeability effects. Brine vaporization rate is at its highest close to the inlet region because of the high capillary driven back-fluxes. As more brine is vaporized, more salt is precipitated into the pores which in turn increase the resistance to flow in this region. Also, at the onset of drying, a larger portion of the core is wetted with brine which reduces the pore space available for CO₂ and thus decreases the relative permeability of CO₂. Thus,

around the injection vicinity, salt precipitation is high and relative permeability to CO₂ is expected to be low. Therefore, maximum CO₂ injectivity impairment is expected around the core inlet, at the startup of the drying process.

As the drying front advances into the core, brine vaporization and salt precipitation decreases as most of the brine are drawn into the inlet region by capillary backflow, leaving the remaining section of the core with less amount of brine available for salt precipitation. When the core is almost completely dried, brine vaporization and salt precipitation in around the effluent end of the core are almost negligible.

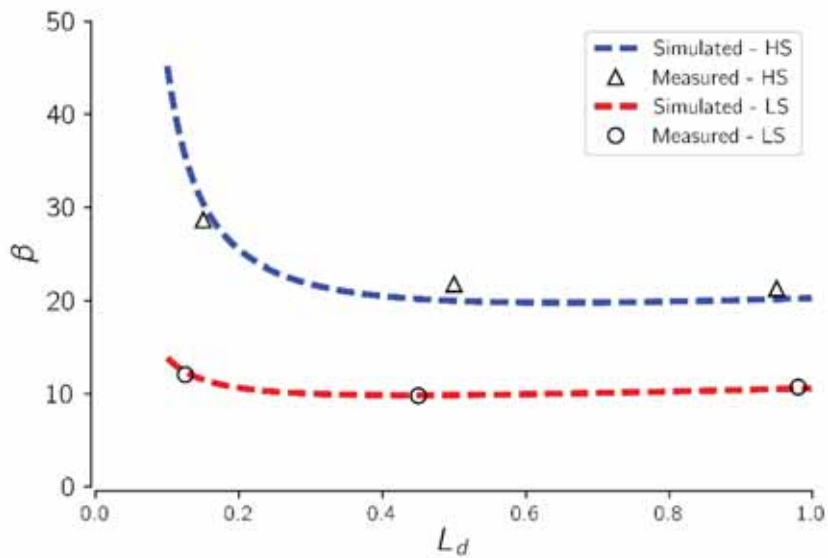


Figure 4.6 The impact of the dry-out length (L_d) on CO₂ injectivity impairment (β) induced by salt precipitation. Magnitude of injectivity impairment increased when brine salinity was doubled from 75 g/L to 150 g/L but successive changes in injectivity impairment was not influenced by change in brine salinity.

CO₂ injectivity impairment increased more than two-fold when brine salinity was doubled from 75 g/L to 150 g/L (Figure 4.6) since the solid salt saturation increases with initial brine salinity. However, successive change in CO₂ injectivity impairment as the drying end advances into the core, was not affected by changes in brine salinity. This suggests that the impact of the

advancing dry-out zone on CO₂ injectivity is independent of initial brine salinity. The two major mechanisms discussed here, rate of salt precipitation during the drying process and relative permeability effects are for the most part dependent on CO₂ injection rate. Increase in brine salinity increases the magnitude of salt precipitated but the rate of precipitation depends primarily on the brine vaporization rate. Also, the relative permeability effects depend on the amount of mobile brine present in the pores which in turn is tied to the sweep efficiency of the flood.

4.1.2.3 Effect of drag forces on precipitated salts

To investigate the effect of drag forces on evolution of CO₂ injectivity, a Berea core sample was initially vacuum saturated with FW and vaporized to complete dryness to precipitate salt into the pores. The liquid CO₂ permeability of the core and pressure drop across two sections of the core were measured with a pressure-tapped core holder. The core was then flooded with about 150 PV of supercritical CO₂ at a constant injection rate of 2.5 mL/min. During this period of CO₂ injection, drag forces will act on the precipitated salts. Permeability and pressure drop across the same sections of the core was measured after CO₂ flooding. The changes in permeability and pressure drop profiles were then analyzed. The experiment was repeated at injection rates of 5 mL/min and 10 mL/min to investigate the effect of injection flow rate. Details of the experimental work can be found in Paper IV. Figure 4.7 shows permeability change induced by the effect of drag forces on precipitated salts at varying injection rates.

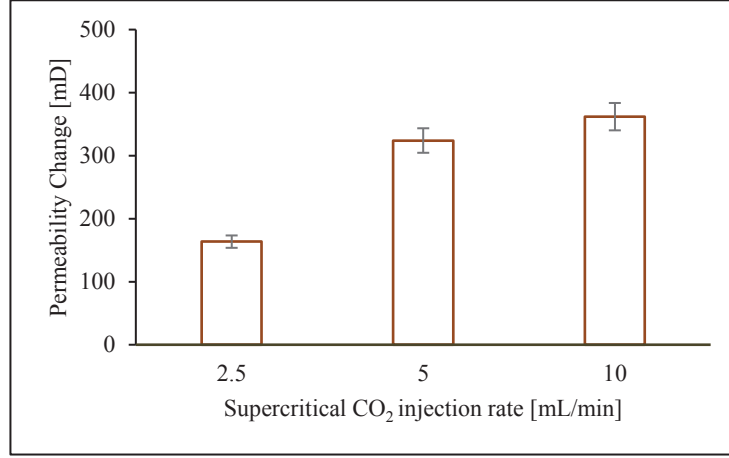


Figure 4.7 The impact of CO₂ injection flow rate on the effect of drag on permeability after salt precipitation. Permeability change is the difference between the core permeability after salt precipitation and before drag test and the permeability after drag test.

The force of drag, F_D experienced by an object is given by (Batchelor, 2000):

$$F_D = \frac{1}{2} \rho v^2 C_D A \quad (4.6)$$

In Eq. (4.6), ρ is the mass density of the fluid, v is the flow velocity relative to the object, C_D is the drag coefficient and A is the reference area.

From Eq. (4.6), the net drag force exerted by supercritical CO₂ on precipitated salts depends strongly on the volumetric injection flow rate (v), increasing with increase in flow rate. The precipitated salts are held to the pore walls mostly by gravitational and electrostatic forces offered by the complex pore structure and rock minerals. If drag forces overcome these attractive forces, the accumulated salts could be dislodged or redistributed in the pores, altering the permeability as a result. The magnitude of permeability change should therefore be proportional to the drag force which in tend depends on the injection flow rate. However, the effect of drag on permeability change is also limited by the amount of precipitated salts in the pores or the solid salt saturation. For a fixed solid salt saturation, there exists a maximum injection flow rate, beyond which no marked additional permeability change can be obtained.

To investigate the effect of initial core permeability, the experiment was repeated with a Kirby core sample. Berea and Kirby cores have similar range of porosity but different permeability. The core was initially saturated with FW and supercritical CO₂ injection flow rate was kept constant at 5 mL/min. The recorded permeability changes are shown in Figure 4.8.

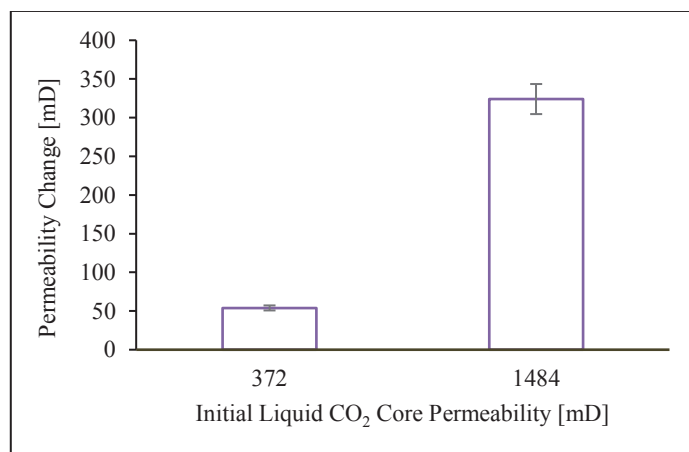


Figure 4.8 Effect of initial core permeability on permeability change induced by the effect of drag forces on precipitated salts. Berea core (1484 mD) and Kirby core (372 mD) were tested. Permeability change seems to increase as the initial permeability is increased.

From Figure 4.8, permeability change induced by drag forces increased with increasing initial core permeability. According to Eq. (4.6), the magnitude of the drag force is also proportional to the reference area, A which in turn depends on the pore area available for salt deposition. Since the two rocks have similar porosities, the Berea (1484 mD) probably has more open and connected pore channels compared to the Kirby core (372 mD). During salt precipitation, more salts and relatively larger aggregates of salts could be deposited in the Berea core compared to the Kirby core as the open pore channels create a larger surface area for the injected gas to displace the precipitated salts. The Berea core showed higher permeability change probably because larger reference area of salt was exposed to the flowing fluid.

4.1.3 CO₂ alternating LSW flooding

We investigated CO₂ alternating low salinity water injection as a potential technique to mitigate salt precipitation effects on CO₂ injectivity. After salt precipitation, a slug of diluent is injected to dissolve the precipitated salts, thus temporarily improving CO₂ injectivity. The diluent used is low salinity water (LSW) which is prepared by diluting FW to lower brine salinity. Details of the experimental and theoretical work presented have been published in Paper V.

The clean Berea core sample was vacuum saturated with FW and aged at 60 °C for 14 days. The aged core was then prepared and flooded with about 50 PV of supercritical CO₂ to vaporize brine and possibly precipitate salts into the pore spaces. After complete dry-out, the initial liquid CO₂ pressure drop across the impaired core was measured to calculate the permeability. The impaired core was then flushed with about 30 PV of the diluent LSW brine at 0.05 mL/min in attempt to dissolve and washout precipitated minerals after which the core was again vaporized with supercritical CO₂ to complete dryness. Liquid CO₂ pressure drop across the treated core was measured to calculate the final permeability. The permeability data was then used to estimate injectivity improvement induced by the mitigation process. The experiment was repeated by gradually reducing the diluent brine salinity. A theoretical model, developed based on fractional flow theory and mass balance was used to simulate the expected injectivity improvement induced by dilution of the saturating brine. Figure 4.9 shows injectivity improvement obtained as a function of mass fraction of salt (X_s) in the diluent brine.

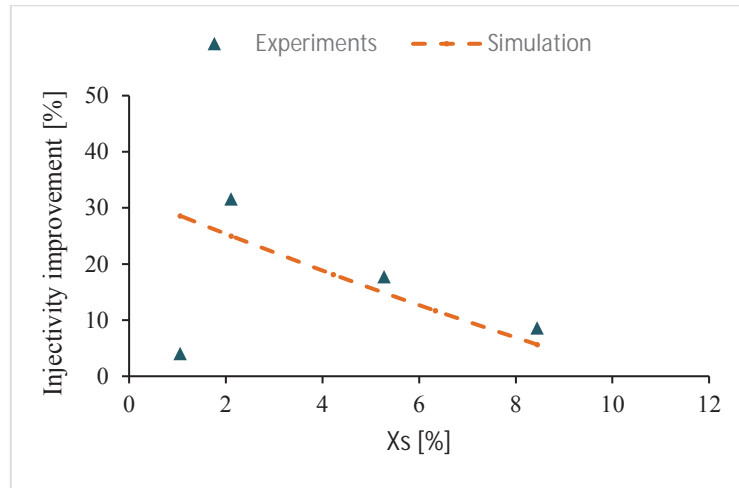


Figure 4.9 Effect of diluent brine Salinity on CO₂ injectivity change induced by alternate injection of supercritical CO₂ and LSW.

In general, CO₂ injectivity improved from 8.66% to 31.62% when the mass fraction of salt in the diluent, X_s was decreased stepwise from 8.44 to about 2.11 (Figure 4.9). We also observe a good match between the experimental data and simulation results, signifying that the same mechanism is responsible for injectivity changes in this range of diluent salinity. The solubility of precipitated minerals in the diluent LSW increases with decreasing brine salinity, because as the brine is further diluted, more free water molecules become available to interact with precipitated salts.

At $X_s = 1.06$, injectivity dropped significantly and the experimental data deviates dramatically from the simulation results, signifying additional injectivity impairment other than salt precipitation. At this point, the diluent starts to interact chemically with the rock minerals. Interaction between rock minerals and the diluent could induce clay swelling and colloidal transport, which have the tendency to aggravate CO₂ injectivity impairment.

4.2 Mineral dissolution and fines mobilization

Preliminary experiments were conducted to investigate the effect of mineral dissolution on CO₂ injectivity. Clay-rich Bentheimer core, was flooded with carbonated water at 80 bar and 60 °C. Bentheimer rock was used because of its

clay content and wider pore spaces. Under these conditions, bicarbonates generated from carbonated water will attack and possibly wear out clay and feldspar minerals into the pore fluid. The suspended particles could then be lifted by the flowing fluid into pore spaces, where they could plug the rock and reduce injectivity. Details of the experimental work can be found in Paper VII.

4.2.1 Evidence of dissolution and fines entrapment

A Bentheimer core, initially fully saturated with FW, was flooded with about 25 pore volumes (PV) of carbonated water at 0.25 mL/min. Pressure drop profiles were recorded during the flooding (Figure 4.10). Effluent samples were collected and filtered with a 0.22 μm filter to collect solid particles that might have been washed out of the core. The sample was then dried and analyzed with a Scanning Electron Microscope (SEM). Energy Dispersive Spectroscopy (EDS) elemental analysis of the sample are shown in Table 4.1.

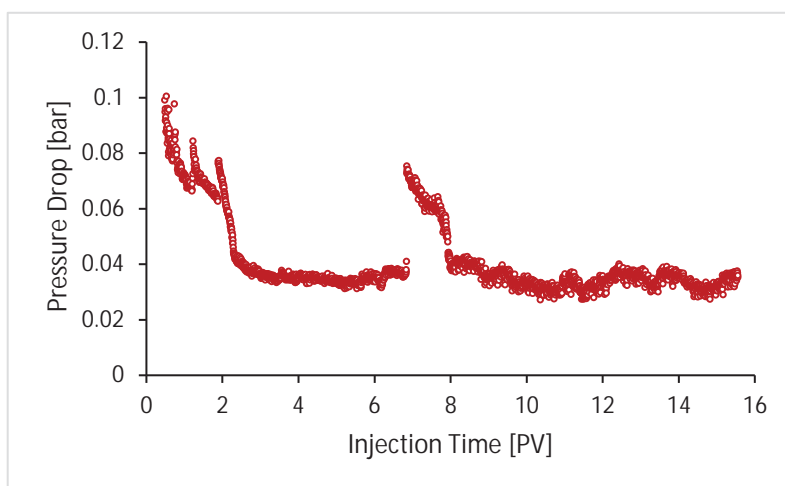


Figure 4.10 Pressure drop profile recorded during injection of carbonated water into a Bentheimer core at flow rate of 0.25 mL/min at 80 bar and 60 °C. The pressure drop is seen to fall sharply until about 3 pore volumes (PV), stabilizes between 3 PV and about 7 PV, and become very unstable afterwards.

In Figure 4.10, we observe a period of immiscible displacement where pressure drop decreased sharply from about 0.1 bar to about 0.04 bar after the core was flooded with about 3 PV of carbonated water. As the displaced FW is replaced by the less dense carbonated water, the pressure drop is seen to fall sharply until carbonated water breakthrough at the effluent end of the core. Pressure drop was stabilized from about 3 PV to about 7 PV. In this period, the core is fully saturated

with carbonated water, leading to stable flow. Unstable flow sets in from about 7 PV to the end of the test. In this period, the pressure drop is seen to rise sharply and fall to a rather haphazard behavior towards the end of the test. We suspect that this is the period in which the resident carbonated water begins to interact chemically with the rock minerals. Dissolution of the rock momentarily decreases the pressure drop as pores are widened. The temporary increase in pressure drop is probably caused by fines entrapment.

The EDS results in Table 4.1 shows the filtered effluent sample is composed predominantly of Na (17.53%) and Cl (29.79%). This is probably because the effluent sample, which is composed mainly of FW, contains about 73.4% NaCl. The injected carbonated water could not have precipitated halite within the rock, since no free CO₂ came into direct contact with the FW during the flooding. The CO₂ was fully dissolved in carbonated water at the flooding conditions. Therefore, the Na and Cl elements are probably components of the effluent FW. The results also reveal the presence of minerals such as Fe, Si, Al, Ni, and Co which were not present in the saturating FW and the injected carbonated water. Therefore, Fe, Si, Al, Ni, and Co were most likely dissolved from the Bentheimer core through the interaction of the carbonated water and the rock minerals. The EDS analysis show low amounts of Fe, Si, Al, Ni, and Co, because only few particles were likely to be washed out of the core.

Table 4.1 EDS elemental analysis of effluent samples collected during carbonated water flooding into Bentheimer core.

Element	wt. %
O	33.56
Fe	7.78
Ni	5.02
Na	17.53
Mg	0.74
Al	2.53
Si	0.35
Cl	29.79
Ca	2.52
Co	0.17
Total	100.00

4.2.2 Effect of dissolution and fines entrapment

Quantitative experiments were then conducted to measure the effect of dissolution on injectivity. A Berea sandstone core sample with known permeability was initially saturated with FW, and then flooded with about 25 PV

of carbonated water at 80 bar and 60 °C at constant injection rate of 0.25 mL/min to release and mobilize fine particles in the rock. The permeability of the core after carbonated water flooding was measured, and injectivity impairment index, β , was calculated. The experiment was then repeated at injection flow rates of 0.5 mL/min and 1.0 mL/min.

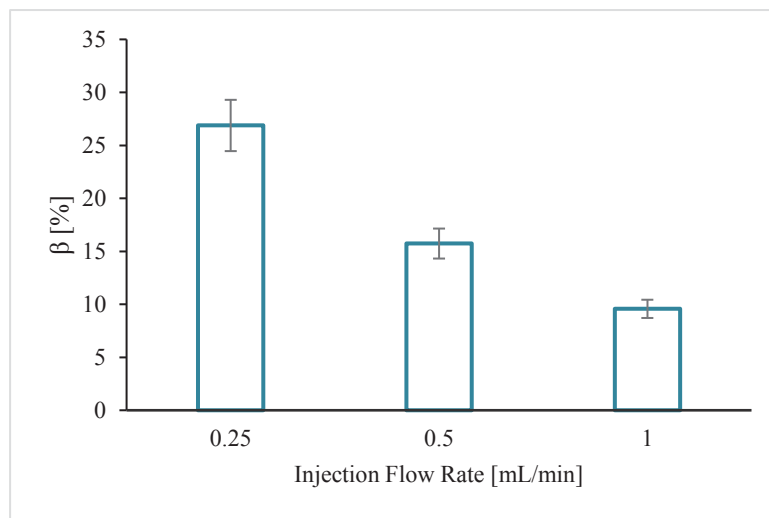


Figure 4.11 Effect of injection flow rate on injectivity impairment induced by fines plugging. Injectivity impairment decreased with increasing carbonated water injection flow rate.

Figure 4.11 shows injectivity impairment decreased with increasing carbonated water injection flow rate. As injection flow rate is increased, carbonated water stays in contact with the rock minerals for a short period of time, since the volume of fluid injected was kept constant in the three experiments. The number of fines generated will then decrease as the injection flow rate is increased. In addition, at high injection flow rate, hydrodynamic forces could lift smaller particles out of the core with the effluent fluid. The number of fines available to plug the rock, and therefore the chances of injectivity impairment, will reduce as carbonated water injection flow rate is increased. Up to 26 % injectivity impairment was induced by mineral dissolution and fines mobilization during carbonated water injection into Berea sandstone cores. Injectivity impairment decreased as injection flow rate was increased.

Under typical storage conditions, CO₂-brine-rock reactions could dissolve the rock and generate secondary minerals including fine particles. During reinjection of CO₂, equilibrium of the suspending particles could be disturbed, leading to mobilization of particles along the flow stream. Entrapment of these

particles in the pore throats could reduce the flow paths and impair injectivity significantly. The variation of injection rate in the experiments was used to investigate the contact time. The experimental findings suggest that the effect of mineral dissolution and fines mobilization increases with time. The longer CO₂ is stored, the more severe will be the effect of dissolution and fines mobilization.

4.3 Salt precipitation and fines mobilization

We compare the effects of fines mobilization to the impact of salt precipitation under linear flow conditions. Attempt was then made to investigate the coupled effect of fines mobilization and salt precipitation on CO₂ injectivity. The objective is to find the dominant injectivity impairment mechanism in the immediate injection area. The full results are published in Paper VI.

4.3.1 Comparing fines and salt effects

Mono-disperse colloid solutions were used to represent the pore fluid containing particles after mineral dissolution. With colloid suspensions, the concentration and size of particles can be optimized. Pore size distribution analysis of Berea sandstone cores suggests an average pore throat size of about 2 μm (Nelson, 2009). The colloid suspension with average particle size of 0.08 μm will yield an average jamming ratio (particle size/pore size) of about 0.04. Natural formation fine particles have average particle sizes in the region of 1 μm , though dissolution under typical CO₂ storage conditions may generate particles of varying sizes over a wide range, depending on the reaction conditions and composition of the rock.

Particles with jamming ratio of about 0.04 could plug the rock through surface deposition, pore bridging, and multi-particle blocking (Khilar and Fogler, 2010). During saturation, the particles are stabilized in the suspending fluid which minimizes surface deposition. Very low particle concentration was used to reduce the chances of pore bridging and multi-particle blocking during saturation. In addition, oil-wet latex particles were used to minimize attachment to the pore walls. Therefore, the particles would stay mono-dispersed within the pore spaces after saturation and prior to CO₂ injection. When CO₂ invades the fluid-filled pores, the stability of the particles in the colloid will be

disturbed, thereby releasing the particles for plugging during CO₂ flooding. This is comparable to CO₂ injection into a reservoir where the formation brine contains fine particles released from the dissolved rock.

A Berea sandstone core sample was initially saturated with mono-disperse colloid solution with average particle size of 0.08 μm and particle concentration of 0.3 wt.%. The composition of mono-disperse colloid suspension used in this study has been described in Table 3.2. The core was then mounted and flooded with about 40 PV of supercritical CO₂ at 5 mL/min to complete dryness. The relative injectivity change, β , was calculated from the permeability of the core measured before and after it was exposed to mineral impairment. The experiment was repeated for particle concentrations of 0.5 wt.% and 1.0 wt.%. We then conducted a salt precipitation experiment by saturating the core with brine containing 10 wt.% of total dissolved salts (FW) prior to supercritical CO₂ drying. Figure 4.12 shows pressure drop profiles recorded during the flooding. Figure 4.13 shows injectivity impairment induced as a function of composition of the pore fluid.

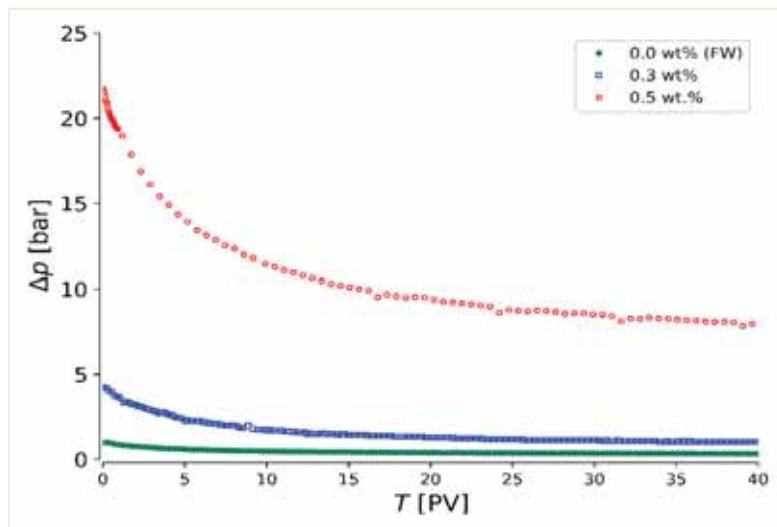


Figure 4.12 Pressure drop profiles recorded during supercritical CO₂ injection into Berea Sandstone cores initially saturated with FW, 0.3 wt.% and 0.5 wt.% colloid solutions with average particle size of 0.08 μm.

Figure 4.12 shows the pressure drop profiles for particle transport followed a trend similar to the pressure drop profiles of brine vaporization and salt precipitation: an early sharp decline rate, followed by gradual decline and constant pressure drop. This suggests that, the mechanisms of CO₂-colloid transport are similar to the mechanisms of CO₂-brine displacement probably because of the drying effect of supercritical CO₂. We also observe that pressure drop was significantly higher for high particle concentrations as the likelihood of fines entrapment increases with particle concentration. Therefore, the pressure drop profiles did not follow the rate-pressure proportionality relationship observed in most brine displacement experiments.

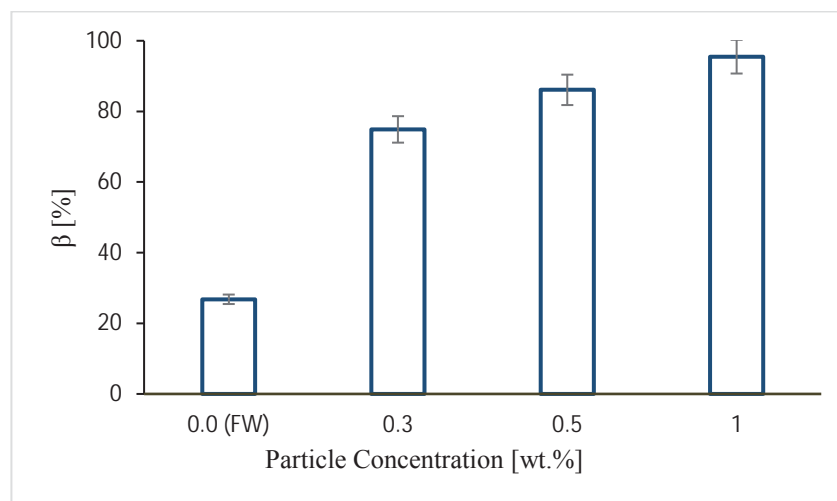


Figure 4.13 The relative impact of fines mobilization and salt precipitation on CO₂ injectivity. Fines migration had a more severe impact on injectivity compared to salt precipitation.

In Figure 4.13, while salt precipitation reduced injectivity by about 26.8%, particle concentration of 0.3 wt.% impaired injectivity by 74.9% through fines mobilization. About 1.0 wt.% of particles in the pore fluid almost plugged the rock. When CO₂ invades the pores, the mono-disperse particles may plug the narrow pore channels through bridging, surface deposition, or multi-particle blocking. As particle concentration increases, the distance between suspended particles shortens, enhancing multi-particle blocking of the invaded pores.

Thus, during fines entrapment, several particles could accumulate in the pore throat and completely plug the pore.

On the other hand, precipitated salts will form a coating on the pore walls to reduce the flow area. While salt precipitation reduces the flow area, fines entrapment could plug and isolate the flow path, making them inaccessible to fluid flow. This could be the reason why about 0.3 wt.% particle concentration in the pore fluid induced over twofold injectivity impairment compared to about 10 wt.% of total dissolved salt in the formation water. The results suggest that, under linear flow conditions, fines mobilization could induce severe CO₂ injectivity impairment comparable to the impact of salt precipitation.

4.3.2 Coupling fines and salt effects

In this section, the bundle-of-tubes model presented in Section 4.1.2.2 was adapted and extended to model the coupled effect of fines mobilization and salt precipitation on CO₂ injectivity. The objective is to investigate fundamental physical mechanisms of the combined effects of fines mobilization and salt precipitation. Details of the theoretical work are presented in Paper VII.

4.3.2.1 Model Formulation

For a bundle of N parallel non-communicating capillary tubes with varying tube radii, r_i and thickness of deposited salts, Δr_i , the total fluid flow rate can be modelled with the Hagen–Poiseuille equation as:

$$q = \frac{\pi}{8\mu} \frac{\Delta p}{L} \sum_{i=1}^N (r - \Delta r)_i^4 \quad (4.7)$$

In Eq. (4.7), $\frac{\Delta p}{L}$ is the overall pressure gradient across the bundle of capillary tubes. For linear flow through a core of radius R and length L , the fluid flow rate is also defined by Darcy's Law:

$$q = \frac{kA}{\mu} \frac{\Delta p}{L} \quad (4.8)$$

In Eq. (4.8), k is the absolute permeability of the core, and $A = \pi R^2$ is the cross-sectional flow area. Combining Eq. (4.7) and Eq. (4.8), the permeability of the core can be expressed as:

$$k = \frac{1}{8R^2} \sum_{i=1}^N (r - \Delta r)_i^4 \quad (4.9)$$

In Eq. (4.9), the permeability depends strongly on the number of open capillary tubes, N , and the thickness of precipitated salts deposited in the tubes, Δr . Injectivity impairment induced by salt precipitation will reduce the value of $(r - \Delta r)$. On the other hand, the entrapment of fine particles will plug the capillary tubes with jamming ratio greater than 1.0, reducing the number of open capillary tubes, N . Thus, by optimizing these parameters, the basic properties of the coupled effect of fines mobilization and salt precipitation could be investigated.

First, the number and distribution of tubes is computed with Eq. (4.3). Eq. (4.4) and (4.5) are then used to compute S_g and Δr respectively. The initial permeability of the core is calculated by setting $\Delta r = 0$ in Eq. (4.9). The permeability ratio, $\frac{k}{k_o}$, is then calculated and the relative injectivity change index, β , computed from Eq. (3.4).

The model does not handle particles of varying sizes as occurs in typical mineral dissolution and particle transport in natural porous media. In addition, fines entrapment through pore bridging and multi-particle blocking have not been included. Only fines entrapment through size exclusion was incorporated in the model.

4.3.2.2 Theoretical results of the coupled effect of fines mobilization and salt precipitation

The results presented are based only on theoretical modelling. We did not verify or compare the data obtained from the model with laboratory core-flood data. However, the results presented here are intuitive and possibly explain the coupled impact of fines and salt effect on CO₂ injectivity.

In the first theoretical experiment, the clean bundle of tubes was exposed to particles of equal sizes. Each capillary tube had an equal chance of being exposed to the particles. Capillary tubes with jamming ratio greater than 1.0 would be plugged through size exclusion. The effect of particle size on injectivity impairment was computed. The experiment was then repeated by first exposing the core to salt precipitation before subjecting them to particle entrapment. Particle sizes up to 20 μm were simulated.

Figure 4.14 shows injectivity impairment induced (β) as a function of average particle size (r_p) for the three cases. For pure fines mobilization (no salt), particle sizes below 5 μm did not induce injectivity impairment. Since an average pore radius of 6 μm was used in the simulation, particles smaller than the average pore size will pipe through most of the pores. For particle sizes greater than 5 μm , injectivity impairment increases with particle size. As the particle size is increased, the number of capillary tubes likely to attain jamming ratios greater than 1.0 increases, and injectivity decreases as more tubes are plugged and isolated.

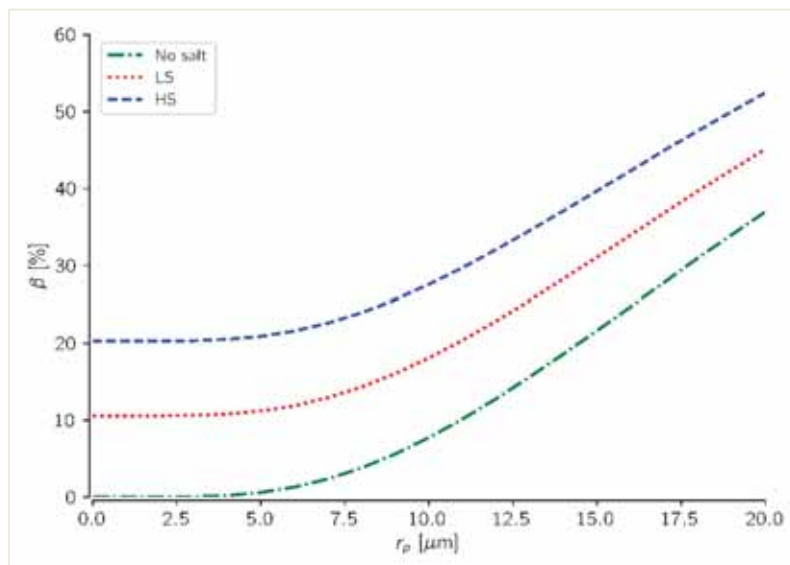


Figure 4.14 The coupled effect of fines mobilization and salt precipitation on CO₂ injectivity. Salt precipitation seems to aggravate injectivity impairment induced by fines migration. Injectivity impairment increased when brine salinity was increased from 75 g/L (LS) to 120 g/L (HS).

Figure 4.14 also shows that injectivity impairment induced by fines mobilization was further aggravated by increase in the saturating brine salinity. As brine salinity is increased, more salts are precipitated in the tubes. The precipitated salts reduce the flow area, increasing the jamming ratio of the tubes for each average particle size. The jamming ratio of the pores increases with increasing brine salinity as more salts are precipitated into the pores. Thus, more tubes will attain jamming ratios greater than 1.0 and eventually get plugged, inducing even more severe injectivity impairment.

The results suggest that salt precipitation could aggravate injectivity impairment induced by fines mobilization. The precipitated salts could reduce the pore radii and increase the jamming ratio of the pores. This effect will in turn increase with saturating brine salinity, as more salts are precipitated into the pore spaces.

5 Discussion

In Chapter 4, we presented experimental and theoretical results on mechanisms of salt precipitation and fines mobilization and their impact on CO₂ injectivity. Important governing parameters were also identified and studied. In the present chapter, the results are discussed with reference to existing literature. Limitations of the work and relevance of the findings to field CO₂ injection are also presented, culminating in proposed future work.

5.1 Results compared to literature

Several researchers (Bacci et al., 2011; Jeddizahed and Rostami, 2016; Kleinitz et al., 2001; Pruess and Muller, 2009) have investigated the mechanisms of salt precipitation around the immediate vicinity of the injection inlet during gas injection into saline formations. However, the mechanisms of salt cake deposition on the surface of the injection inlet have not been properly studied. Most of the mentioned studies, investigated salt precipitation within the dry-out zone in the wellbore vicinity. In the present work, we investigated the underlying mechanisms of salt deposition on the surface of the injection inlet in the form of a filter cake. We identified sweep efficiency and brine salinity as the controlling parameters.

The mechanisms of brine vaporization and salt precipitation within the dry-out region have also been previously studied and documented (André et al., 2014; Miri et al., 2015; Miri and Hellevang, 2016; Peysson et al., 2014; Pruess and Muller, 2009). Pruess, (2009) developed an analytical model based on fractional flow theory and mass balance to characterize the extension of the dry-out zone and estimate the solid salt saturation. However, the quantitative impact of extension of the dry-out zone on the evolution of CO₂ injectivity have not been investigated. In the present work, we developed a model to track extension of the dry-out zone and quantify the impact of the dry-out length on CO₂ injectivity.

Pruess and Muller, (2009) proposed fresh water preflush as a means to mitigate salt precipitation effects. Earlier, Kleinitz et al., (2003) reported implementation of the technique in the field. However, fresh water injection

could induce clay swelling and fines plugging in clay-rich sandstone rocks. Therefore, the application of fresh water preflush is rather risky and limited. In the present work, we proposed alternate injection of CO₂ and diluent low salinity brine. We found that, below brine salinity of about 21 g/L, preflush with diluent low salinity brine did not reduce salt precipitation effects. Injectivity impairment was rather aggravated by clay swelling and fines migration in Berea sandstone cores.

Several researchers (Dawson et al., 2015; Ilgen and Cygan, 2016; Kampman et al., 2014; Rosenbauer et al., 2005; Tang et al., 2016; Tobergte and Curtis, 2013) have investigated CO₂-brine-rock reactions under typical storage conditions and presented evidence of mineral dissolution and potential generation of secondary minerals. Kaszuba et al., (2003) conducted geochemical batch reactions to investigate mineral dissolution under CO₂ sequestration conditions. They reported evidence of mineral dissolution after about 80 days of reaction time. Tang et al., (2016) reported mineral dissolution and precipitation of secondary minerals in batch reactions conducted with Pucheng Oilfield rocks in China. With various evidence of mineral dissolution and possible fines generation, the direct impact of mineral dissolution and fines mobilization on CO₂ injectivity have not been studied. In the present work, we investigated the mechanisms of mineral dissolution and the impact of fines mobilization on CO₂ injectivity.

Due to available evidence of severe injectivity impairment induced by salt precipitation (Miri and Hellevang, 2016), other potential CO₂ injectivity impairment challenges have been generally overlooked. We attempted to compare injectivity impairment induced by fines mobilization to salt precipitation effects. We show that fines mobilization could induce injectivity impairment comparable to salt precipitation in sandstone cores. A theoretical study was then conducted to investigate the coupled effects of fines mobilization and salt precipitation on CO₂ injectivity where salt precipitation was found to aggravate the impact of fines mobilization.

5.2 Limitations of the work

Although our work presents valuable insight and useful practical implications, there are obvious limitations in the underlying methods and applicability of the findings.

First, the findings are based on linear flow conditions. The experimental deductions were based mostly on core-flood studies conducted on sandstone rocks, which can be considered homogeneous with respect to permeability in the linear direction. The theoretical studies were also performed with linear bundle-of-tube models. The main objective of the work was to investigate CO₂ injectivity impairment mechanisms within the immediate injection area of the wellbore. Linear core-flow adequately approximates CO₂ injection into a section in the immediate injection area near the wellbore.

Second, detailed pore-scale analysis of the rock after mineral precipitation was not performed in most of the experiments. The analysis were mostly based on pressure drop profiles recorded during core-flooding and absolute permeability changes measured before and after mineral precipitation. However, the main parameter required to adequately estimate the effect of formation damage, is changes in the flow properties of the rock. Detailed pore-scale scanning techniques, could have improved the evidence presented in some of the studies. Nevertheless, pressure drop profiles and absolute permeability measurements proved adequate within the purview of the current work. In some of the studies, pressure tapped measurements were conducted to minimize uncertainty.

Finally, the work focused mainly on the physical mechanisms of fines mobilization and salt precipitation. However, the operating conditions were designed such that, the impact of chemical effects will be negligible compared to the physical mechanisms. The complexity of the challenges associated with particle transport in porous media under the unique conditions of CO₂ injection, favor the decoupling of physical and chemical effects.

5.3 Field relevance

The impact of fines mobilization on injectivity could be less severe under radial flow conditions where flow velocity decreases more into the formation.

Although typical CO₂ injection rates under storage conditions are high (70 - 600 tonnes/day), as the injected gas moves into the formation, the resultant flow velocity might lag the minimum lift velocity of particles generated at the interface between the CO₂ plume and formation brine away from the wellbore. Although the wellbore fluid might contain particles from drilling fluid and cement, CO₂-brine-rock mineral dissolution is expected to be predominant away from the wellbore. However, the present work has shown that even small amount of particles in the wellbore fluid or the pore fluid within the immediate injection area, could induce dramatic injectivity impairment.

We have shown that mechanisms of immiscible displacement and drying are similar for CO₂ – brine and CO₂ – colloid flooding due to the drying effect of supercritical CO₂. Under typical storage conditions in deep saline reservoirs, both fines and precipitated salts could impair CO₂ injectivity simultaneously. During CO₂ reinjection, if the pore fluid contains fine particles, the rock could be plugged during immiscible CO₂-brine displacement. At irreducible brine saturation, injectivity impairment could be aggravated by brine vaporization and salt precipitation.

Our findings show that alternate injection of supercritical CO₂ and low salinity brine could mitigate the impact of salt precipitation on CO₂ injectivity in sandstone rocks. We propose the diluent brine salinity should be selected above the critical brine salinity to eliminate other geochemical effects such as clay swelling and fines plugging which could further aggravate injectivity loss. This critical brine salinity was found to be about 21 g/L for Kipton Berea Sandstone cores.

The deposition of precipitate salt on the surface of the injection inlet could be minimized by preflush of the wellbore area with low salinity brine and injecting CO₂ at a rate that improves the sweep. Salt cake could form at the injection inlet, if formation brine left behind the injection inlet, reach supersaturation before it is swept into the formation. Improved sweep will minimize brine left behind the inlet and preflush of the wellbore area with diluent delays the brine left behind from reaching supersaturation before it is swept into the formation.

5.4 Proposed further work

The mechanisms and impact of fines mobilization on well injectivity have previously been studied. However, the unique gas-like viscosity and liquid-like density of supercritical CO₂ and the high injection flow rates required to meet emission reduction targets demands further research to adequately understand the mechanisms and impact of fines mobilization under typical CO₂ injection conditions.

The impact of fines mobilization could be affected by salt precipitation because of the drying effect of supercritical CO₂. While salt precipitation within the plugged pores could be limited by flow restrictions, the injected CO₂ could also dislodge pore-bridging particles. It is not clear how these two seemingly opposing processes will impact the injectivity. However, the drying effect of supercritical CO₂ presents additional challenges to the mechanisms of fines mobilization under typical CO₂ storage conditions.

The effects of fines entrapment could be lessened under radial flow conditions where flow velocity decreases away from the wellbore. Under high injection flow rates, plugging through pore-bridging could be moved into the formation as drag forces will tend to break pore bridges around the wellbore vicinity where fluxes are very high. Only pores plugged through size-exclusion are likely to remain plugged in the immediate injection area. Consequently, salt precipitation effects could be the dominant mechanism of injectivity impairment in the immediate injection area. A field-scale simulation will provide insight on how the current and previous findings scale up under typical storage conditions.

Discussion

6 Conclusion

There is an increasing need to adopt drastic measures to halt climate change and its associated threat to human life and the environment. CCUS presents a plausible technique with potential to reduce global emission of CO₂ and sustain the use of hydrocarbons for energy generation. Deep saline aquifers, depleted and existing oil and gas reservoirs have the storage capacity and reliable containment efficiency to hold large volumes of CO₂. However, adequate well injectivity is required to inject large amounts of CO₂ through a minimum number of wells. Therefore, well injectivity is both a technical and economic requirement of CCUS projects.

Salt precipitation and fines mobilization have been found to impair CO₂ injectivity. Although there is no general agreement on the mechanisms of salt precipitation, the impact of salt precipitation on CO₂ injectivity have been previously investigated. The mechanisms of fines mobilization are also well documented. However, the special properties of supercritical CO₂, coupled with the high injection rates required to meet global emission reduction targets, presents the need for extensive research to understand the mechanisms and impact of fines migration in the context of CO₂ injection.

We investigated the physical mechanisms and impact of fines mobilization and salt precipitation on CO₂ injectivity through sandstone core-flood experiments and theoretical modelling. Some practical implications of the findings were also outlined. Some of the highlights of the work include the following:

- Fines mobilization could induce significant injectivity impairment in the immediate injection area. Up to about 26 % injectivity impairment was induced by mineral dissolution and fines mobilization during carbonated water flooding into Berea sandstone cores.
- Injectivity impairment induced by fines mobilization is comparable to salt precipitation effects. About 0.3 wt.% of particles in the pore fluid was found to induce two-fold injectivity impairment compared to about 10 wt.% of salt in the pore fluid.

Conclusion

- Salt precipitation was found to aggravate fines mobilization effects. The precipitated salts reduce the pore spaces and makes the rock more susceptible to fines plugging.
- Alternate injection of CO₂ and diluent low salinity brine could mitigate the impact of salt precipitation on CO₂ injectivity. Up to about 30 % injectivity improvement was obtained in Berea sandstone rocks.
- Improved sweep efficiency and preflush of the wellbore with low salinity brine could reduce salt deposition on the surface of the injection inlet.

Under typical storage conditions, the wellbore fluid could contain particles derived from cement and drilling fluids. Mineral dissolution induced by CO₂-brine-rock reactions could generate secondary minerals in the form of fine particles into the pore fluid. If these particles are mobilized during CO₂ injection, injectivity could be significantly impaired. While salt precipitation remains the dominant injectivity impairment mechanism in the wellbore vicinity, we have shown that fines mobilization could pose a formidable threat to CO₂ injectivity.

7 Bibliography

- Aji, K., 2014. The Experimental and Theoretical Study of Fines Migration in Porous Media under Particle-rock Repulsion and Attraction Kaiser Aji A thesis submitted for the degree of Doctor of Philosophy (PhD) October 2014.
- André, L., Peysson, Y., Azaroual, M., 2014. Well injectivity during CO₂ storage operations in deep saline aquifers – Part 2 : Numerical simulations of drying , salt deposit mechanisms and role of capillary forces. *Int. J. Greenh. Gas Control* 22, 301–312. doi:10.1016/j.ijggc.2013.10.030
- Bacci, G., Durucan, S., Korre, A., 2013. Experimental and Numerical Study of the Effects of Halite Scaling on Injectivity and Seal Performance During CO₂ Injection in Saline Aquifers. *Energy Procedia* 37, 3275–3282. doi:10.1016/j.egypro.2013.06.215
- Bacci, G., Korre, A., Durucan, S., 2011. Experimental investigation into salt precipitation during CO₂ injection in saline aquifers. *Energy Procedia* 4, 4450–4456. doi:10.1016/j.egypro.2011.02.399
- Bachu, S., 2015. Review of CO₂ storage efficiency in deep saline aquifers. *Int. J. Greenh. Gas Control* 40, 188–202. doi:10.1016/j.ijggc.2015.01.007
- Bachu, S., Bonijoly, D., Bradshaw, J., Burruss, R., Holloway, S., Christensen, N.P., Mathiassen, O.M., 2007. CO₂ storage capacity estimation: Methodology and gaps. *Int. J. Greenh. Gas Control* 1, 430–443. doi:10.1016/S1750-5836(07)00086-2
- Bachu, S., Shaw, J.C., Pearson, R.M., 2004. Estimation of oil recovery and CO₂ storage capacity in CO₂ EOR incorporating the effect of underlying aquifers. *SPE/DOE Fourteenth Symp. Improv. Oil Recover.* 3, 1–13. doi:10.2523/89340-MS
- Baines, S.J., Worden, R.H., Jackson, R.E., 2009. Geological Storage of Carbon Dioxide XV, 115–116.
- Batchelor, G.K., 2000. An introduction to fluid dynamics. Cambridge university press.
- Baumann, G., Henniges, J., De Lucia, M., 2014. Monitoring of saturation changes and salt precipitation during CO₂ injection using pulsed neutron-

Bibliography

- gamma logging at the Ketzin pilot site. *Int. J. Greenh. Gas Control* 28, 134–146.
- Birkholzer, J.T., Oldenburg, C.M., Zhou, Q., 2015. CO₂ migration and pressure evolution in deep saline aquifers. *Int. J. Greenh. Gas Control* 40, 203–220.
- Bradshaw, J., Bachu, S., Bonijoly, D., Burruss, R., Holloway, S., Christensen, N.P., Mathiassen, O.M., 2007. CO₂ storage capacity estimation: Issues and development of standards. *Int. J. Greenh. Gas Control* 1, 62–68. doi:10.1016/S1750-5836(07)00027-8
- Christensen, R., 1961. Carbonated Waterflood Results--Texas And Oklahoma. *Annu. Meet. Rocky Mt. Pet.* doi:10.2118/66-MS
- Cinar, Y., Riaz, A., Tchelepi, H.A., 2007. Experimental study of CO₂ injection into saline formations. *SPE Annual Technical Conference and Exhibition*. Society of Petroleum Engineers.
- Cinar, Y., South, N., Riaz, a, Tchelepi, H. a, 2009. Experimental Study of CO₂ Injection Into Saline Formations. *SPE J.* doi:10.2523/110628-MS
- Civan, F., 2007. *Reservoir Formation Damage: Fundamentals, Modelling, Assessment, and Mitigation*. Gulf Professional Publishing, Massachusetts, USA.
- Dake, L.P., 1983. *Fundamentals of Reservoir Engineering*. Elsevier, New York.
- Daniel, R.F., Kaldi, J.G., 2009. Evaluating seal capacity of cap rocks and intraformational barriers for CO₂ containment. *Carbon dioxide sequestration in geological media—State of the science: AAPG Studies in Geology* 59, p. 335–345. DOI:10.1306/13171247St59227
- Davison, J., Freund, P., Smith, A., 2001. Putting carbon back in the ground. *IEA Greenhouse Gas R & D Programme*.
- Dawson, G.K.W., Pearce, J.K., Biddle, D., Golding, S.D., 2015. Experimental mineral dissolution in Berea Sandstone reacted with CO₂ or SO₂-CO₂ in NaCl brine under CO₂ sequestration conditions. *Chem. Geol.* 399, 87–97. doi:10.1016/j.chemgeo.2014.10.005
- Dong, Y., Ishizawa, C., Lewis, E., Dindoruk, B., 2011. Carbonated Water Flood: What We Observed in Sand Pack Experiments. *Int. Symp. Soc. Core Anal.* held Austin, Texas, 18-21 Sept. 1–12.

Bibliography

- Dullien, F.A.L., Dhawan, G.K., 1974. Characterization of pore structure by a combination of quantitative photomicrography and mercury porosimetry. *J. Colloid Interface Sci.* 47, 337–349.
- Fjelde, I., Omekeh, A.V., Sokama-Neuyam, Y.A., 2014. Low Salinity Water Flooding: Effect Of Crude Oil Composition. *SPE Improv. Oil Recover. Symp.* doi:10.2118/169090-MS
- Fogler, H.S., 1984. The Existence of a Critical Salt Concentration for Particle Release. *J. of Colloid and Interface Science* 1, 214–224. doi.org/10.1016/0021-9797(84)90021-3
- Giorgis, T., Carpita, M., Battistelli, A., 2007. 2D modeling of salt precipitation during the injection of dry CO₂ in a depleted gas reservoir. *Energy Convers. Manag.* 48, 1816–1826. doi:10.1016/j.enconman.2007.01.012
- Golghanddashti, H., Saadat, M., Abbasi, S., Shahrabadi, A., 2013. Experimental investigation of water vaporization and its induced formation damage associated with underground gas storage. *J. Porous Media* 16, 89-96. DOI: 10.1615/JPorMedia.v16.i2.10
- Gozalpour, F., Ren, S.R., Tohidi, B., 2005. CO₂ EOR and Storage in Oil Reservoir. *Oil & Gas Science and Technology* 60, 537–546. doi:10.2516/ogst:2005036
- Grude, S., Landrø, M., Dvorkin, J., 2014. Pressure effects caused by CO₂ injection in the Tubåen Fm., the Snøhvit field. *Int. J. Greenh. Gas Control* 27, 178–187.
- Gruesbeck, C., Collins, R.E., 1982. Entrainment and Deposition of Fine Particles in Porous Media. *SPE J.* 22, 10. doi:10.2118/8430-PA
- Gunter, W.D., Wong, S., Cheel, D.B., Sjostrom, G., 1998. Large CO₂ sinks: Their role in the mitigation of greenhouse gases from an international, national (Canadian) and provincial (Alberta) perspective. *Appl. Energy* 61, 209–227.
- Ha-Duong, M., Keith, D., 2003. Carbon storage: the economic efficiency of storing CO₂ in leaky reservoirs. *Reserv. Clean Technol. Environ. Policy* 5, 181–189. doi:10.1007/s10098-003-0213-z
- Hangx, S.J.T., 2005. Subsurface mineralisation: Rate of CO₂ mineralisation and

Bibliography

- geomechanical effects on host and seal formations. *Cato* 1–43.
- Hickok, C.W., Christensen, R.J., Ramsay, H.J., 2013. Progress Review of the K&S Carbonated Waterflood Project. *J. Pet. Technol.* 12, 20–24. doi:10.2118/1474-G
- Holloway, S., 2001. Storage of fossil fuel-derived carbon dioxide beneath the surface of the earth. *Annu. Rev. Energy Environ.* 26, 145–166.
- Hurter, S., Berge, J., Labregere, D., 2007. Simulations for CO₂ injection projects with Compositional Simulator. *Offshore Eur.* 4-7 Sept. doi:10.2118/108540-MS
- IEA, 2015. Storing CO₂ through enhanced oil recovery, International Energy Agency, Paris, France.
- IEA, 2013. Technology roadmap - Carbon capture and Storage. *Technol. Roadmap* 59. doi:10.1007/SpringerReference_7300
- IEA-GHG, E.C.B.M., 1998. Recovery with CO₂ Sequestration, IEA Greenhouse Gas R&D Programme, Report No. PH3/3, August 139.
- Ilgen, A.G., Cygan, R.T., 2016. Mineral dissolution and precipitation during CO₂ injection at the Frio-I Brine Pilot: Geochemical modeling and uncertainty analysis. *Int. J. Greenh. Gas Control* 44, 166–174. doi:10.1016/j.ijggc.2015.11.022
- Jarrell, P.M., 2002. Practical aspects of CO₂ flooding. Richardson, Tex.: Henry L. Doherty Memorial Fund of AIME, Society of Petroleum Engineers.
- Jasinski, R., Sablerolle, W., Amory, M., 1997. ETAP: Scale Prediction and Control for the Heron Cluster. SPE Annual Technical Conference and Exhibition. Society of Petroleum Engineers.
- Jeddizahed, J., Rostami, B., 2016. Experimental investigation of injectivity alteration due to salt precipitation during CO₂ sequestration in saline aquifers. *Adv. Water Resour.* 96, 23–33. doi:10.1016/j.advwatres.2016.06.014
- Kaldi, J., Daniel, R., Tenthorey, E., Michael, K., Schacht, U., Nicol, A., Unterschultz, J., Backe, G., 2013. Containment of CO₂ in CCS: Role of Caprocks and Faults. *Energy Procedia* 37, 5403–5410. doi:10.1016/j.egypro.2013.06.458

Bibliography

- Kampman, N., Bickle, M., Wigley, M., Dubacq, B., 2014. Fluid flow and CO₂-fluid-mineral interactions during CO₂-storage in sedimentary basins. *Chem. Geol.* 369, 22–50. doi:10.1016/j.chemgeo.2013.11.012
- Kaszuba, J.P., Janecky, D.R., Snow, M.G., 2005. Experimental evaluation of mixed fluid reactions between supercritical carbon dioxide and NaCl brine: Relevance to the integrity of a geologic carbon repository. *Chem. Geol.* 217, 277–293. doi:10.1016/j.chemgeo.2004.12.014
- Kaszuba, J.P., Janecky, D.R., Snow, M.G., 2003. Carbon dioxide reaction processes in a model brine aquifer at 200 °C and 200 bars: Implications for geologic sequestration of carbon. *Appl. Geochemistry* 18, 1065–1080. doi:10.1016/S0883-2927(02)00239-1
- Khilar, K.C., Fogler, H.S., 2010. *Migrations of Fines in Porous Media, Theory and Applications of Transport in Porous Media*. Springer Netherlands.
- Khilar, K.C., Fogler, H.S., 1998. *Migrations of fines in porous media*. Springer Science & Business Media.
- Khilar, K.C., Fogler, H.S., 1983. Water Sensitivity of Sandstone. SPE 10103.
- Kim, M., Sell, A., Sinton, D., 2013. Aquifer-on-a-Chip: understanding pore-scale salt precipitation dynamics during CO₂ sequestration. *Lab on a Chip* 13, 2508–2518.
- Kleinitz, W., Dietzsch, G., Köhler, M., 2003. Halite scale formation in gas-producing wells. *Chem. Eng. Res. Des.* 81, 352–358.
- Kleinitz, W., Koehler, M., Dietzsch, G., Gmbh, P.E., 2001. The precipitation of salt in gas producing wells, in: SPE (Ed.), *SPE European Formation Damage Conference*. SPE, The Hague, pp. 1–7. doi:10.2523/68953-MS
- Leung, D.Y.C., Caramanna, G., Maroto-Valer, M.M., 2014a. An overview of current status of carbon dioxide capture and storage technologies. *Renew. Sustain. Energy Rev.* 39, 426–443. doi:10.1016/j.rser.2014.07.093
- Leung, D.Y.C., Caramanna, G., Maroto-Valer, M.M., 2014b. An overview of current status of carbon dioxide capture and storage technologies. *Renew. Sustain. Energy Rev.* 39, 426–443. doi:10.1016/j.rser.2014.07.093
- Li, L., Zhao, N., Wei, W., Sun, Y., 2013. A review of research progress on CO₂ capture, storage, and utilization in Chinese Academy of Sciences. *Fuel* 108, 112–130. doi:10.1016/j.fuel.2011.08.022

Bibliography

- Lin, C., Slattery, J.C., 1982. Three-dimensional, randomized, network model for two-phase flow through porous media. *AIChE J.* 28, 311–324.
- Lombard, J.M., Azaroual, M., Pironon, J., Broseta, D., Egermann, P., Munier, G., Mouronval, G., 2010. CO₂ injectivity in geological storages: An overview of program and results of the GeoCarbone-Injectivity project. *Oil Gas Sci. Technol.* 65, 533–539. doi:10.2516/ogst/2010013
- M.C. Place Jr., J.T.S., 1984. An Unusual Case of Salt Plugging in a High-Pressure Sour Gas Well: SPE (Ed.), 59th Annual Technical Conference and Exhibition. SPE, Houston, Texas, p. 13. doi:<http://dx.doi.org/10.2118/13246-MS>
- Michael Sheppard, 2017. Carbon Capture and Sequestration | Society of Petroleum Engineers. Soc. Pet. Eng. URL <http://www.spe.org/industry/carbon-capture-sequestration.php> (accessed 3.14.17).
- Miri, R., 2015. Effects of CO₂ -Brine-Rock Interactions on CO₂ Injectivity – Implications for CCS. University of Oslo.
- Miri, R., Hellevang, H., 2016. Salt precipitation during CO₂ storage—A review. *Int. J. Greenh. Gas Control* 51, 136–147. doi:10.1016/j.ijggc.2016.05.015
- Miri, R., van Noort, R., Aagaard, P., Hellevang, H., 2015. New insights on the physics of salt precipitation during injection of CO₂ into saline aquifers. *Int. J. Greenh. Gas Control* 43, 10–21. doi:10.1016/j.ijggc.2015.10.004
- Moberg, R., 2001. The Weyburn CO₂ monitoring and storage project. *Greenh. Issues, IEA Greenh. Gas R&D* 57.
- Mohammed, A.S., Ayoub, A., Massoud, M., 2014. Effects of Low Salinity Water Ion Composition on Wettability Alteration in Sandstone Reservoir Rock : A Laboratory Investigation 4, 34–41.
- Muecke, T.W., 1979. Formation fines and factors controlling their movement in porous media. *J. Pet. Technol.* 31, 144–150.
- Muller, N., Qi, R., Mackie, E., Pruess, K., Blunt, M.J., 2009. CO₂ injection impairment due to halite precipitation. *Energy Procedia* 1, 3507–3514. doi:10.1016/j.egypro.2009.02.143
- Nalawade, S.P., Picchioni, F., Janssen, L.P.B.M., 2006. Supercritical carbon dioxide as a green solvent for processing polymer melts: Processing

Bibliography

- aspects and applications. *Prog. Polym. Sci.* 31, 19–43.
doi:10.1016/j.progpolymsci.2005.08.002
- Nelson, P.H., 2009. Pore-throat sizes in sandstones, tight sandstones, and shales. *Am. Assoc. Pet. Geol. Bull.* 93, 329–340.
doi:10.1306/10240808059
- Patton, J.T., Phelan, P., Holbrook, S., 1981. CO₂ Formation Damage Study - First Annual Report. Las Cruces, New Mexico.
- Peksa, A.E., Wolf, K.H.A.A., Zitha, P.L.J., 2015. Bentheimer sandstone revisited for experimental purposes. *Mar. Pet. Geol.* 67, 701–719.
doi:10.1016/j.marpetgeo.2015.06.001
- Peysson, Y., 2012. Permeability alteration induced by drying of brines in porous media. *Eur. Phys. J. Appl. Phys* 60, 12.
doi:http://dx.doi.org/10.1051/epjap/2012120088
- Peysson, Y., André, L., Azaroual, M., 2014. Well injectivity during CO₂ storage operations in deep saline aquifers-Part 1: Experimental investigation of drying effects, salt precipitation and capillary forces. *Int. J. Greenh. Gas Control* 22, 291–300. doi:10.1016/j.ijggc.2013.10.031
- Portier, S., Rochelle, C., 2005. Modelling CO₂ solubility in pure water and NaCl-type waters from 0 to 300 °C and from 1 to 300 bar: Application to the Utsira Formation at Sleipner. *Chemical Geology* 217, 187–199.
doi:10.1016/j.chemgeo.2004.12.007
- Pruess, K., 2009. Formation dry-out from CO₂ injection into saline aquifers: 2. analytical model for salt precipitation. *Water Resour. Res.* 45, 1–6.
doi:10.1029/2008WR007102
- Pruess, K., Muller, N., 2009. Formation dry-out from CO₂ injection into saline aquifers 1: effects of solids precipitation and their mitigation. *Water Resour. Res.* 45, 1–11. doi:10.1029/2008WR007101
- Reeves, S.R., 2003. Enhanced CBM recovery, coalbed CO₂ sequestration assessed. *Oil gas J.* 101, 49–53.
- Reeves, S.R., 2001. Geological sequestration of CO₂ in deep, unmineable coalbeds: an integrated research and commercial-scale field demonstration project. SPE Annual Technical Conference and Exhibition. Society of Petroleum Engineers.

Bibliography

- Reichle, D., Houghton, J., Kane, B., Ekmann, J., 1999. Carbon sequestration research and development. Oak Ridge National Lab., TN (US); National Energy Technology Lab., Pittsburgh, PA (US); National Energy Technology Lab., Morgantown, WV (US).
- Riazi, M., Sohrabi, M., Jamiolahmady, M., Ireland, S., Brown, C., 2009. SPE 121170 Oil Recovery Improvement Using CO₂ — Enriched Water Injection. Proc. Int. Pet. Technol. Conf. 14070. doi:10.2523/14070-ABSTRACT
- Roels, S.M., El, N., Costas, C., Zitha, P.L.J., 2016. Capillary-Driven Transport of Dissolved Salt to the Drying Zone During CO₂ Injection in Homogeneous and Layered Porous Media. *Transp. Porous Media* 111, 411–424. doi:10.1007/s11242-015-0601-y
- Rojas, G., Ali, S.M., 1986. Scaled model studies of carbon dioxide/brine injection strategies for heavy oil recovery from thin formations. *J. Can. Pet. Technol.* 25.
- Rosenbauer, R.J., Koksalan, T., Palandri, J.L., 2005. Experimental investigation of CO₂-brine-rock interactions at elevated temperature and pressure: Implications for CO₂ sequestration in deep-saline aquifers. *Fuel Process. Technol.* 86, 1581–1597. doi:10.1016/j.fuproc.2005.01.011
- Sarkar, A., Sharma, M., 1990. Fines Migration in Two-Phase Flow. *J. Pet. Technol.* 42, 646–652. doi:10.2118/17437-PA
- Sayegh, S.G., Krause, F.F., Girard, M., DeBree, C., 1990. Rock/Fluid Interactions of Carbonated Brines in a Sandstone Reservoir: Pembina Cardium, Alberta, Canada. *SPE Form. Eval.* 5, 399–405. doi:10.2118/19392-PA
- Schembre-McCabe, J.M., Kamath, J., Gurton, R.M., 2007. Mechanistic studies of CO₂ sequestration. International Petroleum Technology Conference. International Petroleum Technology Conference.
- Sen, T.K., Khilar, K.C., 2006. Review on subsurface colloids and colloid-associated contaminant transport in saturated porous media. *Adv. Colloid Interface Sci.* 119, 71–96. doi:10.1016/j.cis.2005.09.001
- Sharma, M.M., Yortsos, Y.C., 1987. Fines migration in porous media. *AIChE J.* 33, 1654–1662.

Bibliography

- Shi, J.Q., Durucan, S., 2005. CO₂ storage in deep unminable coal seams. *Oil Gas Sci. Technol.* 60, 547–558. doi:10.2516/ogst:2005037
- Singh, N., 2008. Deep saline aquifers for sequestration of carbon dioxide, in: *International Geological Congress, Oslo*.
- Sokama-Neuyam, Y.A., Ursin, J., 2016. Experimental and Theoretical Investigations of CO₂ injectivity. *AGH DRILLING, OIL, GAS* 33, 245–257. doi:10.7494/drill.2016.33.2.245
- Sundal, A., Nystuen, J.P., Dypvik, H., Miri, R., Aagaard, P., 2013. Effects of Geological Heterogeneity on CO₂ Distribution and Migration-A Case Study from the Johansen Formation, Norway. *Energy Procedia* 37, 5046–5054.
- Tang, Y., Lv, C., Wang, R., Cui, M., 2016. Mineral dissolution and mobilization during CO₂ injection into the water-flooded layer of the Pucheng Oilfield, China. *J. Nat. Gas Sci. Eng.* 33, 1364–1373. doi:10.1016/j.jngse.2016.06.073
- Tang, Y., Yang, R., Du, Z., Zeng, F., 2015. Experimental study of formation damage caused by complete water vaporization and salt precipitation in sandstone reservoirs. *Transp. Porous Media* 107, 205–218.
- Tobergte, D.R., Curtis, S., 2013. Experimental Perspectives of Mineral Dissolution and Precipitation due to Carbon Dioxide-Water-Rock Interactions. *J. Chem. Inf. Model.* 53, 1689–1699. doi:10.1017/CBO9781107415324.004
- Tunio, S.Q., Tunio, A.H., Ghirano, N.A., El Adawy, Z.M., 2011. Comparison of different enhanced oil recovery techniques for better oil productivity. *Int. J. Appl. Sci. Technol.* 1.
- USDOE, 2007. *Carbon sequestration ATLAS of the United States and Canada*. US Dep. Energy, Off. Foss. Energy, Natl. Energy Technol. Lab.
- Vaidya, R.N., Fogler, H.S., 1990. Formation damage due to colloidally induced fines migration. *Colloids and Surfaces* 50, 215–229. doi:10.1016/0166-6622(90)80265-6
- Verdon, J.P., 2012. Microseismic Monitoring and Geomechanical Modelling of CO₂ Storage in Subsurface Reservoirs 55–81. doi:10.1007/978-3-642-25388-1

-
- Wilkinson, M., Haszeldine, R.S., Fallick, A.E., Odling, N., Stoker, S.J., Gatliff, R.W., 2009. CO₂-Mineral Reaction in a Natural Analogue for CO₂ Storage--Implications for Modeling. *J. Sediment. Res.* 79, 486–494. doi:10.2110/jsr.2009.052
- Wilson, A., 2015. CO₂ Low-Salinity Water Alternating Gas: A Promising New Approach for EOR. *J. Pet. Technol.* 67. doi:10.2118/0115-0084-JPT
- Yang, F., Bai, B., Tang, D., Shari, D.-N., David, W., 2010. Characteristics of CO₂ sequestration in saline aquifers. *Pet. Sci.* 7, 83–92.
- Yanuka, M., Dullien, F.A.L., Elrick, D.E., 1984. Serial sectioning and digitization of porous media for two-and three-dimensional analysis and reconstruction. *J. Microsc.* 135, 159–168.
- Zeidouni, M., Pooladi-Darvish, M., Keith, D., 2009. Analytical solution to evaluate salt precipitation during CO₂ injection in saline aquifers. *Int. J. Greenh. Gas Control* 3, 600–611. doi:10.1016/j.ijggc.2009.04.004
- Zuluaga, E., Muñoz, N.I., Obando, G. a, 2001. An Experimental Study to Evaluate Water Vaporisation and Formation Damage Caused by Dry Gas Flow Through Porous Media. SPE 68335.

Papers

Paper VI

The Impact of Fines Mobilization on CO₂ Injectivity: An Experimental Study.

Yen Adams Sokama-Neuyam, Pahmi U. R. Ginting, Bikram Timilsina, Jann Rune Ursin
University of Stavanger, Norway.

International Journal of Greenhouse Gas Control 65 (2017), 195 – 202.



Contents lists available at ScienceDirect

International Journal of Greenhouse Gas Control

journal homepage: www.elsevier.com/locate/ijggcThe impact of fines mobilization on CO₂ injectivity: An experimental study

Yen Adams Sokama-Neuyam*, Pahmi Utama Raja Ginting, Bikram Timilsina, Jann Rune Ursin

Institute of Petroleum Technology, University of Stavanger, NO-4036 Stavanger, Norway

ARTICLE INFO

Keywords:
CO₂ injectivity
Salt precipitation
Impairment
Fines mobilization
CO₂ storage

ABSTRACT

Adequate well injectivity is required to inject large volumes of CO₂ through minimum number of wells. Presently, salt precipitation is considered the main CO₂ injectivity impairment mechanism in deep saline reservoirs. However, mobilization of formation fines, generated from CO₂-brine-rock reactions, could plug the rock and induce CO₂ injectivity impairment. The unique gas-like viscosity and liquid-like density of CO₂, the drying effect of supercritical CO₂ and the high injection flow rates required to meet emission reduction targets, demands extension of the current knowledge base to adequately understand the mechanisms and impact of fines mobilization under typical CO₂ injection conditions.

The impact of fines mobilization on CO₂ injectivity was investigated by flooding sandstone cores initially saturated with mono-disperse colloid suspensions with dry supercritical CO₂. We found that about 0.5 wt.% particle concentration in the pore fluid reduced CO₂ injectivity by over 80 per cent. CO₂ injectivity impairment increased with increasing particle concentration and CO₂ injection flow rate. Initial rock permeability and average particle size was also found to influence particle entrapment. Attempt was made to quantify the relative importance of fines mobilization and salt precipitation. We also found that, about 0.3 wt.% particle concentration in the pore fluid, induced over two-fold injectivity impairment compared to about 10 wt.% of total dissolved salt in the formation water.

Since most of the current works assumes CO₂ injectivity is mainly impaired by salt precipitation, the present findings serves as a foundation to reconsider the contribution of transport effects such as fines mobilization.

1. Introduction

A suitable geologic formation for Carbon Capture, Utilization and Storage (CCUS) must have robust containment, adequate storage capacity and well injectivity to inject the desired quantity of CO₂ at acceptable rates through a minimum number of wells (IEA, 2013). Lombard et al. (2010) grouped CO₂ injectivity impairment mechanisms into three classes: Transport effects (fines mobilization, drying and relative permeability hysteresis), geochemical effects (dissolution and precipitation) and geomechanical effects. Extensive experimental and numerical studies have revealed significant injectivity reduction induced by brine vaporization and salt precipitation, especially near the wellbore (André et al., 2014; Cinar et al., 2009; Mahadevan et al., 2007; Ott et al., 2015; Pruess, 2009; Pruess and Muller, 2009; Zeidouni et al., 2009). However, these convincing findings seems to discourage the need to investigate other potential injectivity impairment mechanisms such as in-situ fines mobilization.

Carbonates, feldspars and other clay cements in sandstones could be attacked and dissolved by carbonic acid generated by in-situ CO₂-brine reactions (Patton et al., 1981; Sayegh et al., 1990; Tobergte and Curtis,

2013). CO₂-brine-rock batch reaction under conditions relevant to CCUS have shown various amounts of dissolved minerals in solution (Dawson et al., 2015; Ilgen and Cygan, 2016; Kaszuba et al., 2005; Tobergte and Curtis, 2013). In the absence of dynamic forces, mineral dissolution could increase porosity and permeability by etching new pore spaces or widening narrow pore channels, thus temporarily increasing the injectivity (Lombard et al., 2010; Miri, 2015). However, some of the minerals in solution could aggregate into tiny particles in the bulk liquid or form a scale on the pore walls. If the mineral grains are mobilized along the flowing stream, CO₂ injectivity could be severely impaired through plugging of the reservoir rock.

The mechanisms of fines migration in porous media have been studied extensively (Aji, 2014; Gabriel and Inamdar, 1983; Khilar and Fogler, 2010; Muecke, 1979; Scheuerman and Bergersen, 1990; Sharma and Yortsos, 1987). Sarkar and Sharma (1990) investigated fines migration in two-phase flow including the role of wettability and relative permeability. Scheuerman and Bergersen (1990) suggested criteria for optimizing ionic content of injection water to prevent the release of formation fines. Parameters underlying the release and transport of fines have also been identified (Aji, 2014; Khilar and

* Corresponding author.

E-mail address: yen.a.sokama-neuyam@uis.no (Y.A. Sokama-Neuyam).<http://dx.doi.org/10.1016/j.ijggc.2017.08.019>Received 30 September 2016; Received in revised form 2 August 2017; Accepted 28 August 2017
1750-5836/© 2017 Elsevier Ltd. All rights reserved.

Nomenclature		PV	Pore volume
CCUS	Carbon capture, utilization and storage	Δp_i	Initial pressure drop across the core
I	Injectivity	Δp_f	Final pressure drop across the core
K_i	Initial permeability	q_i	Initial injection volumetric flow rate
K_f	Final permeability	q_f	Final injection volumetric flow rate

Fogler, 2010; Scheuerman and Bergersen, 1990; Sharma and Yortsos, 1987). The entrapment of fines in porous media has been found to depend on characteristics of the fine particles, the porous medium and the permeating fluid in which the particles are suspended (Aji, 2014; Sen and Khilar, 2006; Vaidya and Fogler, 1990). The pore structure, size and concentration of fines and the hydrodynamic and colloidal conditions of the suspending medium have also been identified as the deciding parameters. Various levels of permeability and well productivity reduction induced by migratory fines in both consolidated and unconsolidated rocks have also been reported (Gruesbeck and Collins, 1982; Khilar and Fogler, 1983; Sarkar and Sharma, 1990; Sharma et al., 1985; Vaidya and Fogler, 1990).

Supercritical CO₂ has unique combination of gas-like viscosity and liquid-like density (Nalawade et al., 2006) and these properties could influence fines transport. However, the direct effect of the physical and chemical characteristics of supercritical CO₂ on particle transport is beyond the scope of this study. The present work is focused on quantifying the impact of particle entrapment on the magnitude of CO₂ injectivity. Therefore, the objective of the present study is to investigate the impact of fines plugging on CO₂ injectivity and compare the transport effects to the impact of salt precipitation. We present results from core-flood experiments, where dry supercritical CO₂ was injected into sandstone cores initially saturated with mono-disperse colloid suspensions. Pressure drop profiles were monitored during CO₂ injection and injectivity impairment induced by fines entrapment was estimated. The effect of particle concentration, CO₂ injection rate and rock permeability on fines mobilization and CO₂ injectivity were investigated. We then attempted to evaluate the relative impact of fines mobilization and salt precipitation on CO₂ injectivity.

2. Materials and methods

2.1. Rock samples and fluids

Two types of sandstone rocks with similar porosity but different permeability were used in the experiments. Each type of core-plugs were drilled from the same outcrop block in the same direction and can be considered homogeneous with respect to permeability in the linear direction. Berea sandstone core samples were selected as the main reservoir rock because of their suitable range of permeability (60–100mD) and porosity (19–20%). Kirby sandstone samples were used to study effect of permeability as they have almost the same range of porosity (19–20%) but relatively lower permeability (8–9mD). The cylindrical core samples were 20 cm long and 3.81 cm in diameter.

The non-wetting fluid is liquefied CO₂ with purity percentage of about 99.7. For liquid CO₂, the fluid was injected at 80 bar and 26 °C. Liquid CO₂ was used to measure the rock permeability before and after the core was exposed to fines entrapment because it is neutral to both the colloidal particles and the rock samples. The core saturated with the colloid particles was flooded with supercritical CO₂ at 80 bar and 50 °C to displace the particles.

Two types of brine were used in the experiments. A 5 g/L (0.086 M) NaCl brine was used to dilute the concentrated colloid stock solution into mono-disperse colloidal suspensions with specific particle concentrations. Below a critical salt concentration (CSC) of about 0.071 M, NaCl brine could interact with and possibly detach formation fine particles from the pore walls into the flowing stream (Khilar and Fogler,

1984). Brine concentration of 0.086 M is adequately above the CSC for fines detachment and also low enough to prevent salt precipitation from brine vaporization. To investigate the effect of brine vaporization and salt precipitation on CO₂ injectivity, we used synthetic formation water (FW) with 10.09 wt.% of total dissolved salt and salinity of 105.5 g/L (NaCl 77.4 g/L; CaCl₂·2H₂O 21.75 g/L; MgCl₂·6H₂O 3.56 g/L; SrCl₂·6H₂O 2.25 g/L; Na₂SO₄ 0.13 g/L; KCl 0.42 g/L) (Fjelde et al., 2014). This brine did not contain colloids.

Mono-disperse colloid suspensions were prepared from concentrated fumed alumina latex particles stock solution. Alumina was selected for this study because of its high resistance to wear and its stability in CO₂ and organic and inorganic solvents. They are oil wet particles and this minimizes attachment to the rock surface. The particles were stabilized in low salinity brine at near-neutral pH conditions to prevent particle aggregation. Typical formation fines have average particle diameter between 0.01 μm and 1 μm (Khilar and Fogler, 2010). Two particle sizes were selected for the experiments: I and II with average particle diameter of 0.08 μm and 0.14 μm respectively. Characteristics of the colloid stock solution are presented in Table 1. Mono-disperse suspensions with specific mass concentration were prepared from the stock solution.

2.2. Experimental set up and methodology

The cylindrical core sample, wrapped in a tight rubber sleeve was loaded into the horizontal Hassler core holder and positioned in the oven at controlled temperature (Fig. 1). A confinement pressure of about 150 bar was applied in the annular space between the core and the core holder. A differential pressure gauge and a pressure transducer were connected across the core holder to monitor the pressure drop across the core and the pore pressure respectively. An ISCO CO₂ pump receives liquid CO₂ from the gas container through a pressure regulator. Depending on the injection conditions, either liquid or supercritical CO₂ are injected. The Quizix pump deliver brine through a connected piston cell into the inlet. The injected fluid passes a long coiled tubing, positioned in the oven, to hold the fluid and secure a preset temperature in the oven. A backpressure of 80 bar was set at the outlet, during CO₂ injection and the effluent fluid was safely collected in a piston cell for analysis and safe disposal.

The core samples were initially dried in an oven at 60 °C for about 24 h to remove moisture. The experiment consists of the following steps:

1. Measurement of initial liquid CO₂ pressure drop (ΔP_i) and permeability (K_i) across the clean core sample.
2. Saturating the core with either brine or colloidal suspension.

Table 1
Characteristics of fumed alumina stock solution used to prepare the colloid suspensions. Colloids with different particle size were used in the experiment: type I and II.

	I	II
Particle size (μm)	0.08 μm	0.14 μm
Al ₂ O ₃ content (%)	39–41	29–31
Viscosity (mPa/s)	< 70	< 2000
pH	6.0–9.0	3.0–5.0
Density (g/cc)	1.39	1.26

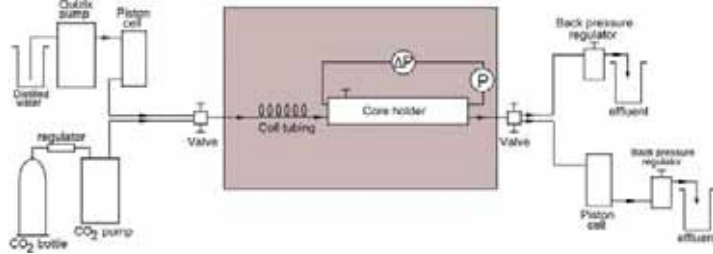


Fig. 1. Experimental set-up for the CO₂ core-flooding experiments.

3. Supercritical CO₂ flooding and drying of the core sample.
4. Measurement of the final liquid CO₂ pressure drop (ΔP_f) and permeability (K_f).

To prevent CO₂ leakage, the core sample was wrapped in Teflon tape and tightly covered in shrinking plastic sleeve before it was mounted in the Viton membrane inside the cell. In step 2, the core was either saturated with FW to investigate salt precipitation effects or mono-disperse colloid suspension to study the impact of fines migration. In step 3, about 40 pore volumes (PV) of supercritical CO₂ was injected into the core at constant injection rate to displace the saturating fluid and dry the core sample. Pressure drop profiles were closely monitored during supercritical CO₂ flooding.

3. Results

3.1. Estimation of injectivity impairment

During supercritical CO₂ flooding, pressure drop profiles were recorded to monitor the resistance to flow associated with particle displacement and entrapment. Detailed 3D analysis of pore-scale events can be obtained from direct X-ray scanning, SEM, μ CT imaging and other advanced analytical methods (Bacci et al., 2013; Ott et al., 2015; Peysson et al., 2014; Roels et al., 2014). These advanced analytical scanning techniques could have provided information on the accumulation and distribution of minerals within the rock. However, the most important parameter in the present work is the resistance offered to fluid flow by the entrapped minerals. This parameter can be estimated by measuring the change in absolute permeability. To understand the evolution of permeability and injectivity during the flooding process, pressure drop profiles were monitored during supercritical CO₂ injection.

Fluid injectivity, I , is defined as the ratio of volumetric injection flow rate, q , to the pressure drop, Δp . Assuming the core has constant absolute permeability k_i and k_f before and after it was exposed to precipitated minerals respectively and that viscosity of the fluid used in the measurement (liquid CO₂) can be considered constant, the injectivity, before and after mineral entrapment can be expressed from Darcy's law as:

$$I_i = \frac{q_i}{\Delta p_i} = k_i \cdot C \quad (1)$$

$$I_f = \frac{q_f}{\Delta p_f} = k_f \cdot C \quad (2)$$

In Eqs. (1) and (2), C is a constant defined as $C = \frac{A}{\mu L}$, for constant A and L . If liquid CO₂ is injected at a constant rate during injectivity measurements ($q_i = q_f$), we define a Relative Injectivity Change (RIC) index as:

$$RIC = \left(\frac{I_i - I_f}{I_i} \right) = 1 - \left(\frac{I_f}{I_i} \right) \quad (3)$$

Substituting Eqs. (1) and (2) into (3) yields:

$$RIC = 1 - \left(\frac{\Delta p_i}{\Delta p_f} \right) = 1 - \left(\frac{K_f}{K_i} \right) \quad (4)$$

Plugging of the pores by precipitated minerals or fines would reduce the flow area and increase pressure drop across the core, Δp . Thus, in Eq. (4), $\Delta p_f > \Delta p_i$ and $K_i > K_f$ after permeability impairment. Therefore, a positive RIC value indicates injectivity impairment. RIC was expressed as a percentage in the current work. Although the RIC can be considered a rather linear injectivity measurement technique, it is an indirect method for estimating injectivity impairment independent of the chemical properties of the pore-plugging material. This is particularly useful as a neutral technique to compare the effects of fines plugging and salt deposition.

3.2. Uncertainty analysis

Particle transport in natural porous media is a highly uncertain process. The particles are displaced in a highly random flow path into very tortuous pore network distribution. Therefore, the repeatability of particle flow experiments in even homogeneous natural rocks is expected to be low. However, attempt was made to quantify and minimize uncertainty in the measurements.

For pressure drop $\Delta p = y$, the measured data was reported as:

$$y_{measured} = y_{avg} \pm \Delta y_{avg} \quad (5)$$

In Eq. (5), y_{avg} is the mean value of the stabilized liquid CO₂ Δp across the core before and after supercritical CO₂ injection, mineral precipitation and potential particle entrapment and Δy_{avg} is the estimated uncertainty in y_{avg} . Initial and final pressure drop measurements are recorded when liquid CO₂ pressure drop across the core become stable. y_{avg} and Δy_{avg} are calculated from:

$$y_{avg} = \frac{\sum y}{N} \quad (6)$$

$$\Delta y_{avg} = \frac{y_{max} - y_{min}}{\sqrt{N}} \quad (7)$$

In Eqs. (6) and (7), N is the total number of recorded data points, y_{max} and y_{min} are the maximum and minimum pressure drop values respectively.

The uncertainty in pressure drop was found to depend on the differential pressure gauge, injection flow rate and the type of mineral plugging. A very sensitive differential pressure gauge which measures to an accuracy of about 0.009% was used. We found that, low injection flow rate minimized the uncertainty. Similarly, colloidal entrapment induced higher uncertainty compared to salt precipitation. Injection flow rate of about 5 ml/min was found to be optimal liquid CO₂ injection rate for the measurements. The minimum estimated uncertainty (4%) was associated with salt precipitation and maximum uncertainty (9%) for particle transport experiments. However, the maximum uncertainty of 9% was applied across board, assuming a worst-case

scenario.

3.3. Drying and salt precipitation

Brine vaporization and salt precipitation are almost inevitable when dry gas is injected into saline formations. Therefore, to effectively study the impact of fines mobilization on CO₂ injectivity, water vaporization and salt precipitation effects must be decoupled.

Formation fines are either attached to the pore walls or interspersed in the pore liquid (Khilar and Fogler, 2010; Sen and Khilar, 2006). Initially, injected CO₂ might immiscibly displace the colloid suspension where particle entrapment could reduce CO₂ injectivity. During immiscible two-phase displacement, brine vaporization into the gaseous phase is minimal (Miri and Hellevang, 2016; Miri et al., 2015; Ott et al., 2015; Roels et al., 2016). However, at irreducible brine saturation, brine vaporization could dry the rock and precipitate salts. Therefore, under typical storage conditions, fines plugging and salt precipitation could simultaneously impair CO₂ injectivity.

First, we investigated the effect of salt precipitation in Berea Sandstone core. The clean core with known initial permeability was saturated with FW – synthetic formation brine representative of North-Sea reservoir pore fluid. About 40 PV of dry supercritical CO₂ was injected into the saturated core at injection flow rate of 2 ml/min. Pressure drop profiles were recorded during supercritical CO₂ flooding. After drying and potential salt precipitation, the permeability of the core was measured to compute the effect of salt deposition on injectivity. The experiment was then repeated at 5 ml/min and 10 ml/min. Recorded pressure drop profiles and estimated injectivity impairment induced by salt precipitation are presented in Fig. 2.

The pressure drop profiles show three distinct periods during the drying process (Fig. 2(A)). First, the pressure drop declines sharply, then a more gradual decline period is observed after about 5 PV of CO₂ injection followed by constant pressure drop towards the end of the experiment. The sharp linear decline period corresponds to two-phase immiscible displacement of brine. As brine is replaced with supercritical CO₂, the pressure drop declines sharply until CO₂ breakthrough at the outlet. This period is also relatively short (about 5 PV) because it terminates when producible brine within the inter-connected pores have been evacuated. Brine evaporation during two-phase displacement is minimal (Miri and Hellevang, 2016). The second period is dominated by capillary backflow of brine when capillary pressure gradient overcomes the injection pressure gradient and drive water towards the evaporation front (Ott et al., 2015; Peysson et al., 2014; Roels et al., 2016). At residual brine saturation, water evaporates into the CO₂ stream, increasing the salt concentration of the trapped brine. When the concentration of brine exceeds supersaturation, salt is precipitated (Zuluaga et al., 2001). The third period is probably dominated by salt precipitation at residual brine saturation.

Supercritical CO₂ injection rate strongly influence the pressure drop profiles (Fig. 2(A)). The two-phase displacement period was shorter for high CO₂ injection rates as brine displacement speed increased. Under laminar flow conditions, pressure drop is proportional to volumetric flow rate. The pressure drop curves show strong proportionality between volumetric CO₂ injection rate and pressure drop as expected.

An average of about 26% injectivity impairment was induced by the drying process (Fig. 2(B)). Practically, supercritical CO₂ injection rate did not impose a marked influence on injectivity loss. Increasing the CO₂ injection rate, increases the speed of brine displacement and the drying rate. However, the solid salt saturation depends mainly on brine salinity and irreducible brine saturation. Brine vaporization at irreducible water saturation is the dominant mechanism for salt precipitation under linear flow conditions. For near-homogeneous cores, residual brine saturation is almost the same in the core samples regardless of CO₂ injection rate. Probably, this is why the tested range of gas injection rate did not seem to affect injectivity impairment markedly.

3.4. Fines mobilization

To investigate the effect of fines mobilization on CO₂ injectivity, the core samples were initially saturated with mono-disperse colloid solution. We did not analyze the pore size distribution of the sandstone used in this study. However, studies conducted on similar Berea sandstone rocks suggest an average pore throat size of about 2 μm (Nelson, 2009). The two sets of colloids used in this work have average particle sizes of 0.08 μm and 0.14 μm yielding average jamming ratio (particle size/pore size) of about 0.04 and 0.07 respectively. Natural formation fine particles have average particle sizes in the regions of 1 μm (Khilar and Fogler, 2010). However, dissolution of sandstone minerals under typical CO₂ storage conditions may yield particles of varying sizes over a wide range depending on the reaction conditions and composition of the rock mass.

Khilar and Fogler (2010) reported that particles with jamming ratio between 0.04 and 0.07 could be entrapped (Table 2). Particles within this size range could plug the rock through surface deposition, pore bridging and multi-particle blocking. If the particles are stabilized in the suspending fluid, surface deposition would be greatly reduced and at very low particle concentration, the chances of pore bridging and multi-particle blocking could be greatly minimized. Therefore, the particles would stay mono-disperse within the pore spaces after saturation and prior to CO₂ injection. When CO₂ invades the fluid-filled pores, the stability of the particles in the colloid will be disturbed thereby releasing the particles for plugging during CO₂ flooding. This is assumed to be comparable to CO₂ injection into a reservoir where the formation brine contains fine particles.

The CO₂ injection flow rates adopted in this work eliminates or at least minimizes all known likely chemical reactions during flooding. Therefore, we focus on investigating the physical effects of colloidal transport in the porous medium and the subsequent effect of fines

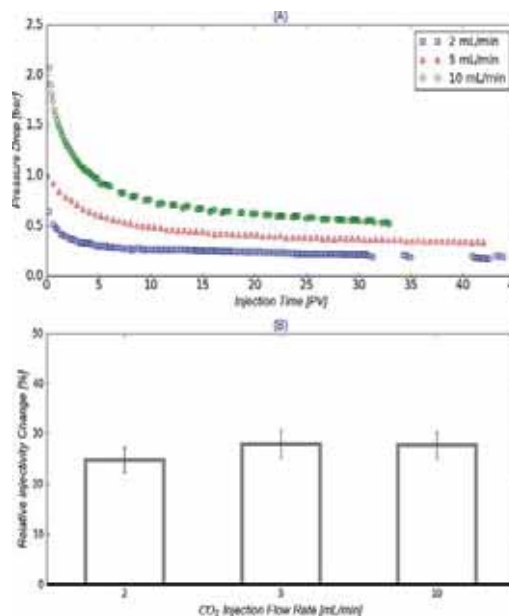


Fig. 2. (A) Pressure drop profiles recorded during supercritical CO₂ injection into Berea Sandstone core initially saturated with FW. Generally, pressure drop decreased with injection time for supercritical CO₂ injection rates of 2 ml/min, 5 ml/min and 10 ml/min. (B) Estimated injectivity impairment induced by salt precipitation as a function of CO₂ injection flow rate. The RIC did not show a marked change with CO₂ injection flow rate.

Table 2

Dependence of pore plugging or piping on the ratio of size of fines to size of pore constrictions (Khilar and Fogler, 2010).

Fines size/Pore Size	Occurrence
≥ 1	Plugging due to blocking or size exclusion
0.1 to 0.6	Plugging due to bridging, and multi-particle blocking
0.04 to 0.10	Plugging due to surface deposition, bridging, and multi-particle blocking
0.01 to 0.04	Surface deposition and multi-particle blocking
Less than 0.01	Piping

plugging on CO₂ injectivity. Some important parameters considered are the effect of rock permeability, CO₂ injection rate, particle concentration and particle size.

3.4.1. Effect of particle concentration

Two Berea sandstone cores were used to investigate the effect of particle concentration on CO₂ injectivity. In each experiment, the core sample was initially saturated with colloid solution of particle size 0.08 μm and concentrations of 0.3 wt.% and 0.5 wt.%. Results from the salt precipitation experiment presented in Section 3.3, was used as reference (labelled FW). About 40 PV supercritical CO₂ was injected into the colloid-saturated core at a constant rate of 5 ml/min until all producible liquid was drained. During CO₂ flooding, pressure drop profiles were recorded in real time to study the transport process (Fig. 3(A)) and the effect of fines mobilization on CO₂ injectivity was estimated and displayed in Fig. 3(B).

Generally, the pressure drop profiles for particle transport followed a trend comparable to the pressure drop profiles of brine displacement and salt precipitation: an early sharp decline rate, followed by gradual decline and constant pressure drop. However, at 0.5 wt.% particle concentration, the constant pressure drop period was not observed. This is probably due to particle dislodgement after brine advection. At dry-out, the entrapped particles in the pore channels could be dislodged and redistributed by injected CO₂ and this might continue to alter the pressure drop. At low particle concentration, the effect of particle dislodgement on pressure drop might not be significant as fewer trapped particles are available to be displaced. We also observe pressure drop was significantly higher for high particle concentrations as the likelihood of fines entrapment increases with particle concentration. Therefore, the pressure drop profiles did not follow the same rate-pressure proportionality relationship observed in the salt precipitation experiments.

From Fig. 3(B), injectivity impairment increased by about 11 percentage points when concentration of mono-disperse particles in solution was increased from 0.3 wt.% to 0.5 wt.%. While salt precipitation from FW reduced injectivity by about 26.8%, particle concentration of 0.3 wt.% reduced injectivity by 74.9% through fines entrapment and plugging of the pore channels.

When CO₂ invade the pores, resident mono-disperse particles may plug the narrow pore channels through bridging, surface deposition or multi-particle blocking. Khilar and Fogler (2010) reported that when the jamming ratio is in the range of 0.01 and 0.1, the concentration of particles will be a key parameter in determining whether entrapment or piping occurs. As particle concentration increases, the distance between suspended particles shortens, enhancing multi-particle blocking of the invaded pores. In salt precipitation, the deposited salts form a coating that reduce the pore spaces but during fines entrapment, several particles could accumulate in a pore channel and completely plug the pore. This is probably why even low concentration of fine particles had higher impact on injectivity compared to salt precipitation.

3.4.2. Effect of CO₂ injection rate

Supercritical CO₂ injection rate of 2 ml/min and 10 ml/min were investigated by initially saturating the Berea sandstone cores with

0.5 wt.% colloidal brine solution prepared with 0.08 μm particles. Pressure drop profiles and estimated injectivity reduction data are presented in Fig. 4.

At the onset of the experiments, when CO₂ injection flow rate was raised from 2 ml/min to 10 ml/min, the pressure drop increased by about 50 bar (Fig. 4(A)). However, the difference in pressure drop decreased as more PV of CO₂ was injected. At residual liquid saturation, the difference in pressure drop reduced to less than 10 bar. Plugging of the rock during fines migration is a random process and as fluxes increase, the randomness of particle movement increases. At high CO₂ injection rate, increased random movement of particles could introduce a more heterogeneous plugging of the pores thereby increasing the pressure drop. In addition, the constant pressure drop period was not observed at 10 ml/min flow rate probably because of particle dislodgement at residual liquid saturation. High injection rate increases drag and particle dislodgement which probably continued to fluctuate the pressure drop even at dry-out.

Increasing the CO₂ injection flow rate from 2 ml/min to 10 ml/min induced about 14 percentage points of additional injectivity impairment (Fig. 4(B)). At injection low flow rate and high particle density, the particles could settle at the bottom of the pore space. For the particles selected for this work, Brownian motion may dominate particle movements. High flow rate increases random particle movements and induces heterogeneous plugging. However, at high injection velocity, the particles bridging the pore channels could be dislodged by the high fluxes which could open some of the plugged channels. At lower flow rates, the rate of dislodgement of plugged particles could be reduced but the fluxes are not high enough to randomly lift particles into narrow pore channels which results in a more uniform plugging of the pore channels.

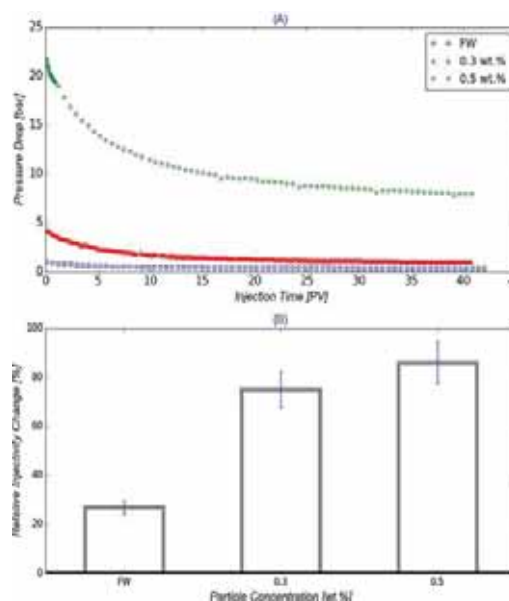


Fig. 3. (A) Pressure drop profiles of supercritical CO₂ injection into Berea Sandstone cores initially saturated with 0.3 wt.% and 0.5 wt.% colloid solutions with average particle size of 0.08 μm . The pressure drop profiles were then compared to the pressure drop profile recorded in Section 3.3 where the core was saturated with FW prior to CO₂ injection. A constant CO₂ injection rate of 5 ml/min was maintained through the experiments. (B) The impact of particle concentration on the Relative Injectivity Change. Injectivity impairment increased when the concentration of mono-disperse particles in the resident brine was increased.

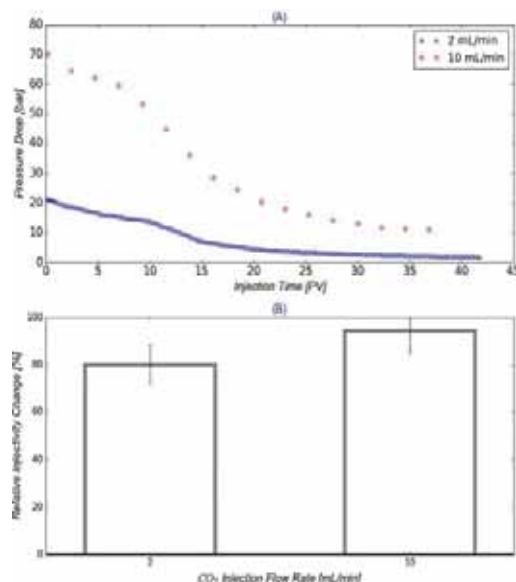


Fig. 4. (A) Pressure drop profiles of supercritical CO₂ injection into Berea sandstone core initially saturated with brine containing 0.5 wt.% mono-disperse particle with average particle diameter of 0.08 μm . Two experiments were conducted at constant supercritical CO₂ injection rates of 2 ml/min and 10 ml/min. (B) Estimated Relative Injectivity Change measured as function of CO₂ injection flow rate. CO₂ injectivity impairment increased when the injection flow rate was increased from 2 ml/min to 10 ml/min.

3.4.3. Effect of core permeability

Berea (64 mD) and Kirby (9 mD) sandstone core samples were initially saturated with 0.5 wt.% colloid solution with average particle size of 0.08 μm . Supercritical CO₂ was injected at 5 ml/min flow rate. Fig. 5 shows the recorded pressure drop profiles and estimated injectivity impairment.

From Fig. 5(A), pressure drop was higher in Berea compared to Kirby. The pressure drop profile for Kirby displayed very gradual and almost linear decline, deviating from the three-stage pressure decline observed in the previous tests. The 9 mD Kirby core has narrower pore channels and therefore should be more susceptible to plugging. Therefore, we expected a higher pressure drop in Kirby than the Berea core. However, during colloid saturation, a filter cake was built at the inlet of the Kirby core (Fig. 6). Some particles in solution were filtered at the inlet of the core due to the narrow pore channels and probably only few particles entered the core. Under storage conditions, the dissolved rock particles may have already been deposited into the pore fluids and therefore filter cake might not form within the rock. However, if the wellbore fluids contain fine particles, filter cake could be deposited at the injection inlet depending on the rock permeability.

If the particle size is equal to or greater than the size of the pore throat, entrapment or filtration of fine particles will inevitably occur (Khilar and Fogler, 2010). Injectivity impairment was about 28 percentage points higher in Berea core compared to Kirby (Fig. 5(B)). The filter cake at the inlet of the Kirby core was removed and cleaned properly before the final permeability was measured to reduce the impact of the filtrate on CO₂ injectivity. The filtration of particles will obviously reduce the concentration of particles available for entrapment and plugging. With large number of particles filtered out, 57.5% injectivity impairment in the Kirby core is higher than expected. But with 9 mD permeability, Kirby is probably characterized by a high percentage of narrow pore constrictions where the particles that made

their way into the core will have high chances of being entrapped.

3.4.4. Effect of particle size

To investigate the effect of particle size on injectivity impairment, the Berea sandstone core was initially saturated with 0.5 wt.% mono-disperse colloid solution with average particle size of 0.14 μm . Supercritical CO₂ was injected into the core at a rate of 5 ml/min to displace the colloids and mobilize fine particles. Fig. 7 shows injectivity loss as a function of particle size.

In the process of saturating the core sample with the liquid suspension, we found that a filter cake was deposited at the inlet of the core. The effluent liquid concentration was found to be lower than the concentration of the inlet solution. Because of the increased particle size, some particles could not penetrate the narrow pore channels at the inlet. However, some of the particles flowed through the open pore channels into the core. The filter cake was cleaned properly before final permeability was measured.

Fig. 7 shows that injectivity loss decreased by about 24 percentage points when the particle size was increased from 0.08 μm to 0.14 μm . The filtration of particles at the inlet reduced the concentration of particles in the saturating solution. During displacement, fewer particles in the open pore channels were probably mobilized. With fewer mobilized particles, the effect on petrophysical properties of the rock was reduced and probably that is why CO₂ injectivity loss was lower. Practically, filtration at the injection inlet might increase pressure drop in the near well vicinity even at high CO₂ injection rates. If the filter cake was not removed, the measured injectivity loss could have been higher.

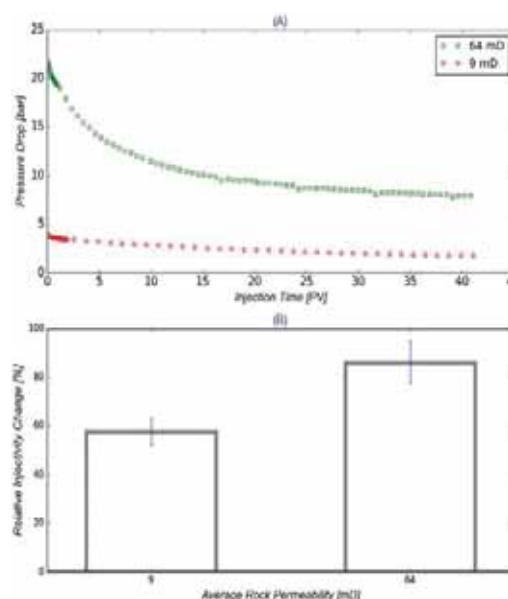


Fig. 5. (A) Pressure drop profiles of supercritical CO₂ injection into Sandstone cores initially saturated with 0.5 wt.% colloid solution with average particle size of 0.08 μm . Berea and Kirby sandstone cores with almost the same porosity but permeability of 64 mD and 9 mD respectively were used in the study. Constant CO₂ injection rate of 5 ml/min was maintained through the experiments. (B) Estimated CO₂ injectivity impairment as a function of average rock permeability. Injectivity impairment was low in Kirby because of particle filtration at the inlet of the core.



Fig. 6. A picture showing filter cake (white substance) formed at the core inlet during injection of 0.5 wt.% colloidal solution containing 0.08 μm size particles into Kirby sandstone core. The narrow pore channels in Kirby core prevented some of the particles from penetrating the inlet of the core.

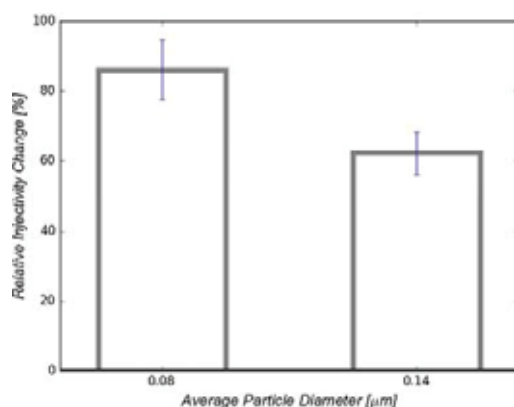


Fig. 7. Estimated Relative Injectivity Change as a function of colloid particle average diameter when supercritical CO_2 was injected into Berea sandstone core that was initially saturated with 0.5 wt.% colloidal solution. CO_2 was injected at a constant injection flow rate of 5 ml/min. Injectivity impairment decreased when particle size was increased from 0.08 μm to 0.14 μm due to filtration of particles at the core inlet.

4. Discussion and practical implications

Analysis of pressure drop profile presented in the previous section, suggest that mechanisms of immiscible displacement and drying are similar for CO_2 -brine and CO_2 -colloid flooding within the current experimental conditions. Although attempt was made to decouple salt precipitation and fines mobilization effects, under typical storage conditions in deep saline reservoirs, both mechanisms could impair CO_2 injectivity simultaneously, especially in the wellbore vicinity. During reinjection of CO_2 , if the pore fluid contains fine particles, the rock could be plugged during immiscible CO_2 -brine displacement. At irreducible brine saturation, injectivity impairment could be compounded by brine vaporization and salt precipitation. While salt precipitation within the plugged pores could be limited by flow restrictions, the injected CO_2 could also dislodge plugged particles if the interstitial flow velocity is above the minimum velocity required to lift and displace the particles. It is not clear how these two seemingly opposing processes

will impact the overall injectivity. However, the drying effect of supercritical CO_2 presents additional challenges to the mechanisms of fines mobilization under typical CO_2 storage conditions.

Although, a field-scale simulation is required to fully understand the impact of fines mobilization on injectivity, the effects of fines entrapment could be lessened under radial flow conditions where flow velocity decreases more into the formation. Although CO_2 injection rates under storage conditions are high, as the gas moves into the formation, the resultant flow velocity might lag the minimum lift velocity of particles generated at the interface between the CO_2 plume and formation brine away from the wellbore. Mineralization and potential particle generation are expected to be predominant within the formation compared to the wellbore vicinity. However, the present work has shown that even small amount of particles in the wellbore fluid or the pore fluid within the immediate injection area could induce dramatic injectivity impairment.

The force required to lift particles, depends on the density of the fluid, the square of the velocity, viscosity and compressibility of the fluid and the size and shape of the particles (NASA, 2017). The gas-like viscosity and liquid-like density of supercritical CO_2 increases the hydrodynamic force acting on the particles. Typical CO_2 injection rates under storage conditions is around 1Mt/pa (Ghaderi et al., 2009). For example, CO_2 injection rate in the Weyburn project is between 74 and 588 t per day per well (Verdon, 2012). To meet global emission reduction targets, higher CO_2 injection rates will be required. Under such high injection flow rates, plugging through pore-bridging could be pushed into the formation as drag forces will tend to break pore bridges around the wellbore vicinity where fluxes are very high. Only pores plugged through size-exclusion are likely to remain plugged in the immediate injection area. Consequently, salt precipitation effects could be the dominant mechanism of injectivity impairment in the immediate injection area. Therefore, the nature of the plugging and the distribution of entrapment will also depend to a large extent on the size of particles generated. Again, further work is required to understand the nature of fines entrapment under these extreme conditions and the impact on CO_2 injectivity. Thus, the current literature on fines mobilization needs to be extended to fully understand the impact of the unique properties and conditions of CO_2 injection under typical storage conditions.

5. Conclusions

Mineral dissolution induced by CO_2 -brine-rock reactions could generate fine particles into the pore fluid. During CO_2 injection, these fine particles could be lifted into the reservoir and possibly plug the pore channels depending on the petrophysical characteristics of the rock, the size of the particles and the hydrodynamic conditions. Entrapment of fine particles in the pore constrictions could severely reduce permeability and consequently CO_2 injectivity. Other probable sources of fine particles during CO_2 injection include drilling fluids and casing cements.

We flooded sandstone cores initially saturated with mono-disperse colloidal solutions with supercritical CO_2 to investigate the impact of fines mobilization on CO_2 injectivity. The experiments were designed to adequately represent fines mobilization under CO_2 storage conditions. Important governing parameters were identified and studied. Some highlights of the work include the following:

- Fines mobilization could be more severe to CO_2 injectivity impairment compared to drying and salt precipitation under linear flow conditions. About 0.3 wt.% particle concentration in the pore fluid, induced up to two-fold injectivity impairment compared to about 10 wt.% of total dissolved salt in the pore water.
- CO_2 injectivity impairment increased with increase in fine particle concentration. About 1.0 wt.% of particle concentration in the formation fluid plugged the rock completely.

- CO₂ injection rate did not impose a marked impact on CO₂ injectivity reduction induced by fines entrapment.
- Depending on the particle size and rock permeability, fine particles could form filter cake at the core inlet.

The unique gas-like viscosity and liquid-like density of supercritical CO₂ and the high injection flow rates required to meet emission reduction targets presents the need to extend current knowledge base to adequately understand the mechanisms and impact of fines mobilization under typical CO₂ injection conditions. In addition, the drying effect of supercritical CO₂ makes salt precipitation almost inevitable during fines mobilization. The coupled effect of these mechanisms also require further studies. The present work serves as a preliminary investigation to quantify the impact of fines mobilization on CO₂ injectivity as compared to salt precipitation effects under linear flow conditions. Attempt was also made to identify some practical implications of the current findings.

Acknowledgements

The authors would like to acknowledge PGNiG Upstream International AS, Norway and the Institute of Petroleum Technology (IPT) of the University of Stavanger for funding the project.

References

- Aji, K., 2014. The experimental and theoretical study of fines migration in porous media under particle-rock repulsion and attraction Kaiser Aji. A Thesis Submitted for the Degree of Doctor of Philosophy (PhD) October 2014.
- André, L., Peysson, Y., Azaroual, M., 2014. Well injectivity during CO₂ storage operations in deep saline aquifers – Part 2: numerical simulations of drying, salt deposit mechanisms and role of capillary forces. *Int. J. Greenh. Gas Control* 22, 301–312. <http://dx.doi.org/10.1016/j.ijggc.2013.10.030>.
- Bacci, G., Durucan, S., Korre, A., 2013. Experimental and numerical study of the effects of halite scaling on injectivity and seal performance during CO₂ injection in Saline aquifers. *Energy Procedia* 37, 3275–3282. <http://dx.doi.org/10.1016/j.egypro.2013.06.215>.
- Cinar, Y., South, N., Riaz, a., Tchelepi, H.a., 2009. Experimental study of CO₂ injection into Saline formations. *SPE J.* <http://dx.doi.org/10.2523/110628-MS>.
- Dawson, G.K.W., Pearce, J.K., Biddle, D., Golding, S.D., 2015. Experimental mineral dissolution in Berea Sandstone reacted with CO₂ or SO₂-CO₂ in NaCl brine under CO₂ sequestration conditions. *Chem. Geol.* 399, 87–97. <http://dx.doi.org/10.1016/j.chemgeo.2014.10.005>.
- Fjelde, I., Omekeh, A.V., Sokama-Neuyam, Y.A., 2014. Low salinity water flooding: effect of crude oil composition. *SPE Improv. Oil Recover. Symp.* <http://dx.doi.org/10.2118/169090-ms>.
- Gabriel, G.A., Inamdar, G.R., 1983. An experimental investigation of fines migration in porous media. In: *SPE Annual Technical Conference and Exhibition*. Society of Petroleum Engineers. San Francisco, California. <http://dx.doi.org/10.2118/12168-MS>.
- Ghaderi, S.M., Keith, D.W., Leonenko, Y., 2009. Feasibility of injecting large volumes of CO₂ into aquifers. *Energy Procedia* 1, 3113–3120. <http://dx.doi.org/10.1016/j.egypro.2009.02.092>.
- Gruesbeck, C., Collins, R.E., 1982. Entrainment and Deposition of Fine Particles in Porous Media 22, 10. <http://dx.doi.org/10.2118/8430-PA>.
- IEA, 2013. Technology roadmap – carbon capture and storage. *Technol. Roadmap* 59. http://dx.doi.org/10.1007/SpringerReference_7300.
- Ilgen, A.G., Cygan, R.T., 2016. Mineral dissolution and precipitation during CO₂ injection at the Frio-I Brine Pilot: geochemical modeling and uncertainty analysis. *Int. J. Greenh. Gas Control* 44, 166–174. <http://dx.doi.org/10.1016/j.ijggc.2015.11.022>.
- Kaszuba, J.P., Janecky, D.R., Snow, M.G., 2005. Experimental evaluation of mixed fluid reactions between supercritical carbon dioxide and NaCl brine: relevance to the integrity of a geologic carbon repository. *Chem. Geol.* 217, 277–293. <http://dx.doi.org/10.1016/j.chemgeo.2004.12.014>.
- Khilar, K.C., Fogler, H.S., 1983. Water sensitivity of sandstone. *Spe* 10103.
- Khilar, K., Fogler, H., 1984. The existence of a critical salt concentration for particle release. *J. Colloid Interface Sci.* 101, 214–224. [http://dx.doi.org/10.1016/0021-9797\(84\)90021-3](http://dx.doi.org/10.1016/0021-9797(84)90021-3).
- Khilar, K.C., Fogler, H.S., 2010. *Migrations of Fines in Porous Media, Theory and Applications of Transport in Porous Media*. Springer, Netherlands.
- Lombard, J.M., Azaroual, M., Pironon, J., Brosseta, D., Egermann, P., Munier, G., Mouronval, G., 2010. CO₂ injectivity in geological storages: an overview of program and results of the GeoCarbone-Injectivity project. *Oil Gas Sci. Technol.* 65, 533–539. <http://dx.doi.org/10.2516/ogst/2010013>.
- Mahadevan, J., Sharma, M.M., Yortsos, Y.C., 2007. Water removal from porous media by gas injection: experiments and simulation. *Transp. Porous Media* 66, 287–309. <http://dx.doi.org/10.1007/s11242-006-0030-z>.
- Miri, R., Hellevang, H., 2016. Salt precipitation during CO₂ storage—A review. *Int. J. Greenh. Gas Control* 51, 136–147. <http://dx.doi.org/10.1016/j.ijggc.2016.05.015>.
- Miri, R., van Noort, R., Aagaard, P., Hellevang, H., 2015. New insights on the physics of salt precipitation during injection of CO₂ into saline aquifers. *Int. J. Greenh. Gas Control* 43, 10–21. <http://dx.doi.org/10.1016/j.ijggc.2015.10.004>.
- Miri, R., 2015. *Effects of CO₂ – Brine-Rock Interactions on CO₂ Injectivity – Implications for CCS*. University of Oslo.
- Muecke, T.W., 1979. Formation fines and factors controlling their movement in porous media. *J. Pet. Technol.* 31, 144–150.
- NASA, 2017. The Lift Equation. URL: <https://www.grc.nasa.gov/www/k-12/airplane/lifteq.html> (accessed 8.2.17).
- Nalawade, S.P., Picchioni, F., Janssen, L.P.B.M., 2006. Supercritical carbon dioxide as a green solvent for processing polymer melts: processing aspects and applications. *Prog. Polym. Sci.* 31, 19–43. <http://dx.doi.org/10.1016/j.progpolymsci.2005.08.002>.
- Nelson, P.H., 2009. Pore-throat sizes in sandstones, tight sandstones, and shales. *Am. Assoc. Pet. Geol. Bull.* 93, 329–340. <http://dx.doi.org/10.1306/10240808059>.
- Ott, H., Roels, S.M., De Kloe, K., 2015. Salt precipitation due to supercritical gas injection: i. Capillary-driven flow in unimodal sandstone. *Int. J. Greenh. Gas Control* 43, 247–255. <http://dx.doi.org/10.1016/j.ijggc.2015.01.005>.
- Patton, J.T., Phelan, P., Holbrook, S., 1981. *CO₂ Formation Damage Study – First Annual Report*. Las Cruces, New Mexico.
- Peysson, Y., André, L., Azaroual, M., 2014. Well injectivity during CO₂ storage operations in deep saline aquifers-Part 1: Experimental investigation of drying effects, salt precipitation and capillary forces. *Int. J. Greenh. Gas Control* 22, 291–300. <http://dx.doi.org/10.1016/j.ijggc.2013.10.031>.
- Pruess, K., Muller, N., 2009. Formation dry-out from CO₂ injection into saline aquifers: 1. effects of solids precipitation and their mitigation. *Water Resour. Res.* 45, 1–11. <http://dx.doi.org/10.1029/2008WR007101>.
- Pruess, K., 2009. Formation dry-out from CO₂ injection into saline aquifers: 2. Analytical model for salt precipitation. *Water Resour. Res.* 45, 1–6. <http://dx.doi.org/10.1029/2008WR007102>.
- Roels, S.M., Ott, H., Zitha, P.L.J., 2014. μ -CT analysis and numerical simulation of drying effects of CO₂ injection into brine-saturated porous media. *Int. J. Greenh. Gas Control* 27, 146–154. <http://dx.doi.org/10.1016/j.ijggc.2014.05.010>.
- Roels, S.M., El, N., Costas, C., Zitha, P.L.J., 2016. Capillary-driven transport of dissolved salt to the drying zone during CO₂ injection in homogeneous and layered porous media. *Transp. Porous Media* 111, 411–424. <http://dx.doi.org/10.1007/s11242-015-0601-y>.
- Sarkar, A., Sharma, M., 1990. Fines migration in two-phase flow. *J. Pet. Technol.* 42, 646–652. <http://dx.doi.org/10.2118/17437-PA>.
- Sayegh, S.G., Krause, F.F., Girard, M., DeBree, C., 1990. Rock/fluid interactions of carbonated brines in a sandstone reservoir: pembina cardium, Alberta, Canada. *SPE Form. Eval.* 5, 399–405. <http://dx.doi.org/10.2118/19392-PA>.
- Scheuerman, R.F., Bergersen, B.M., 1990. Injection-water salinity, formation pretreatment, and well-operations fluid-selection guidelines. *J. Pet. Technol.* 42, 836–845.
- Sen, T.K., Khilar, K.C., 2006. Review on subsurface colloids and colloid-associated contaminant transport in saturated porous media. *Adv. Colloid Interface Sci.* 119, 71–96. <http://dx.doi.org/10.1016/j.cis.2005.09.001>.
- Sharma, M.M., Yortsos, Y.C., 1987. Fines migration in porous media. *AIChE J.* 33, 1654–1662.
- Sharma, M.M., Yortsos, Y.C., Handy, L.L., 1985. Release and Deposition of Clays in Sandstones. <http://dx.doi.org/10.2118/13562-ms>.
- Tobertge, D.R., Curtis, S., 2013. Experimental perspectives of mineral dissolution and precipitation due to carbon dioxide-water-rock interactions. *J. Chem. Inf. Model.* 53, 1689–1699. <http://dx.doi.org/10.1017/CBO9781107415324.004>.
- Vaidya, R.N., Fogler, H.S., 1990. Formation damage due to colloids induced fines migration. *Colloids Surf.* 50, 215–229. [http://dx.doi.org/10.1016/0166-6622\(90\)80265-6](http://dx.doi.org/10.1016/0166-6622(90)80265-6).
- Verdon, J.P., 2012. Microseismic Monitoring and Geomechanical Modelling of CO₂ Storage in Subsurface Reservoirs 55–81. <http://dx.doi.org/10.1007/978-3-642-25388-1>.
- Zeidouni, M., Pooladi-Darvish, M., Keith, D., 2009. Analytical solution to evaluate salt precipitation during CO₂ injection in saline aquifers. *Int. J. Greenh. Gas Control* 3, 600–611. <http://dx.doi.org/10.1016/j.ijggc.2009.04.004>.
- Zuluaga, E., Muñoz, N.I., Obando, G.a., 2001. An Experimental Study to Evaluate Water Vaporisation and Formation Damage Caused by Dry Gas Flow Through Porous Media.

Paper VII

The Coupled Effect of Fines Mobilization and Salt Precipitation on CO₂ Injectivity.

Yen Adams Sokama-Neuyam, Sindre L. Forsetløykken, Jhon-Eirik Lien, Jann Rune Ursin
University of Stavanger, Norway.

Energies **2017**, *10*(8), 1125.

Article

The Coupled Effect of Fines Mobilization and Salt Precipitation on CO₂ Injectivity

Yen Adams Sokama-Neuyam * , Sindre Langås Forsetløyken, Jhon-eirik Lien and Jann Rune Ursin

Department of Petroleum Engineering, University of Stavanger, 4036 Stavanger, Norway; SL.Forsetløyken@stud.uis.no (S.L.F.); Jh.Lien@stud.uis.no (J.-e.L.); jann-rune.ursin@uis.no (J.R.U.)

* Correspondence: yen.a.sokama-neuyam@uis.no; Tel.: +47-5183-1821

Received: 6 June 2017; Accepted: 26 July 2017; Published: 1 August 2017

Abstract: In terms of storage capacity and containment efficiency, deep saline aquifers are among the best candidates for CO₂ storage. However, salt precipitation in the wellbore vicinity and fines mobilization ensued from in situ mineral dissolution could impair CO₂ injectivity and reduce the quality and capacity of deep saline reservoirs for CO₂ storage. The mechanisms of salt precipitation and its impact on CO₂ injectivity have been studied, but the effects of fines mobilization have not been properly investigated. We conducted core-flood experiments and theoretical studies to investigate the impact of fines mobilization on CO₂ injectivity, the relative contribution of fines mobilization and salt precipitation to injectivity impairment, and the coupled effect of salt precipitation and fines mobilization. We found that, mineral dissolution and transport effects could induce up to about 26% injectivity impairment. The findings also suggest that about 0.3 wt % particle concentration in the pore fluid could induce over twofold injectivity impairment compared to about 10 wt % of total dissolved salt in the formation water. Salt precipitation was also found to compound injectivity impairment induced by fines mobilization. The present study provides important insight, and could serve as a foundation to inspire further experimental and theoretical investigation into the effects of mineral dissolution and fines mobilization in the context of CO₂ injectivity.

Keywords: fines mobilization; salt precipitation; CO₂ injectivity impairment; carbon storage

1. Introduction

CO₂ Capture, Utilization, and Storage (CCUS) has potential to reduce the concentration of CO₂ in the atmosphere and prevent climate change. The storage potential of a geological CCUS candidate is defined by its storage capacity and well injectivity [1]. Lombard et al. [2] classified CO₂ injectivity impairment mechanisms into three main groups: transport effects such as fines mobilization, geochemical effects such as mineral dissolution, and salt precipitation and geomechanical processes. Among these injectivity impairment challenges, salt precipitation effects have attracted the highest attention over the past years [3–7]. The effect of fines mobilization on CO₂ injectivity has not been given its deserved attention, probably because of available evidence of massive injectivity impairment induced by salt precipitation.

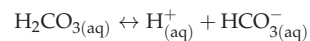
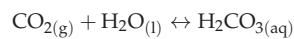
Salt precipitation was already known to impair well injectivity in natural gas production. Kleinitz et al. [8] reported field experience of severe halite scaling in the injection region during natural gas production in Northern German gas reservoirs. A dramatic reduction in the production rate due to complete plugging of the flow path by precipitated salts caused the well to be shut down. Similar field experiences have been reported during gas production, injection, and storage [9–11]. In the context of field CO₂ injection experience, Baumann et al. [12] and Grude et al. [13] have reported convincing evidence of salt precipitation effects in the Ketzin pilot reservoir and the Snøhvit field,

respectively. Permeability impairment between 13% and 83% and porosity reduction ranging from 2% to 15% have been reported from laboratory core-flood experiments [5,14–18]. These experimental findings have also been confirmed by theoretical and numerical simulations [19–22].

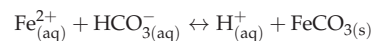
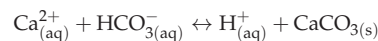
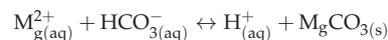
Miri and Hellevang [3] identified the processes leading to salt precipitation as: (1) immiscible two-phase CO₂-brine displacement; (2) vaporization of brine into the flowing CO₂ stream; (3) capillary back-flow of brine toward the inlet; (4) diffusion of dissolved salt in the porewater; (5) gravity override of CO₂; and (6) salt self-enhancing. While numerical experiments by Roels et al. [23] suggested that precipitated salt accumulates far from the wellbore, several research works [6,14,24,25] show that precipitated salt accumulates near the wellbore.

Pruess et al. [25] suggested that a preflush of the injection region with freshwater could reduce salt precipitation. However, Kleinitz et al. [8] have shown that freshwater injection could not mitigate salt precipitation if the flow area is completely plugged by solid salt. Sokama-Neuyam and Ursin [18] reported that freshwater injection could induce other injectivity impairment challenges such as clay swelling and the release of fine particles in sandstone rocks if the brine salinity is below a certain critical value. They proposed alternate injection of CO₂ and diluent low salinity brine.

Under typical storage conditions, CO₂ could dissolve in formation brine at the CO₂-brine interface to form carbonic acid and then bicarbonates according to the following equations:



The bicarbonates could react with cations in the rock and formation water to form stable carbonates, as shown in the following equations [26–28]:



The carbonates in solution (M_gCO_{3(s)}, CaCO_{3(s)}, FeCO_{3(s)}, etc.) could aggregate into tiny particles in the bulk liquid or form a scale on the pore walls. If these mineral grains are mobilized along the flow stream, CO₂ injectivity could be severely impaired through plugging of the reservoir rock.

The mechanisms of in situ fines migration and the impact of particle transport on the petrophysical properties of reservoir rocks have been well-researched. Khilar and Fogler [29] presented the mechanisms of colloidal and hydrodynamic induced release of fine particles in porous media. Muecke [30] investigated parameters controlling the movement of fines particles within the pore spaces. They identified the pH and salinity of the formation brine, flow rate, and temperature as some of the underlying parameters. Khilar and Fogler [31] reported that there exists a critical salt concentration below which the pore fluid could weaken the Van der Waal's forces holding fine particles to the pore wall. Gruesbeck and Collins [32] investigated the effect of hydrodynamic forces on the release and transport of fines. They identified a minimum interstitial velocity for fines entrainment. The effect of two-phase flow and rock wettability on fines entrainment has been experimentally investigated by Sarkar and Sharma [33]. They found that the wettability of the core could affect the extent and rate of permeability impairment induced by migratory fines. Analytical models have been developed by Sharma and Yortsos [34] to investigate the mechanisms of size exclusion and quantify the effect of particle entrapment on rock permeability. A thorough analysis of formation damage induced by migratory fines can be found in Civan [35].

During particle transport in natural porous media, the entrapment or piping of fines depends on the jamming ratio (particle size/pore size) [29]. According to Aji Kaiser [36], only particles with a jamming ratio greater than 1.0 could be entrapped through size exclusion. Depending on the

particle size, the suspending medium, hydrodynamic properties, and petrophysical properties of the reservoir rock, the pores could also be plugged through pore bridging, surface deposition, and multi-particle blocking.

We conducted laboratory core-flood experiments with sandstone core samples to investigate the effect of salt precipitation and fines mobilization on CO₂ injectivity. We then attempted to model the coupled effects of salt precipitation and fines mobilization using a tractable bundle-of-tubes model. The objective is to study the underlying fundamental mechanisms of fines migration and salt precipitation in sandstone rocks in the context of CO₂ injection.

2. Materials and Methods

The experimental work is in two parts. First, preliminary experiments were conducted to investigate the effect of mineral dissolution on injectivity impairment. Bentheimer core, containing high amounts of clay minerals (2.68%) and feldspars (4.86%), was flooded with carbonated water at 80 bar and 65 °C. Under these conditions, bicarbonates generated from carbonated water could attack and wear out clay and feldspar minerals into the pore fluid. The suspended particles could then be lifted by the flowing fluid into the pore channels, where they could plug the rock and affect injectivity.

Second, the quantitative effect of fines mobilization on CO₂ injectivity was investigated. To control the concentration of particles in the pore fluid, the core was saturated with mono-disperse colloid solution prior to CO₂ injection. By optimizing the contents of the pore fluid, we attempted to compare the effects of fines mobilization to the impact of salt precipitation under linear flow conditions. A theoretical model was also developed to study the coupled effect of salt precipitation and fines mobilization.

2.1. Materials

2.1.1. Rocks

Outcrop cylindrical sandstone core samples were used in the experiments. The characteristics of the rock samples are shown in Table 1. Each type of core sample was drilled from the same block, and with the exception of the Bandera cores, all of the samples can be considered homogeneous with respect to permeability. The cores were 20 cm long with a diameter of 3.81 cm.

Table 1. Characteristics of sandstone core samples used in the experiments.

Rock	Permeability (mD)	Porosity (%)
Berea	90–120	17–19
Bentheimer	1200–2000	22–24
Bandera	4–10	19–21

According to measurements conducted by Peksa et al. [37], Bentheimer sandstone rock is composed mainly of quartz (91.70 wt %), feldspars (4.86 wt %), clay minerals (2.68 wt %), and pyrite and iron oxides (0.17 wt %). The rock has an average pore body diameter of 0.014 mm and pore throat diameter of 0.012 mm [37]. With such open pore channels, dissolved rock particles could pipe through the rock to provide evidence of mineral dissolution. That was another reason for selecting this core for the mineral dissolution tests, apart from its clay-rich contents.

The Kipton Berea sandstone rock used in this study is composed mainly of Silica (86.47 wt %), Alumina (7.31 wt %), and Oxides (Iron Oxide, Titanium Oxide, Calcium Oxide, and Magnesium oxide) [38]. The Berea rock has pore throat sizes between 0.5 and 5.0 µm, and pore body sizes ranging from 5.0 to 50 µm [39]. Berea cores were used for the particle injection experiments because of their smaller range of pore sizes, which makes them capable of trapping released minerals during the

displacement of the pore fluid. The Bandera core was mainly used to investigate the sensitivity of initial rock permeability.

2.1.2. Formation Water

We used synthetic formation water (FW) with salinity of about 105.5 g/L (NaCl, 77.4 g/L; CaCl₂·2H₂O, 21.75 g/L; MgCl₂·6H₂O, 3.56 g/L; SrCl₂·6H₂O, 2.25 g/L; Na₂SO₄, 0.13 g/L; KCl 0.42 g/L) [40]. This FW is representative of typical North Sea reservoir brine. The FW was used in salt precipitation investigations as the initial saturating fluid. In the fines mobilization experiments, FW was used to prepare carbonated water and to measure the permeability of the core, before and after mineral dissolution and fines mobilization. NaCl brines (HS (High Salinity), 150 g/L and LS (Low Salinity), 75 g/L) were used in the modelling experiments to investigate the coupled effects of fines mobilization and salt precipitation.

2.1.3. Carbonated Water

Carbonated water was used to generate fine particles in the rock. Figure 1 shows a schematic of the setup used to prepare carbonated water. CO₂ is soluble in brine, with solubility strongly dependent on temperature, pressure, and brine salinity. A tight piston cell was filled with about 1000 mL of FW. CO₂ was then injected into the brine at a constant pressure of 80 bar and 20 °C for about 48 h. The injection pressure was kept at 80 bar until the pump delivered insignificant volume of CO₂ (<0.0001 mL/min) into the brine, signifying complete saturation. Experimental data reported by Portier and Rochelle [41] suggests CO₂ solubility in Utsira formation brine with similar composition as the FW used in the current experiment, under the current working conditions is in the range of 1.26–1.36 mol Kg⁻¹ H₂O. The connected pressure gauge was used to monitor fluid pressure in the piston cell.

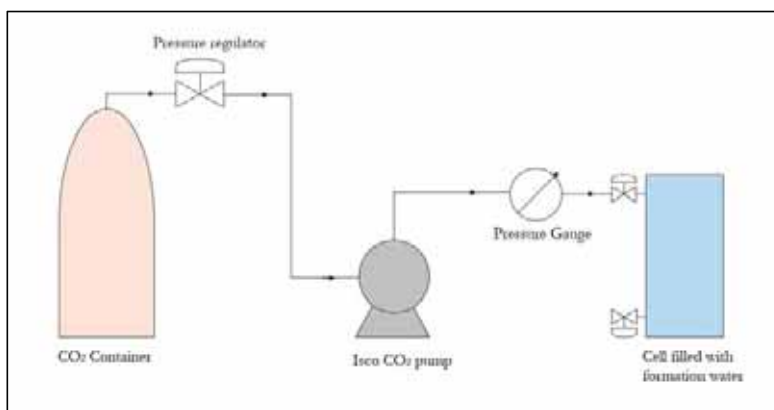


Figure 1. Schematic of the carbonated water preparation apparatus.

2.1.4. CO₂

Liquefied CO₂ with purity percentage of about 99.7 was used as the injected gas. Liquid CO₂ was injected to measure injectivity impairments associated with salt precipitation and fines migration because the precipitated salts are insoluble in this fluid. To obtain liquid CO₂, the gas was injected at 80 bar and 26 °C. Supercritical CO₂, which was used as the displacing and drying fluid, was injected at 80 bar and 50 °C.

2.1.5. Colloid Suspension

Mono-disperse colloid suspensions prepared from concentrated, fumed alumina latex particles stock solution were used to investigate the effect of fines migration on CO₂ injectivity. Alumina was selected for this study because of its high resistance to wear and its stability in CO₂, and because they are oil wet particles with minimized attachment to the pore walls.

The particles were stabilized in low salinity brine at near-neutral pH conditions to prevent particle aggregation. A 5 g/L (0.086 mol/L) NaCl brine was used to dilute the concentrated colloid stock solution into mono-disperse colloidal suspensions. Below a critical salt concentration (CSC) of about 0.071 mol/L, NaCl brine could detach formation fine particles from the pore walls into the flowing stream [42]. A brine concentration of 0.086 mol/L was used, because it is adequately above the CSC for fines detachment and low enough to prevent salt precipitation through brine vaporization. The characteristics of the colloid stock solution are presented in Table 2. Specific concentrations of mono-disperse suspensions, prepared from the stock solution were used in various experiments.

Table 2. Characteristics of fumed alumina stock solution used to prepare the colloid suspensions.

Properties	Data
Particle size (μm)	0.08
Al ₂ O ₃ content (%)	39–41
Viscosity (mPa/s)	<90
pH	6.0–9.0
Density (g/cc)	1.39

2.2. Experimental Setup

A schematic of the core flooding apparatus used in the tests is shown in Figure 2. Prior to the test, the core was loaded in a horizontal Hassler core-holder. The Quizix pump was used to deliver fluid through the connected piston cell into the core inlet. Either brine or carbonated water was injected. The Isco CO₂ pump was used to deliver CO₂. The injected fluid was positioned in the oven to secure a preset temperature. A differential pressure gauge and a pressure transducer were used to monitor the pressure drop across the core and record the absolute pore pressure, respectively. A backpressure of 80 bar was set at the outlet during Carbonated water and CO₂ injection, and the effluent fluid was safely collected in a piston cell for analysis and safe disposal.

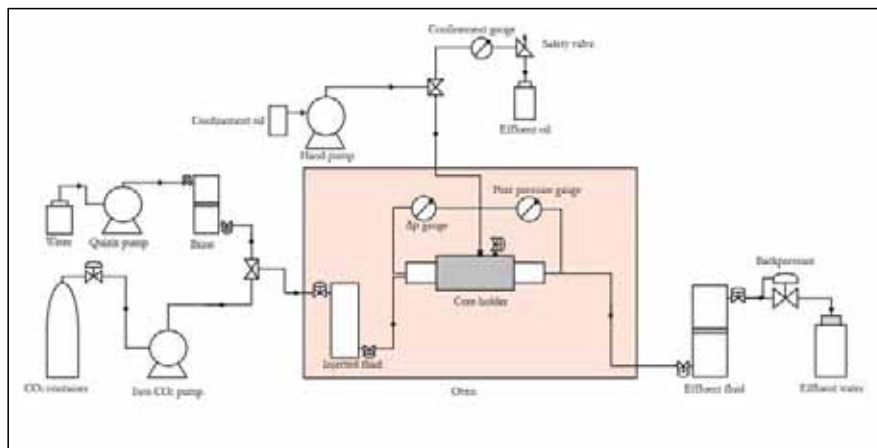


Figure 2. Schematic of the experimental setup used in the core-flood experiments: the CO₂ flow rig.

2.3. Methods

2.3.1. Experimental Procedure

The clean core sample was first dried at 65 °C for about 24 h. The core was then wrapped in shrinking Teflon sleeve to prevent leakage, before it was inserted into the rubber sleeve and horizontally mounted in the core holder. A confining pressure of about 150 bar was applied in the annular space between the core and the core holder during the supercritical CO₂ injection. The confining pressure was reduced to 20 bar during the injection of FW. The experimental procedure consists of the following general steps:

1. The initial permeability (K_i) of the core was measured.
2. The core was saturated with brine and flooded with either carbonated water or supercritical CO₂ to generate fines or dry the core, respectively.
3. The experiment was stopped and the core was cooled for all trapped CO₂ to boil out.
4. The permeability of the core after mineral impairment (K_f) was measured.

In Step 1 and Step 4, either liquid CO₂ or FW was used to measure the permeability depending on the solubility of the precipitated minerals in the fluid. Details of each experimental process are presented with the results.

2.3.2. Injectivity Impairment Quantification

Fluid injectivity, I , is defined as the ratio of volumetric injection flow rate, q , to the pressure drop, Δp . Assuming the core has constant absolute permeability, k_i and k_f before and after it has been exposed to impairment, respectively, and that the viscosity of the fluid used in the measurement is constant, the injectivity before and after permeability impairment can be expressed from Darcy's law as:

$$I_i = \frac{q_i}{\Delta p_i} = k_i \cdot C, \quad (1)$$

$$I_f = \frac{q_f}{\Delta p_f} = k_f \cdot C, \quad (2)$$

In Equations (1) and (2), C is a constant defined as $C = \frac{A}{\mu L}$, for constants A and L . If the measuring fluid is injected at a constant rate during injectivity measurements ($q_i = q_f$), we can define a Relative Injectivity Change (RIC) index, β , as:

$$\beta = \left(\frac{I_i - I_f}{I_i} \right) = 1 - \left(\frac{I_f}{I_i} \right), \quad (3)$$

Substituting Equations (1) and (2) into (3) yields:

$$\beta = 1 - \left(\frac{\Delta p_i}{\Delta p_f} \right) = 1 - \left(\frac{k_f}{k_i} \right), \quad (4)$$

The plugging of the pores by precipitated minerals would reduce the flow area and increase the pressure drop across the core, Δp . Thus, in Equation (4), $\Delta p_f > \Delta p_i$ and $K_i > K_f$ after permeability impairment. Consequently, a positive β value indicates injectivity impairment. In the present work, β was expressed as a percentage. Although β is a rather linear injectivity measurement technique, it provides an indirect method for estimating injectivity impairment independently of the chemical properties of the pore-plugging material.

2.3.3. Uncertainty in Experimental Data

Particle transport in natural porous media is a highly uncertain process. The particles are displaced in a highly random flow path into a very tortuous pore network distribution. Therefore, the repeatability of particle flow experiments in even homogeneous natural rocks is expected to be low. However, an attempt was made to quantify and minimize the uncertainty in the measurements.

The measured injectivity data I , was reported as:

$$I_{measured} = I_{avg} \pm \Delta I_{avg}, \quad (5)$$

In Equation (5), I_{avg} is calculated from the mean value of the stabilized liquid CO₂ or brine Δp across the core before and after supercritical CO₂ injection, mineral precipitation, and particle entrapment, and ΔI_{avg} is the estimated uncertainty in I_{avg} . Initial and final pressure drop measurements are recorded when the liquid CO₂ or brine pressure drop across the core stabilizes. I_{avg} and ΔI_{avg} are calculated as:

$$I_{avg} = \frac{\sum I}{N}, \quad (6)$$

$$\Delta I_{avg} = \frac{I_{max} - I_{min}}{\sqrt{N}}, \quad (7)$$

In Equations (6) and (7), N is the total number of recorded data points, and I_{max} and I_{min} are the maximum and minimum values, respectively.

The uncertainty in injectivity was dependent upon the differential pressure gauge, injection flow rate, and the type of mineral plugging. A very sensitive differential pressure gauge, which measures to an accuracy of about 0.009%, was used. We found that a low injection flow rate also minimized the uncertainty. Similarly, colloidal entrapment induced higher uncertainty compared to salt precipitation. An injection flow rate of about 5 mL/min was found to be the optimal liquid CO₂ injection rate. A maximum uncertainty of about 5% was then applied across the board.

3. Theoretical Modelling

In this section, we present a tractable bundle-of-tubes model in an attempt to model the coupled effect of fines mobilization and salt precipitation on CO₂ injectivity. The objective is to develop a model capable of capturing the main fundamental physical mechanisms of fines mobilization and salt precipitation without complicating the process with details.

3.1. Background and Assumptions

The cylindrical core, with radius R and length L , was reconstructed into a bundle of parallel cylindrical capillary tubes with varying radii ($r_1, r_2, r_3, \dots, r_N$) interspersed between non-porous mass (grey regions) representing the rock matrix (Figure 3). The model is sectioned into a dry-out zone (L_1), where salt has been precipitated into the tubes and the uncontaminated zone (L_2), representing the part of the core which has not been dried by supercritical CO₂.

In the dry-out zone, we assume that solid salt accumulates on the walls of the pore constriction (black shades in Figure 3). We also assume that the accumulated salt in the dry-out region would reduce the cross-flow area by Δr_1 for r_1 ; Δr_2 for r_2 ; Δr_3 for r_3 ; \dots , Δr_N for r_N , for N total number of capillary tubes in the porous medium.

A dimensionless dry-out length, $I_d = \frac{L_1}{L}$, defined as the ratio of the length of the dry-out region to the total length of the core, was introduced to track the development of the dry-out zone and characterize the distribution of precipitated salt.

In the present study, we investigate fines entrapment induced by size exclusion of particles. Fines plugging caused by pore bridging, multiparticle blocking, and surface deposition have not been included in the model.

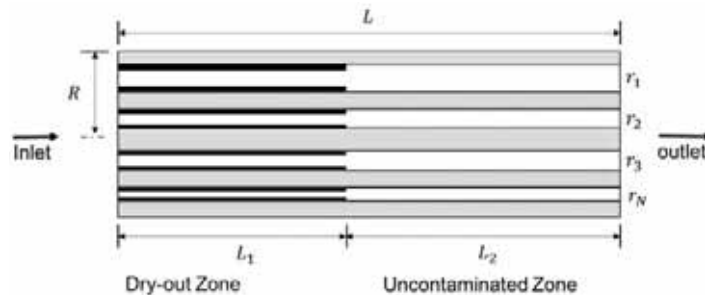


Figure 3. A schematic of the bundle-of-tubes model. The core of length L and radius R was reconstructed into a bundle of parallel cylindrical capillary tubes with varying radii interspersed between non-porous mass.

3.2. Model Formulation

For a bundle of N parallel non-communicating capillary tubes with varying tube radii, r_i and thickness of deposited salts, Δr_i , the total fluid flow rate can be modelled with the Hagen–Poiseuille equation as:

$$q = \frac{\pi \Delta p}{8\mu L} \sum_{i=1}^N (r - \Delta r)_i^4, \quad (8)$$

In Equation (8), μ is the fluid viscosity, and $\frac{\Delta p}{L}$ is the overall pressure gradient across the bundle of capillary tubes. For linear flow through a core of radius R and length L , the fluid flow rate is also defined by Darcy's Law:

$$q = \frac{kA \Delta p}{\mu L}, \quad (9)$$

In Equation (9), k is the absolute permeability of the core, and $A = \pi R^2$ is the cross-sectional flow area. Combining Equation (8) and Equation (9), the permeability of the core can be expressed as:

$$k = \frac{1}{8R^2} \sum_{i=1}^N (r - \Delta r)_i^4, \quad (10)$$

In Equation (10), the permeability depends strongly on the number of open capillary tubes, N , and the thickness of precipitated salts deposited in the tubes, Δr . Salt precipitation will impair the permeability by reducing $(r - \Delta r)$. On the other hand, the entrapment of fine particles will plug the capillary tubes with jamming ratio greater than 1.0, consequently impairing permeability by reducing the number of open capillary tubes, N . Thus, by controlling these factors, the coupled effect of fines mobilization and salt precipitation could be investigated.

The initial permeability of the core can be estimated by setting $\Delta r = 0$. The permeability ratio, $\frac{k}{k_0}$, can therefore be calculated and the relative injectivity change index, β , computed from Equation (4).

3.3. Number of Capillary Tubes and Distribution of Precipitated Salt

The pore volume of the core, V_p , is assumed to be approximately equal to the internal volume of all the capillary tubes.

$$V_p = \pi L \sum_{i=1}^N r_i^2 \approx \pi L N \bar{r}_i^2, \quad (11)$$

In Equation (11), \bar{r}_i^2 is the average of the square of the tube radii. From the definition of porosity and Equation (11), the total number of capillary tubes can be derived as:

$$N \approx \frac{3}{4} \phi \left(\frac{R}{\bar{r}_i} \right)^2, \quad (12)$$

In Equation (12), we have used the relation $\overline{r_i^2} = \frac{4}{3}\overline{r_i}^2$. Equation (12) shows that the total number of capillary tubes depends on the porosity of the core, ϕ , average pore radius, $\overline{r_i}$, and the radius of the core, R .

Based on a pore size distribution analysis using mercury injection in sandstone cores, Shi et al. [43] have found an average pore radius of about 6.7 μm . From this data, we calibrated our model to an average tube size of 6 μm using a lognormal distribution of tube radii, as shown in Figure 4.

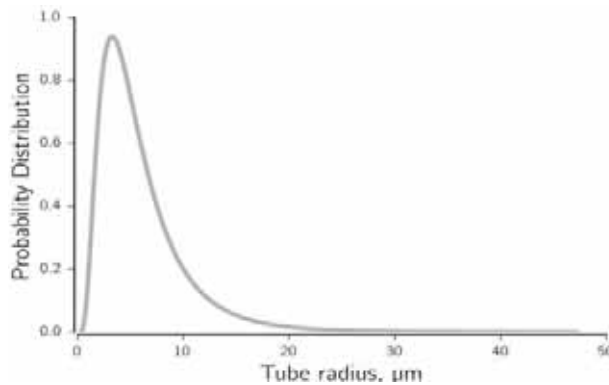


Figure 4. Distribution of capillary tube radii used in the attempt to reconstruct the characteristics of sandstone core.

Natural reservoir rocks consist of pore bodies connected by two or more pore throats depending on the coordination number. In this work, the pore chambers and throats were represented as individual non-interacting tubes. The average coordination number in sandstones is between 4 and 8 [44,45]. The pore size distribution in Figure 4 compares favorably with this range of coordination numbers.

Under linear flow, solid salt distribution will depend on the linear interconnection of pores. The bundle-of-tubes model could adequately characterize the principal mechanisms of salt deposition under linear flow conditions, where the horizontal interconnection of pores can be represented as capillary tubes.

By fitting experimental data, we derived a correlation for the deposited solid salt saturation by modifying the mass balance equation previously derived by Karsten Pruess [21], as:

$$S_s = (a + bl_d) \frac{\rho_{aq} X_s}{\rho_s}, \quad (13)$$

In Equation (13), a and b are constants. By fitting initial experimental data, $a = 0.85$ and $b = 0.1$ were found to be the optimum correlation constants for the current studies.

From mass balance, it can be shown that the thickness of solid salt in each capillary tube can be estimated from:

$$\Delta r_i \approx \frac{2}{3} \frac{S_s r_i}{l_d}, \quad (14)$$

Equation (14) shows that the thickness of solid salt, Δr_i , in each capillary tube, r_i , is dependent on the total precipitated solid salt saturation, S_s , and the distribution of salt in the pores, which is determined by the dry-out length, l_d .

3.4. Implementation of the Model

To estimate injectivity impairment induced by the coupled effect of fines mobilization and salt precipitation, the following steps were followed:

1. The number and distribution of capillary tubes for given properties of the core was calculated from Equation (12) by specifying the average pore radius.
2. The initial permeability of the core was calculated from Equation (10) by setting $\Delta r = 0$. The calculated permeability was then compared to the measured permeability of the core. If the agreement is not favourable, Step 1 is optimized until the agreement is acceptable.
3. base case is established by exposing the tubes to fine particles with average particle size r_p . For simplicity, we assumed that the flowing fluid contains particles of the same size and that each capillary tube has equal chance of being exposed to the particles. Tubes with a jamming ratio greater than 1.0 are isolated and the permeability of the core is recalculated from Equation (10).
4. The relative injectivity change, β , induced by fines entrapment is calculated from Equation (4).
5. For given properties of the saturating formation brine, the thickness of precipitated salt in each capillary tube is computed from Equations (13) and (14).
6. Steps 3 and 4 are then repeated to calculate the combined effect of salt precipitation and fines mobilization.

The model does not handle particles of varying sizes as occurs in typical mineral dissolution and particle transport in natural porous media. In addition, fines entrapment through pore bridging and multiparticle blocking have not been included. However, the fundamental mechanisms of salt precipitation and fines migration have been captured in the model. Salt precipitation reduces the flow area by coating the pore walls. The reduced flow area then makes the pore constrictions even more susceptible to fines entrapment through the jamming ratio.

4. Results and Discussion

4.1. Injectivity Impairment Induced by Fines Mobilization

To investigate the effect of mineral dissolution and fines migration on CO₂ injectivity, sandstone core samples were flooded with carbonated water at 80 bar and 60 °C. A Bentheimer core, which was initially fully saturated with FW, was flooded with about 25 pore volumes (PV) of carbonated water at 0.25 mL/min. Figure 5 shows part of the pressure drop profiles recorded during carbonated water flooding. Effluent was collected and filtered with a 0.22 µm filter to collect any solid particles that might have been washed out of the core. The sample was then dried and analyzed with a Scanning Electron Microscope (SEM) process. Energy Dispersive Spectroscopy (EDS) elemental analysis of the sample is provided in Table 3.

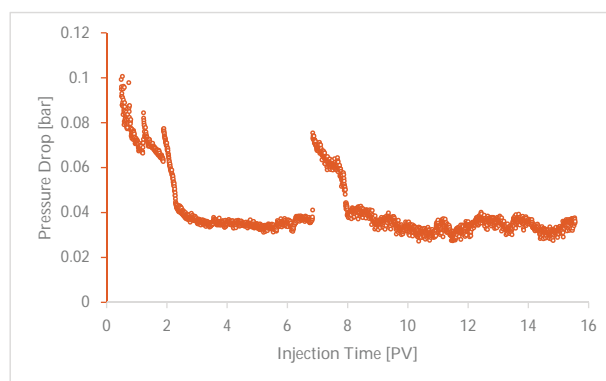


Figure 5. Pressure drop profile recorded during injection of carbonated water into a Bentheimer core at a flow rate of 0.25 mL/min at 80 bar and 60 °C. The pressure drop is seen to fall sharply until about 3 pore volumes (PV), stabilizes between 3 PV and about 7 PV, and become very unstable afterwards.

In Figure 5, the pressure drop decreased sharply from about 0.1 bar to about 0.04 bar after the core was flooded with about 3 PV of carbonated water. This is the period of immiscible displacement of the saturating pore water (FW) by carbonated water. As the displaced FW is replaced by the less dense carbonated water, the pressure drop is seen to fall sharply until carbonated water breakthrough at the effluent end of the core. The pressure drop remained practically stable from 3 PV to about 7 PV. In this period, the core is fully saturated with carbonated water, leading to stable flow. However, the pressure drop became unstable from about 7 PV to the end of the test. In this period, the pressure drop is seen to rise sharply and fall to a rather haphazard behavior towards the end of the test. We suspect that this is the period in which the resident carbonated water begins to interact chemically with the rock minerals. The dissolution of the rock momentarily decreases the pressure drop. As the dissolved minerals are produced out of the core, some of the particles could plug the smaller pores and temporarily increase the pressure drop. However, due to the large pore channels of the Bentheimer core, few particles are likely to plug the pores, as seen in the magnitude of the momentary changes in pressure drop.

The EDS results in Table 3 reveal that the sample is composed predominantly of Na (17.53%) and Cl (29.79%), probably because the filtered effluent sample, which is composed mainly of FW, contains about 73.4% NaCl (Section 2.1.2). The injected carbonated water could not have precipitated halite within the rock, since CO₂ was dissolved in FW. Salt could have been precipitated in the pores only if high amounts of free CO₂ came into direct contact with the FW during the flooding. The present experimental conditions eliminate the possibility of brine vaporization and salt precipitation. Therefore, the Na and Cl elements are probably components of the effluent FW. Table 3 also indicates the presence of minerals such as Fe, Si, Al, Ni, and Co which were not present in the saturating FW and the injected carbonated water. Therefore, Fe, Si, Al, Ni, and Co were most likely dissolved from the Bentheimer core through the interaction of the carbonated water and the rock minerals. The EDS analysis show low amounts of Fe, Si, Al, Ni, and Co, because only few particles were probably washed out of the core.

Table 3. Energy Dispersive Spectroscopy (EDS) analysis of effluent samples collected during carbonated water flooding into Bentheimer core.

Element	wt %
O	33.56
Fe	7.78
Ni	5.02
Na	17.53
Mg	0.74
Al	2.53
Si	0.35
Cl	29.79
Ca	2.52
Co	0.17
Total	100.00

Quantitative experiments were then conducted to measure the effect of dissolution on injectivity. The quantification process described in Section 2.3.2 was used to estimate the injectivity effects. An attempt was also made to investigate the effect of carbonated water injection flow rate and initial rock permeability.

4.1.1. Effect of Injection Flow Rate

A Berea sandstone core sample with known permeability was initially saturated with FW, and then flooded with about 25 PV of carbonated water at 80 bar and 60 °C at constant injection rate of 0.25 mL/min to release and mobilize fine particles in the rock. The permeability of the core after carbonated water flooding was measured, and the injectivity impairment index, β , was calculated. The experiment was then repeated at injection flow rates of 0.5 mL/min and 1.0 mL/min.

Figure 6 shows that the injectivity impairment decreased with increasing carbonated water injection flow rate. As injection flow rate is increased, the injected fluid stays in contact with the rock minerals for a short period of time, since the volume of injected fluid was kept constant in the three experiments. The number of fines generated will then decrease as the injection flow rate is increased. In addition, at a high injection flow rate, hydrodynamic forces could lift the smaller particles out of the core with the effluent fluid. The number of fines available to plug the rock, and therefore the chances of injectivity impairment, will reduce as the carbonated water injection flow rate is increased.

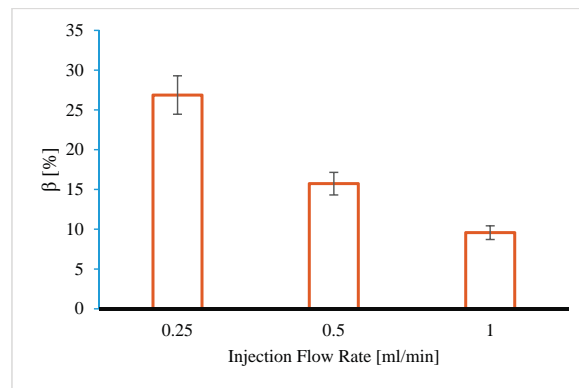


Figure 6. Effect of injection flow rate on injectivity impairment induced by fines migration. Injectivity impairment decreased with increasing rate of carbonated water injection flow rate.

4.1.2. Effect of Initial Core Permeability

To investigate the effect of initial rock permeability, the experiment was repeated with three sandstone rocks with varying initial permeability (Bentheimer: 1013 mD, Berea: 101 mD, Bandera 5 mD). It was assumed that the effect of variations in chemical properties of the sandstone cores on injectivity impairment is negligible compared to the flow properties of the cores. Carbonated water was injected into each rock at a constant flow rate of 0.25 mL/min. Figure 7 shows the impact of initial rock properties on injectivity impairment induced by mineral dissolution.

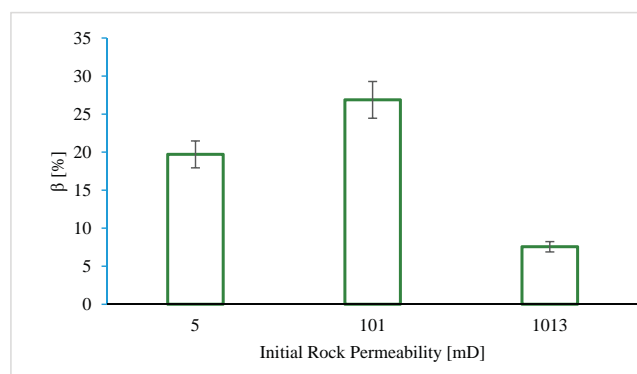


Figure 7. The influence of initial rock permeability on injectivity impairment induced by mineral dissolution. There was no obvious correlation between injectivity impairment and initial rock permeability.

Figure 7 shows that there was no obvious correlation between initial rock permeability and effect of dissolution on CO₂ injectivity. The impact of mineral dissolution on CO₂ injectivity will depend on the number of particles generated and the fraction of particles entrapped. The pore throats in low permeability rocks are very narrow, and have poor interconnections. The contact between injected carbonated water and the rock minerals will be low in this case, generating fewer particles as a result. However, due to the narrow pore channels, most of the generated particles have high chances of plugging the pores. Conversely, sandstone rocks with very high permeability will have more open and interconnected pore channels, which leads to improved contact between injected carbonated water and the rock minerals. More particles will be generated as a result. However, because most of the pores are open and connected, the released particles will have high chances of piping through the rock with the effluent and a low chance of plugging the pores. In sandstone rocks with medium permeability, fines generation and entrapment could both be enhanced to favor injectivity impairment.

4.2. Comparing the Effects of Salt Precipitation and Fines Mobilization

After establishing that mineral dissolution could impair CO₂ injectivity, we attempted to compare the contribution of each mechanism to CO₂ injectivity impairment. In order to optimize the properties of the fine particles, we used colloid suspensions as the formation fluid.

A Berea sandstone core sample was initially saturated with mono-disperse colloid solution with an average particle size of 0.08 μm and a particle concentration of 0.3 wt %. The composition of the mono-disperse colloid suspension used in this study has been described in Table 2. The core was then mounted and flooded with about 40 PV of supercritical CO₂ at 5 ml/min to complete dryness. The relative injectivity change, β , was calculated from the permeability of the core measured before and after it was exposed to mineral impairment. The experiment was repeated for particle concentrations of 0.5 wt % and 1.0 wt %. We then conducted a salt precipitation experiment by saturating the core with brine containing 10 wt % of total dissolved salts (FW) prior to supercritical CO₂ drying. Figure 8 shows the experimental results.

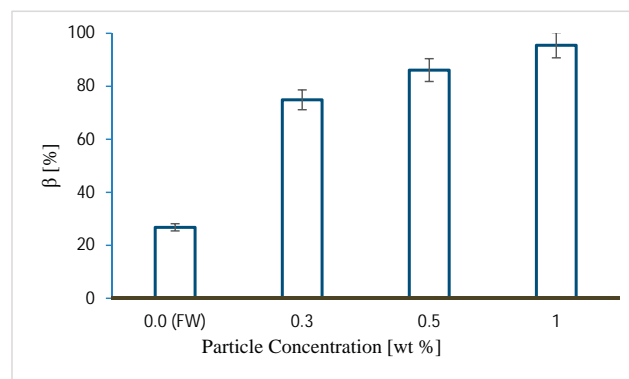


Figure 8. The relative impact of fines mobilization and salt precipitation on CO₂ injectivity. Fines migration had a more severe impact on injectivity compared to salt precipitation.

Pore size distribution analysis of similar Berea sandstone cores suggests an average pore throat size of about 2 μm [46]. The colloid with average particle size of 0.08 μm will yield an average jamming ratio of about 0.04. Natural formation fine particles have average particle sizes in the region of 1 μm [29,47]. However, the dissolution of sandstone under typical CO₂ storage conditions may yield particles of varying sizes over a wide range, depending on the reaction conditions and composition of the rock.

Particles with a jamming ratio of about 0.04 could plug the rock through surface deposition, pore bridging, and multi-particle blocking [29]. During saturation, if the particles are stabilized in the suspending fluid, the surface deposition would be greatly reduced. At very low particle concentration, the chances of pore bridging and multi-particle blocking could be greatly minimized. Therefore, the particles would stay mono-dispersed within the pore spaces after saturation and prior to CO₂ injection. When CO₂ invades the fluid-filled pores, the stability of the particles in the colloid will be disturbed, thereby releasing the particles for plugging during CO₂ flooding. This is comparable to CO₂ injection into a reservoir where the formation brine contains fine particles released from the dissolved rock.

In Figure 8, CO₂ injectivity impairment increased by about 20 percentage points when the concentration of mono-disperse particles in the saturating pore fluid was increased from 0.3 wt % to 1.0 wt %. While salt precipitation due to the drying of the FW reduced injectivity by about 26.8%, the particle concentration of 0.3 wt % reduced the injectivity by 74.9% through fines mobilization. When CO₂ invades the pores, the mono-disperse particles may plug the narrow pore channels through bridging, surface deposition, or multi-particle blocking. As the particle concentration increases, the distance between suspended particles shortens, enhancing the multi-particle blocking of the invaded pores.

After salt precipitation, the deposited salts will form a coating on the pore walls to reduce the flow area. However, during fines entrapment, several particles could accumulate in the pore throat and completely plug the pore. While salt precipitation reduces the flow area, fines entrapment could plug and isolate the flow path, making it inaccessible to fluid flow. This could be the reason why about 0.3 wt % particle concentration in the pore fluid induced over twofold injectivity impairment compared to about 10 wt % of total dissolved salt in the formation water. The results suggest that, under linear flow conditions, fines mobilization could induce severe CO₂ injectivity impairment comparable to the impact of salt precipitation.

4.3. Coupled Effect of Fines Mobilization and Salt Precipitation

The coupled effect of salt precipitation and fines mobilization was modelled with the bundle-of-tubes model described in Section 3. The results and conclusions drawn from this section are based only on theoretical modelling. We did not verify or compare the data obtained from the model with laboratory core-flood data. Although very preliminary, we believe the results presented here are intuitive and adequately explain the coupled impact of fines and salt effect on CO₂ injectivity.

In the first theoretical experiment, the clean bundle of tubes was exposed to particles of the same size. Each capillary tube had an equal chance of being exposed to the particles. Capillary tubes with a jamming ratio greater than 1.0 would be plugged through size exclusion. The effect of particle size on injectivity impairment was computed. The experiment was then repeated by first exposing the core to salt precipitation before subjecting them to particle entrapment. It was assumed that the precipitated salts would reduce the flow area, and render the capillary tubes more susceptible to fines entrapment. Particle sizes up to 20 μm were simulated.

Figure 9 shows the injectivity impairment induced (β) as a function of average particle size (r_p) for the three cases. For pure fines mobilization (no salt), particle sizes below 5 μm did not induce injectivity impairment. Since an average pore radius of 6 μm was used in the simulation, particles smaller than the average pore size will pipe through most of the pores. For particle sizes greater than 5 μm, injectivity impairment increases with particle size. As the particle size is increased, the number of capillary tubes likely to attain jamming ratios greater than 1.0 increases, and injectivity decreases as more tubes are plugged and isolated.

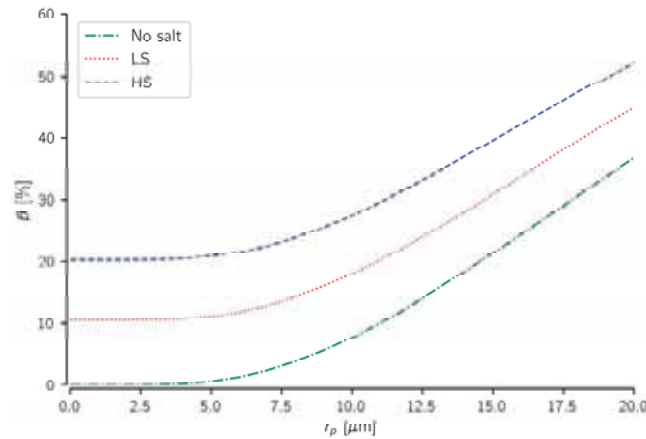


Figure 9. The coupled effect of fines mobilization and salt precipitation on CO_2 injectivity. Salt precipitation seems to compound injectivity impairment induced by fines migration. HS, high salinity brine; LS, low salinity brine.

Figure 9 also shows that injectivity impairment induced by fines mobilization was further compounded by increase in the saturating brine salinity. As brine salinity is increased, more salts are precipitated in the tubes. The precipitated salts reduce the flow area, increasing the jamming ratio of the tubes for each average particle size. The jamming ratio of the pores increases with increasing brine salinity as more salts are precipitated into the pores. Thus, more tubes will attain jamming ratios greater than 1.0 and eventually get plugged, inducing massive injectivity impairment.

The results suggest that salt precipitation could compound the injectivity impairment induced by fines mobilization. The precipitated salts could reduce the pore radii and increase the jamming ratio of the pores. This effect will in turn increase with saturating brine salinity, as more salts are precipitated into the pore spaces.

5. Conclusions

CO_2 injectivity impairment affects both the technical and economic planning and implementation of CCUS projects. Salt precipitation near the wellbore vicinity and in situ fines mobilization during CO_2 injection into deep saline reservoirs have been identified as potential CO_2 injectivity impairment mechanisms. The effect of salt precipitation on CO_2 injectivity has been researched, but the impact of fines mobilization is yet to receive its deserved attention. During CO_2 reinjection into deep saline reservoirs, salt precipitation and fines mobilization could simultaneously impair CO_2 injectivity.

We conducted preliminary core-flood experiments to investigate the impact of fines mobilization on CO_2 injectivity. The relative contribution of fines mobilization and salt precipitation to injectivity impairment was also investigated. A tractable bundle-of-tubes model was then used to study the coupled effect of salt precipitation and fines mobilization on injectivity. Some of the highlights of this work include:

1. Fines mobilization could induce severe CO_2 injectivity impairment. The experimental results suggest up to about a 26% injectivity impairment could be induced by fines migration.
2. Under linear flow conditions, CO_2 injectivity impairment induced by fines mobilization could be comparable to injectivity impairment caused by salt precipitation. About a 0.3 wt % particle concentration in the pore fluid induced over twofold injectivity impairment compared to about 10 wt % of total dissolved salt in the formation water.

- The findings also suggest that salt precipitation could compound the impact of fines mobilization on CO₂ injectivity. The precipitated salts reduce the pore spaces, making them more susceptible to particle plugging and injectivity reduction.

Although the methods adopted in this study were simple and rather linear, the findings will make a relevant contribution to the fundamental mechanisms of fines mobilization within the context of CO₂ injectivity. The results also provide important insight and could serve as a foundation to inspire further experimental and theoretical investigation into the effects of fines mobilization on CO₂ injectivity.

Acknowledgments: The authors would like to thank PGNiG Upstream International, Norway, and the Institute of Petroleum Technology (IPT) of the University of Stavanger for funding this project.

Author Contributions: Yen Adams Sokama-Neuyam established the research direction, designed the methods, and wrote the paper; Sindre Langås Forsetløyken and Jhon-eirik Lien conducted the experiments and collected data; Jann Rune Ursin contributed to data analysis and edited the paper.

Conflicts of Interest: The authors declare no conflict of interest.

Abbreviations

CCUS	CO ₂ Capture, Utilization and Storage
FW	Formation Water
I	Injectivity
HS	High Salinity brine
LS	Low Salinity brine

References

- Miri, R. Effects of CO₂-Brine-Rock Interactions on CO₂ Injectivity—Implications for CCS. Ph.D. Thesis, University of Oslo, Oslo, Norway, July 2015.
- Lombard, J.M.; Azaroual, M.; Pironon, J.; Broseta, D.; Egermann, P.; Munier, G.; Mouronval, G. CO₂ injectivity in geological storages: An overview of program and results of the GeoCarbone-Injectivity project. *Oil Gas Sci. Technol.* **2010**, *65*, 533–539. [[CrossRef](#)]
- Miri, R.; Hellevang, H. Salt precipitation during CO₂ storage—A review. *Int. J. Greenh. Gas Control* **2016**, *51*, 136–147. [[CrossRef](#)]
- Bacci, G.; Durucan, S.; Korre, A. Experimental and Numerical Study of the Effects of Halite Scaling on Injectivity and Seal Performance During CO₂ Injection in Saline Aquifers. *Energy Procedia* **2013**, *37*, 3275–3282. [[CrossRef](#)]
- Muller, N.; Qi, R.; Mackie, E.; Pruess, K.; Blunt, M.J. CO₂ injection impairment due to halite precipitation. *Energy Procedia* **2009**, *1*, 3507–3514. [[CrossRef](#)]
- Peysson, Y.; André, L.; Azaroual, M. Well injectivity during CO₂ storage operations in deep saline aquifers-Part 1: Experimental investigation of drying effects, salt precipitation and capillary forces. *Int. J. Greenh. Gas Control* **2014**, *22*, 291–300. [[CrossRef](#)]
- Zuluaga, E.; Muñoz, N.I.; Obando, G. An Experimental Study to Evaluate Water Vaporisation and Formation Damage Caused by Dry Gas Flow Through Porous Media. In Proceedings of the International Symposium on Oilfield Scale, Aberdeen, UK, 30–31 January 2001.
- Kleinitz, W.; Dietzsch, G.; Köhler, M. Halite scale formation in gas-producing wells. *Chem. Eng. Res. Des.* **2003**, *81*, 352–358. [[CrossRef](#)]
- Jasinski, R.; Sablerolle, W.; Amory, M. ETAP: Scale Prediction and Control for the Heron Cluster. In Proceedings of the SPE Annual Technical Conference and Exhibition, San Antonio, TX, USA, 5–8 October 1997.
- Golghanddashti, H.; Saadat, M.; Abbasi, S.; Shahrabadi, A. Experimental investigation of water vaporization and its induced formation damage associated with underground gas storage. *J. Porous Media* **2013**, *16*. [[CrossRef](#)]
- Place, M.C., Jr.; Smith, J.T. An Unusual Case of Salt Plugging in a High-Pressure Sour Gas Well. In Proceedings of the 59th Annual Technical Conference and Exhibition, Houston, TX, USA, 16–19 September 1984; p. 13.

12. Baumann, G.; Hennings, J.; De Lucia, M. Monitoring of saturation changes and salt precipitation during CO₂ injection using pulsed neutron-gamma logging at the Ketzin pilot site. *Int. J. Greenh. Gas Control* **2014**, *28*, 134–146. [[CrossRef](#)]
13. Grude, S.; Landrø, M.; Dvorkin, J. Pressure effects caused by CO₂ injection in the Tubåen Fm., the Snøhvit field. *Int. J. Greenh. Gas Control* **2014**, *27*, 178–187. [[CrossRef](#)]
14. Bacci, G.; Korre, A.; Durucan, S. Experimental investigation into salt precipitation during CO₂ injection in saline aquifers. *Energy Procedia* **2011**, *4*, 4450–4456. [[CrossRef](#)]
15. Kim, M.; Sell, A.; Sinton, D. Aquifer-on-a-Chip: Understanding pore-scale salt precipitation dynamics during CO₂ sequestration. *Lab Chip* **2013**, *13*, 2508–2518. [[CrossRef](#)] [[PubMed](#)]
16. André, L.; Peysson, Y.; Azaroual, M. Well injectivity during CO₂ storage operations in deep saline aquifers—Part 2: Numerical simulations of drying, salt deposit mechanisms and role of capillary forces. *Int. J. Greenh. Gas Control* **2014**, *22*, 301–312. [[CrossRef](#)]
17. Tang, Y.; Yang, R.; Du, Z.; Zeng, F. Experimental study of formation damage caused by complete water vaporization and salt precipitation in sandstone reservoirs. *Transp. Porous Media* **2015**, *107*, 205–218. [[CrossRef](#)]
18. Sokama-Neuyam, Y.A.; Ursin, J. Experimental and Theoretical Investigations of CO₂ injectivity. *AGH Drilling Oil Gas* **2016**, *33*, 245–257. [[CrossRef](#)]
19. Giorgis, T.; Carpita, M.; Battistelli, A. 2D modeling of salt precipitation during the injection of dry CO₂ in a depleted gas reservoir. *Energy Convers. Manag.* **2007**, *48*, 1816–1826. [[CrossRef](#)]
20. Hurter, S.; Berge, J.; Labregere, D. Simulations for CO₂ injection projects with Compositional Simulator. In Proceedings of the Offshore Europe, Aberdeen, UK, 4–7 September 2007.
21. Pruess, K. Formation dry-out from CO₂ injection into saline aquifers: 2. analytical model for salt precipitation. *Water Resour. Res.* **2009**, *45*, 1–6. [[CrossRef](#)]
22. Zeidouni, M.; Pooladi-Darvish, M.; Keith, D. Analytical solution to evaluate salt precipitation during CO₂ injection in saline aquifers. *Int. J. Greenh. Gas Control* **2009**, *3*, 600–611. [[CrossRef](#)]
23. Roels, S.M.; Ott, H.; Zitha, P.L.J. μ -CT analysis and numerical simulation of drying effects of CO₂ injection into brine-saturated porous media. *Int. J. Greenh. Gas Control* **2014**, *27*, 146–154. [[CrossRef](#)]
24. Kleinitz, W.; Koehler, M.; Dietzsch, G.; Gmbh, P.E. The precipitation of salt in gas producing wells. In Proceedings of the SPE European Formation Damage Conference, The Hague, The Netherlands, 21–22 May 2001; pp. 1–7.
25. Pruess, K.; Muller, N. Formation dry-out from CO₂ injection into saline aquifers: 1. Effects of solids precipitation and their mitigation. *Water Resour. Res.* **2009**, *45*, 1–11. [[CrossRef](#)]
26. Patton, J.T.; Phelan, P.; Holbrook, S. *CO₂ Formation Damage Study—First Annual Report*; U.S. Department of Energy: Las Cruces, NM, USA, 1981.
27. Sayegh, S.G.; Krause, F.F.; Girard, M.; DeBree, C. Rock/Fluid interactions of carbonated brines in a sandstone reservoir: Pembina Cardium, Alberta, Canada. *SPE Form. Eval.* **1990**, *5*, 399–405. [[CrossRef](#)]
28. Tobergte, D.R.; Curtis, S. Experimental perspectives of mineral dissolution and precipitation due to carbon dioxide-water-rock interactions. *J. Chem. Inf. Model.* **2013**, *53*, 1689–1699.
29. Khilar, K.C.; Fogler, H.S. *Migrations of Fines in Porous Media*; Kluwer Academic Publisher: Dordrecht, The Netherlands, 1998; Volume 12.
30. Muecke, T.W. Formation fines and factors controlling their movement in porous media. *J. Pet. Technol.* **1979**, *31*, 144–150. [[CrossRef](#)]
31. Khilar, K.C.; Fogler, H.S. Water Sensitivity of Sandstone. *Soc. Pet. Eng. J.* **1983**, *23*, 55–64. [[CrossRef](#)]
32. Gruesbeck, C.; Collins, R.E. Entrainment and Deposition of Fine Particles in Porous Media. *Soc. Pet. Eng. J.* **1982**, *22*, 847–856. [[CrossRef](#)]
33. Sarkar, A.; Sharma, M. Fines Migration in Two-Phase Flow. *J. Pet. Technol.* **1990**, *42*, 646–652. [[CrossRef](#)]
34. Sharma, M.M.; Yortsos, Y.C. Fines migration in porous media. *AIChE J.* **1987**, *33*, 1654–1662. [[CrossRef](#)]
35. Civan, F. *Reservoir Formation Damage: Fundamentals, Modelling, Assessment, and Mitigation*; Gulf Professional Publishing: Waltham, MA, USA, 2007.
36. Aji, K. The Experimental and Theoretical Study of Fines Migration in Porous Media under Particle-rock Repulsion and Attraction. Ph.D. Thesis, University of Adelaide, Adelaide, Australia, October 2014.
37. Peksa, A.E.; Wolf, K.H.A.A.; Zitha, P.L.J. Bentheimer sandstone revisited for experimental purposes. *Mar. Pet. Geol.* **2015**, *67*, 701–719. [[CrossRef](#)]

38. Mohammed, A.S.; Ayoub, A.; Massoud, M. Effects of Low Salinity Water Ion Composition on Wettability Alteration in Sandstone Reservoir Rock: A Laboratory Investigation. *J. Nat. Sci. Res.* **2014**, *4*, 34–41.
39. Dullien, F.A.L.; Dhawan, G.K. Characterization of pore structure by a combination of quantitative photomicrography and mercury porosimetry. *J. Colloid Interface Sci.* **1974**, *47*, 337–349. [[CrossRef](#)]
40. Fjelde, I.; Omekeh, A.V.; Sokama-Neuyam, Y.A. Low Salinity Water Flooding: Effect Of Crude Oil Composition. In Proceedings of the SPE Improved Oil Recovery Symposium, Tulsa, OK, USA, 12–16 April 2014.
41. Portier, S.; Rochelle, C. Modelling CO₂ solubility in pure water and NaCl-type waters from 0 to 300 C and from 1 to 300 bar Application to the Utsira Formation at Sleipner. *Chem. Geol.* **2005**, *217*, 187–199. [[CrossRef](#)]
42. Fogler, H.S. The Existence of a Critical Salt Concentration for Particle Release. *J. Colloid Interface Sci.* **1984**, *101*, 214–224.
43. Shi, J.Q.; Xue, Z.; Durucan, S. Supercritical CO₂ core flooding and imbibition in Berea sandstone—CT imaging and numerical simulation. *Energy Procedia* **2011**, *4*, 5001–5008. [[CrossRef](#)]
44. Lin, C.; Slattery, J.C. Three-dimensional, randomized, network model for two-phase flow through porous media. *AIChE J.* **1982**, *28*, 311–324. [[CrossRef](#)]
45. Yanuka, M.; Dullien, F.A.L.; Elrick, D.E. Serial sectioning and digitization of porous media for two- and three-dimensional analysis and reconstruction. *J. Microsc.* **1984**, *135*, 159–168. [[CrossRef](#)]
46. Nelson, P.H. Pore-throat sizes in sandstones, tight sandstones, and shales. *Am. Assoc. Pet. Geol. Bull.* **2009**, *93*, 329–340. [[CrossRef](#)]
47. Sen, T.K.; Khilar, K.C. Review on subsurface colloids and colloid-associated contaminant transport in saturated porous media. *Adv. Colloid Interface Sci.* **2006**, *119*, 71–96.



© 2017 by the authors. Licensee MDPI, Basel, Switzerland. This article is an open access article distributed under the terms and conditions of the Creative Commons Attribution (CC BY) license (<http://creativecommons.org/licenses/by/4.0/>).